NASA CONTRACTOR REPORT

NASA CR – 137645

FEASIBILITY STUDY OF LOW ANGLE PLANETARY ENTRY

by R. E. DeFrees

Prepared by
MCDONNELL DOUGLAS ASTRONAUTICS COMPANY – EAST
St. Louis, Missouri 63166 (314) 232-0232

NATIONAL AERONAUTICS AND SPACE ADMINISTRATION • WASHINGTON, D.C. • MAY 1975

TABLE OF CONTENTS

TABLE OF CONTENTS

LIST OF PAGES

Title, ii thru viii

Report 1 thru 144

LIST OF FIGURES

LIST OF FIGURES

LIST OF FIGURES

LIST OF FIGURES

ACKNOWLEDGEMENTS

This data presented in this report was generated by members of the Outer Planets Probe group at the McDonnell Douglas Astronautics Company-East. The efforts of these individuals are acknowledged: J. H. Carter, W. H. Gustin, C. A. Hinrichs, D. L. Jenkins, W. C. Kessler, J. W. Kiefer, R. L. Kloster, S. A. Mezines, B. T. Miller, G. D. Mitchell, J. C. Murray, R. N. Rezentes, R. D. Rochat, E. L. Rusert, J. L. Sedwick, M. E. Siegrist, J. A. Smittkamp. Mr. T. L. Grant was especially helpful in clarifying the presentation of the communication link; his advice is gratefully appreciated. The assistance in preparation by M. F. Aubuchon and T. M. Bytnar and in editing by F. E. Bradley and W. D. Cowan were especially appreciat d by the author.

SUMMARY

An entry probe is described which is capable of release near an outer planet's sphere of influence; which descends to a predetermined target entry point in the planet's atmosphere, survives the trapped particle radiation belts (if present) and through an entry heating pulse, and that descends in a stable dynamic condition while gathering and relaying data to an overflying spacecraft bus. It is 889 mm (35 in.) in diameter and weighs 150 kg (or less). It is configured as a sphere-cone fore body and a hemisphere after body. Because ground-based and flyby measurements are susceptible to various conflicting interpretations, in situ measurements of local physical properties and chemical composition within the atmosphere are needed to remove the dependence on atmospheric modeling and lead directly to the utilization of prior remotely acquired data. The types of experiments that have the highest priority for in situ measurements on an entry probe are concerned with atmospheric structure and chemical composition. A tri-axial accelerometer provides data on atmospheric densities. These data, when combined with direct low altitude measurements of ambient temperatures and pressures, provide profiles of the physical structure of the atmosphere. The chemical composition of the atmosphere is determined by mass spectrometry and gas chromatography. These data are gathered in the troposphere, where the atmosphere is homogeneous.

The atmosphere of Jupiter can be successfully explored in the early 1980's because of three major developments. These developments have come to fruition through the combined efforts of the National Aeronautics and Space Administration, aerospace industry, and individual researchers. By utilizing the technology gained while carefully proving each element of the configuration step by step, an atmospheric probe can be made available for launching in 1979 on an interplanetary spacecraft. The probe carrying bus may be a Mariner based or a Pioneer based design, the probe requires only changes in the antenna and, perhaps, transmitter characteristics to adapt to either bus.

This study is aimed at determining the range of parameters which make feasible a Jovian entry by a probe originally designed for Saturn and Uranus entries. The massiveness of Jupiter, which produces high relative entry

velocities, necessitates thickening the forward heat shield, reformatting of data collection and transmission, increasing transmitter power, and optimizing the receiving equipment. The pertinent data for this probe are summarized in Figure 1. The study has substantiated confidence in the feasibility of an early Jupiter entry mission.

The three developments that have produced this feeling of confidence are:

1) The characterization of the Jovian magnetosphere by Pioneer 10 which permits more accurate prediction of component environments. Knowing the nature and severity of the exposure, functional elements can be hardened to survive the effects of trapped particle radiation. The exact character of the environment is still incomplete within the 3 to 1 R_J layer. However, the passage of Pioneer 11 will improve current modeling in this layer; thereby permitting thorough analysis of protection needed and already provided.

2) The refinement in ephemeris resulting from the Jupiter flyby in 1973 by Pioneer 10. The precision in knowing Jupiter's mass properties and its locus as a function of time permits accurate planning of an atmospheric entry mission at a few degrees flight path angle from the skip-out boundary. By keeping the angle low, the heating environment can be accommodated with current state of the art thermal protection materials. Although entry conditions into the Jovian atmosphere are the most severe of any planet, the combination of precision in trajectory targeting and material fabrication assure survival through the peak heating environment.

3) The evolution of convolutional coding techniques and communication linkages that can operate in a noisy, turbulent environment at or above the adverse tolerances present at the outer planets. Again, each planet's synchrotron noise and other conditions which influence communicability are not completely understood. The level of understanding and the tools to overcome the problems have evolved to the point where alternative solutions can be defined and selection criteria established. These in turn will permit the development of a workable link when needed.

The anticipated hazards (trapped particles and entry heating) are considered to be tractable at this time. The remainder of this report is directed at detail examination of the design problems foreseen and solutions which, as yet,

LOW ANGLE ENTRY PROBE FOR JUPITER

LAUNCH VEHICLE	TITAN IIIE/CENTAUR D1-T/TE364-4	
SPACECRAFT	MODIFIED PIONEER F/G	
MISSIONS:	PROBE '79	ORBITER-PROBE '80
MISSION DESIGNATOR	PJ_P 79	PJO_P 80
LAUNCH DATES	8 NOV 79	6 DEC 80
ARRIVAL DATES	11 MAR 82	14 FEB 83
S/C PERIAPSIS RADIUS, R_J	1.8	1.8
PROBE DIAMETER (mm/in)	889/35	889/35
PROBE WEIGHTS (kg/lb)	140/308.8	146.5/323
PROBE SEPARATION RADIUS (R_J)	500	500
S/C DEFLECTION ΔV (m/s)	80	
ENTRY LATITUDE (deg)	+4.8	+4.8
EXOSPHERIC DESCENT TIME (days)	53.2	50
ATMOSPHERIC DESCENT TIME (min)	30	30
INERTIAL VELOCITY @ ENTRY (km/s)	59.8	59.8
INERTIAL ENTRY ANGLE (DEG @ 450 km)	-7.5	-7.5
BALLISTIC COEFFICIENT, M/C_DA(kg/m^2)	125 (average)	158.1 (initial)
ANGLE OF ATTACK: W S/C DEFLECTION	0	0
NO S/C DEFLECTION	29	16.6
COMMUNICATION DURATION (min)	24.6	30
PROBE BEAMWIDTH (deg)	66	66
S/C PHASING TIME (hr BEFORE ENTRY)	0.4	0.4
S/C BEAMWIDTH (deg)	50	50
S/C BEAM CENTER (deg FROM AXIS)	65	56
PROBE TRANSMITTER POWER (W)	40	60
PROBE DATA RATE (bps)	44	44
PROBE DATA STORAGE (kbits)	17.4/31.2	25.5
HEAT SHIELD WEIGHT (kg/lb)	68.5/151.2	68.6/151.5
PEAK HEAT FLUX ($BTU/ft^2/s$)	17	17
PEAK DECELERATION (g_E)	264	286
ELECTRICAL POWER REQUIRED (W-hrs)	98	125.2
ENGINEERING SENSORS	17	23
SCIENCE INSTRUMENTS	ACCELEROMETER PRESSURE TEMPERATURE MASS SPECTROMETER NEPHELOMETER	SAME +
		GAS CHROMATO-GRAPH VISIBLE-IR FLUX ENERGETIC PARTICLES

FIGURE 1

are not necessarily optimal. Continuing study may reveal atlernate paths over or around the hazards. The work described has been performed by the McDonnell Douglas Astronautics Company-East under contract to NASA/Ames Research Center (Contract NAS2-8377).

This report describes probe variations for two similar missions. In the first a flyby of Jupiter by a Pioneer spacecraft launched during the 1979 (PJ_p'79) opportunity is examined parametrically. The discussion is concentrated in the section labeled Mission Analysis. In the second mission an orbiter based on Pioneer and launched in 1980 (PJO_p'80) is defined in more specific terms. This discussion is concentrated in "Probe Description" and "Subsystem Design". Occasional interminging occurs to illustrate certain factors not computed with both mission analyses. The differences rest in the science payload and directly affected wiring and electronics packages. Since weights are approximately the same for both, only dynamic effects are involved. The six-degree-of-freedom data indicates that, although the center of gravity is aft of the theoretical intersection of cone and aft sphere, the dynamic stability characteristics are satisfactory for the heavier, more aft-c.g. version (Pioneer Jupiter Orbiter Probe for 1980). The initial baseline mission (Pioneer Jupiter Probe for 1979) served as the basis for most analytical studies. In almost all instances the differences between missions and configurations have only secondary effects on performance of the probe.

INTRODUCTION

The successful entry of a probe into one of the outer planets requires a design that can overcome the hazards of radiation, severe heat pulses, and uncertainties of the trajectory and of the atmospheres to be encountered. The severity of each hazard is greater at Jupiter than at the planets that are further removed from the sun. In References 1 and 2 a probe design is described that can enter either Saturn's or Uranus' atmosphere with a high probability of providing in situ measurements of their atmospheres. A potential exists for adapting that configuration for entry into Jupiter's atmosphere and, perhaps, that of the satellites to the outer planets. This study investigates some of the known variations of Jupiter's environment. The effects are presented with first iterations on design parameters to demonstrate feasibility.

Feasibility is defined as ability to withstand the severe conditions without adding undue penalties of cost or time to develop and deploy the probe. Evaluations are presented of primary and subsidiary solutions from allied studies that are also under contract to the NASA/Ames Research Center.

Background

The Saturn/Uranus Atmospheric Entry Probe (SUAEP) System Level Definition Study was initiated as contract number NAS2-7328 in November 1972 with a final report published on 18 July 1973 (Reference 1). This effort has been extended and expanded as shown in Figure 2 to cover important considerations that were brought to light in the basic study. One such aspect is the difficulty of entering a Jovian atmosphere because its gravitational attraction causes very high velocities which produce severe heating conditions. Prior work on Jovian entries (e.g. Reference 3) demonstrated an amelioration of the environment effects by reduction of the entry angle into Jupiter's atmosphere. Thus, this study was directed at angles of entry (γ) from the skip-out boundary ($\gamma \cong -4°$ @ 450 km) down to $\gamma = -12.5°$. In this range of entry angles, longer, lower-level decelerations are encountered. The result is some relief in peak heat flux, especially radiant energy.

PROBE PHASE II CONTRACTED RESEARCH

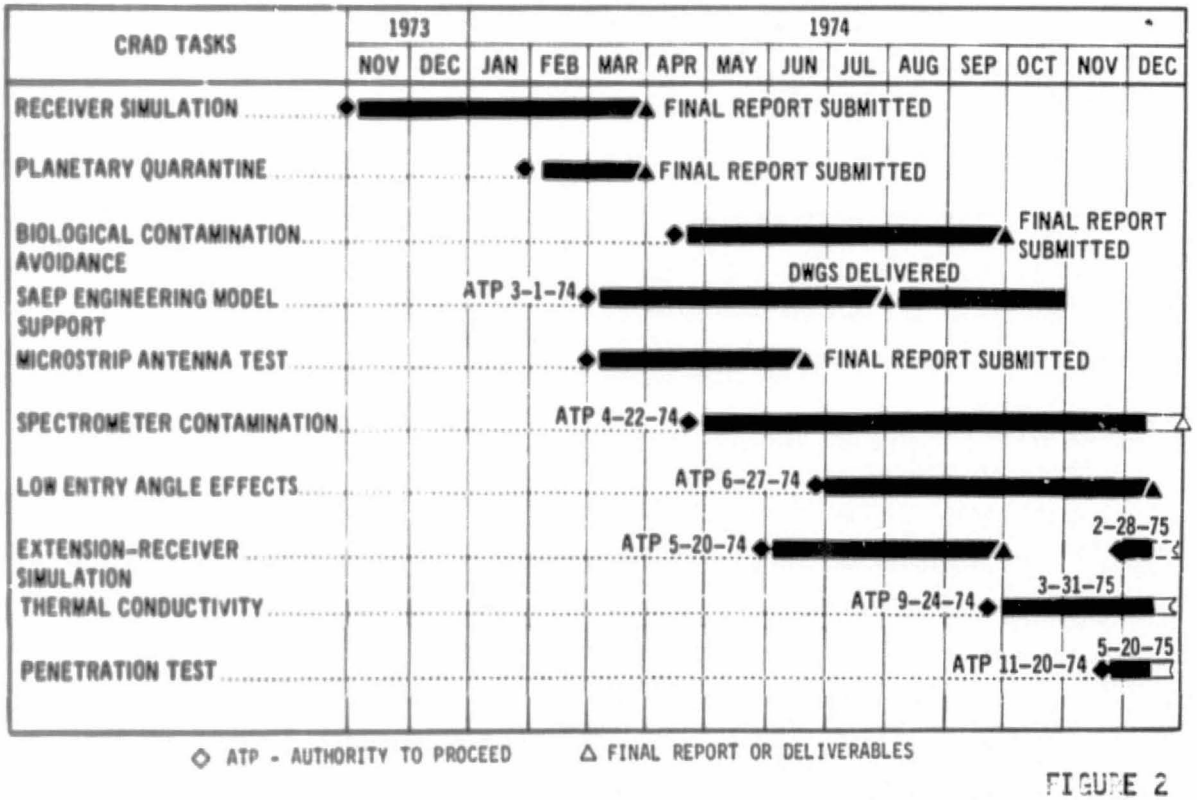

FIGURE 2

This study contract (NAS2-8377) was initiated on 27 June 1974; the study is completed with submission of this report. The statement of work tasks are included in Reference 4.

Study Objectives

"To perform a feasibility study of conducting definitive atmospheric science during descent into a planetary atmosphere by using extremely small flight path angles (near the skipout boundary). The study shall establish the requirements of a probe heat protection system, communication link, and science data-gathering which are compatible with survival of the high heating environments for outer planets entry."

The science objectives are determination of atmospheric constituents; characterization of pressure, temperature, and density profiles; and observation of the cloud layers. Consideration of infrared radiant energy measurement and energetic particle counting were added after contract start.

Scope of Effort

Direct effects of low angle entry into a Jovian atmosphere are covered. Secondary effects, such as structural redesign or battery reduction for shorter durations are also included. The study is restricted to Jupiter since moderately steep entries are feasible into Saturn and Uranus (see Section 4.2.1 of Reference 1) with carbon-phenolic material.

The scope of this study also is limited to analysis; only design changes reflecting individual components are included. Complete drawings, similar to Part V of Reference 1, were not made. The changes, though not superficial, are of a nature that understanding is possible without complete drawings.

Baseline Definition

The baseline mission initially was for the 1979 opportunity using the Titan IIIE/Centaur D1-T/TE364-4 launch vehicle and a modified Pioneer F,G type of spacecraft bus. During the interplanetary flight, the probe's temperature is controlled by the spacecraft but without a closed loop sensor - heat transport mechanism. The study constraints are summarized in the succeeding section.

A summary of baseline data for this mission and configuration is presented in Figure 3. These parameters are shown with two columns: (1) the initial or SUAEP value, and (2) the Jupiter nominal value. The latter are somewhat non-optimal because iterations are incomplete. In some instances only two of three (or four) model atmospheres are exercised in the interest of bracketing problems. All required atmosphere definitions would have to be studied before a baseline finalization could be made.

The primary function of this probe is to collect and transmit data that aids in characterizing the atmosphere of Jupiter. To date, all data have been obtained remotely. However, even the close-up measurements of Pioneer 10 are not in agreement; for example, the infrared radiometer data conflict with the radio occultation. To obtain absolute values and to permit correlation of existing data, in situ measurements will enhance our understanding of some of the planetary atmosphere processes. As the probe enters the atmosphere, an onboard accelerometer senses a threshold, in this case ($-0.0004\ g_E$); the data handling system continues to record deceleration values at moderate rates until the deceleration peak occurs. This is defined as $a = -0.01\ g_E$ (axially) on the ascending side of the peak, and this serves as the rate-change cue. Because this specific value cues several probe functions, the accelerometer is backed up by a g-switch. Subsequently, other deceleration cues trigger other functions such as instrument deployment and radio transmission. This sequence of events is correlated with time and altitude and the usually defined cloud layers in Figure 4.

BASELINE DEFINITION COMPARISON

OPERATION/PARAMETER	SUAEP(1)	PJ_p'79
PRELAUNCH		
LAUNCH PERIOD,	T5	SAME
PAYLOAD, lbs (kg)	1050 (476)	
PROBE WEIGHT, lbs (kg)	308.8 (140)	
PROBE DIAMETER, in (m)	35 (0.89)	SAME
PRELAUNCH CONDITIONING	FORCED AIR	SAME
TEMPERATURE REGIME	80°F (GROUND) 30°F (FLIGHT)	
LAUNCH VEHICLE	TITAN IIIE/CENTAUR/ TE364-4	SAME
S/C(3) INTERPLANETARY		
INFLIGHT CONDITIONING	HEATED ADAPTER	SAME
TARGETING	BY S/C; S/C DEFLECTION	SAME
SEPARATION TIMING	S/C TRIGGERED	SAME
S/C ORIENTATION	EARTH-LOCKED	SAME
BATTERY CHARGING (BOOSTRAP)	S/C RTG'S	SAME
(MAIN)	PRE-CHARGED	SAME
DESCENT TO ENTRY		
TIMING (WARMUP & ACCELEROMETER)	PRE-SET ACCUTRON	SAME
PREENTRY SCIENCE	NONE	SAME
ENTRY ANGLE,	(ь) -30° (б) -40°	(ъ)-7.5°
ENTRY LATITUDE	(ъ) +30°	(ъ)+4.8°
PEAK DECELERATION, g_E	800	250
ATMOSPHERIC ENTRY		
CONFIGURATION	60° SPHERE CONE; HEMISPHERE	SAME
COMM INITIATION - METHOD	ACCELEROMETER; G-SWITCH	SAME
- LEVEL, g_E	-2	-3
TRANSMISSION FREQUENCY, GHz	0.4	0.6-0.8
TRANSMITTER	NONCOHERENT FREQUENCY SHIRT KEYED	SAME
ANTENNA PATTERNS-PROBE	ROLL AXIS; CONICAL	SAME
-S/C	SPINNING; PANCAKE	SAME
ANTENNA BEAMWIDTH-PROBE	66°	SAME
-S/C	30°-105°	SAME
INSTRUMENT DEPLOYMENT-CUE	ACCELEROMETER,	SAME
-LEVEL, g_E	-6	-30
-METHOD	THRU HEATSHIELD	SAME
SCIENCE INSTRUMENTS	NEUTRAL MASS SPEC	SAME
	TEMPERATURE GAGE	SAME
	PRESSURE GAGE	SAME
	ACCELEROMETERS	SAME
	NEPHELOPMETER	SAME
		RADIOMETER
INITIAL ANGLE OF ATTACK	(α_1) = 12.6°	(α) = 29° or 0° (PIONEER DEPENDENT)
HEAT SHIELD - CONFIGURATION	RETAINED	SAME
- FORWARD	CARBON-PHENOLIC	SAME
- AFT	SILICONE ELASTOMER	SAME

(1) SUAEP-SATURN/URANUS ATMOSPHERIC ENTRY PROBE
(2) PJ_p'79 - PIONEER JUPITER PROBE IN 1979
(3) S/C - SPACECRAFT BUS

FIGURE 3

DATA COLLECTION SEQUENCE

• JUPITER 1980 NOMINAL MISSION

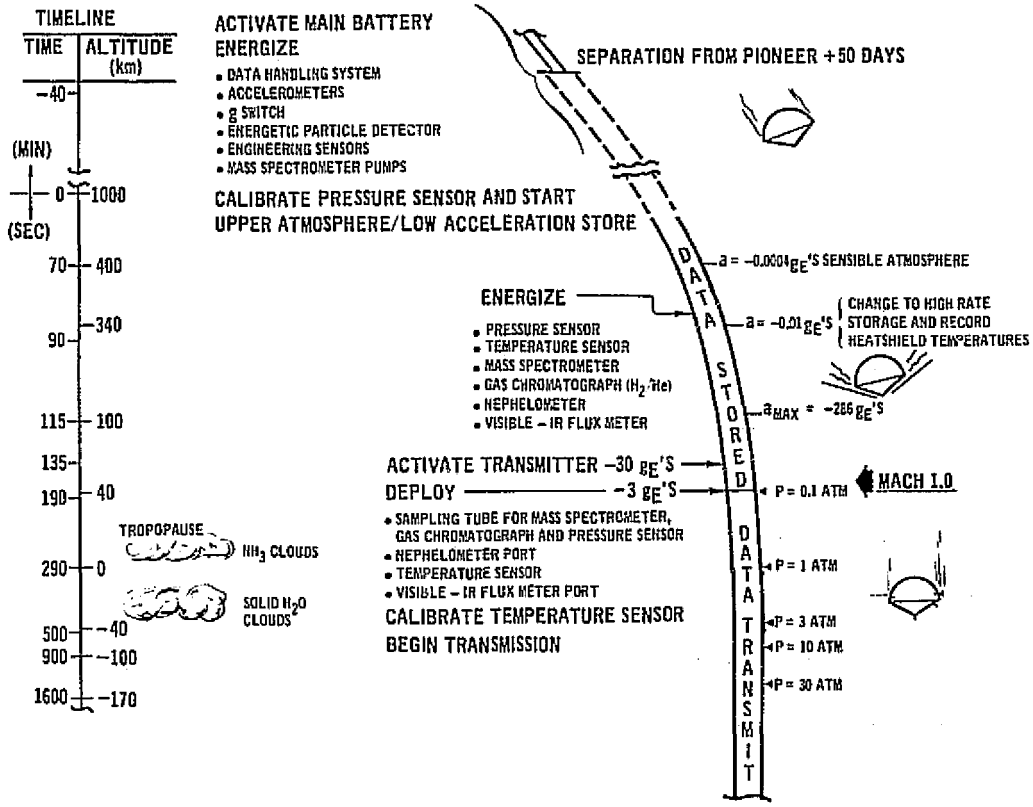

FIGURE 4

GUIDELINES & CONSTRAINTS

This study is directed at an examination of entry angles into Jupiter's atmosphere which produce decelerations that can be accommodated by the structure designed for the Saturn/Uranus Atmospheric probe described in Reference 1. The probe heat protection is adjustable in thickness but aluminum and honeycomb characteristics and overall diameter are to be unchanged from the reference values. The design is based on NASA monograph atmosphere models as defined in Reference 5 with emphasis placed on the envelope of Nominal and Warm definitions. (Note that other definitions were studied, but no other was specified.) Pioneer 10 data indicate that the Cool model is an improbable condition.

The guidelines and constraints employed in this study are itemized in the following table.

Guidelines

1)	Launch Vehicle	Titan III E/Centaur D1-T/TE364-4
2)	Spacecraft	Modified Pioneer F, G, H
3)	Temperature Control (to separation)	Open-Loop by Spacecraft
4)	Minimum Science Payload (see Reference 1)	Mass Spectrometer Accelerometer Temperature and Pressure Gauges Nephelometer

[N.B. Instrument ranges to be adjusted to meet environments to be encountered.]

5)	Flight Opportunities	1979, 1980
6)	Planetary Quarantine	Considered as part of another contract.
7)	Data Collection Objective	30 min. (minimum)

Constraints

1)	Representative probe design shall be based on the results of Contract NAS2-7328 (Reference 1).	
2)	Probe Diameter	$\leq$ 36 inches (91.5 cm)
3)	Probe Weight (including margins)	$\leq$ 300 pounds (136 kg)
4)	Data Gathering	10 bar minimum
5)	Atmospheric Models	Reference 5 Nominal & Warm

Although the study was to be confined by these guidelines and constraints, some latitude in studying alternatives beyond these limits was encouraged by ARC personnel in order to evaluate potentials "just over the next hill". These excursions permitted: (1) better interpolation at boundaries, and (2) provide alternate mission potential for NASA review. For example, the weight of the probe for the Pioneer Jupiter Orbiter Probe mission in 1980 is profusively illustrated herein. It weighs 146.5 kg (323 lbs). Its capability for better atmosphere definition warrants strong consideration of its use over a 300 lb limit probe.

MISSION ANALYSIS

The Earth-to-Jupiter mission profile is similar to that used for the SUAEP study. Two missions are considered: (1) a Jupiter flyby and probe deposition in 1979 (PJ_p '79), and (2) a Jupiter orbiter and probe in 1980 (PJO_p '80). The representative interplanetary trajectory was chosen by Ames Research Center. A plane change ascent is required at Earth departure for the interplanetary trajectory selected. Details of the interplanetary track properly belong in descriptions of the spacecraft. Suffice it to say that from initial insertion by the final stage rocket (TE364-4 solid rocket motor), the spacecraft and probe are aimed to be captured by the target planet. As tracking continues with time, the aim point is refined in accuracy by corrective maneuvers. The final correction is made shortly ($\sim$1 or 2 days) prior to release.

Flyby Mission (PJp '79)

Except for the addition of a post-deflection corrective maneuver to the spacecraft, the mission profile utilized for Jovian entries is similar to that featured in the various SUAEP studies. As depicted in Figure 5, the spacecraft (with probe) is targeted for the probe entry point. For this treatment, the targeted entry point is an inertial path angle of -7.5 degrees at an altitude of 450 km with probe and spacecraft equatorially inclined at 10 and 20 degrees.

The principal independent variables (trajectory,mission parameters) utilized in the study of planetary trajectories are spacecraft periapsis radius and spacecraft phasing time. For complete understanding of this text certain parameters are defined in Figure 6.

The spacecraft and probe are targeted at the probe entry point as depicted in Figure 7. At a distance from Jupiter that is within its sphere of influenc , herein taken at 500 R_J, the probe is released. The spacecraft is retargeted via a deflection maneuver for a near overfly of the probe by the spacecraft; this is phased to occur during the probe's data gathering descent into the Jovian atmosphere and prior to spacecraft insertion into orbit. Phasing is accomplished during the deflection and consists of a deceleration of the spacecraft to cause a lag. The probe mission is completed when the probe and spacecraft are no longer in communications view of each other.

MISSION PROFILE FOR JUPITER PROBE STUDY

1979 OPPORTUNITY

NOMINAL MISSION	
LAUNCH	8 NOV 79
ARRIVAL	11 MAR 82
DURATION, DAYS	854
SEPARATION, R_J	500
DESCENT, DAYS	53.2
ENTRY ANGLE, DEG	-7.5
PHASING, HRS	0.4
S/C PERIAPSIS, R_J	1.8

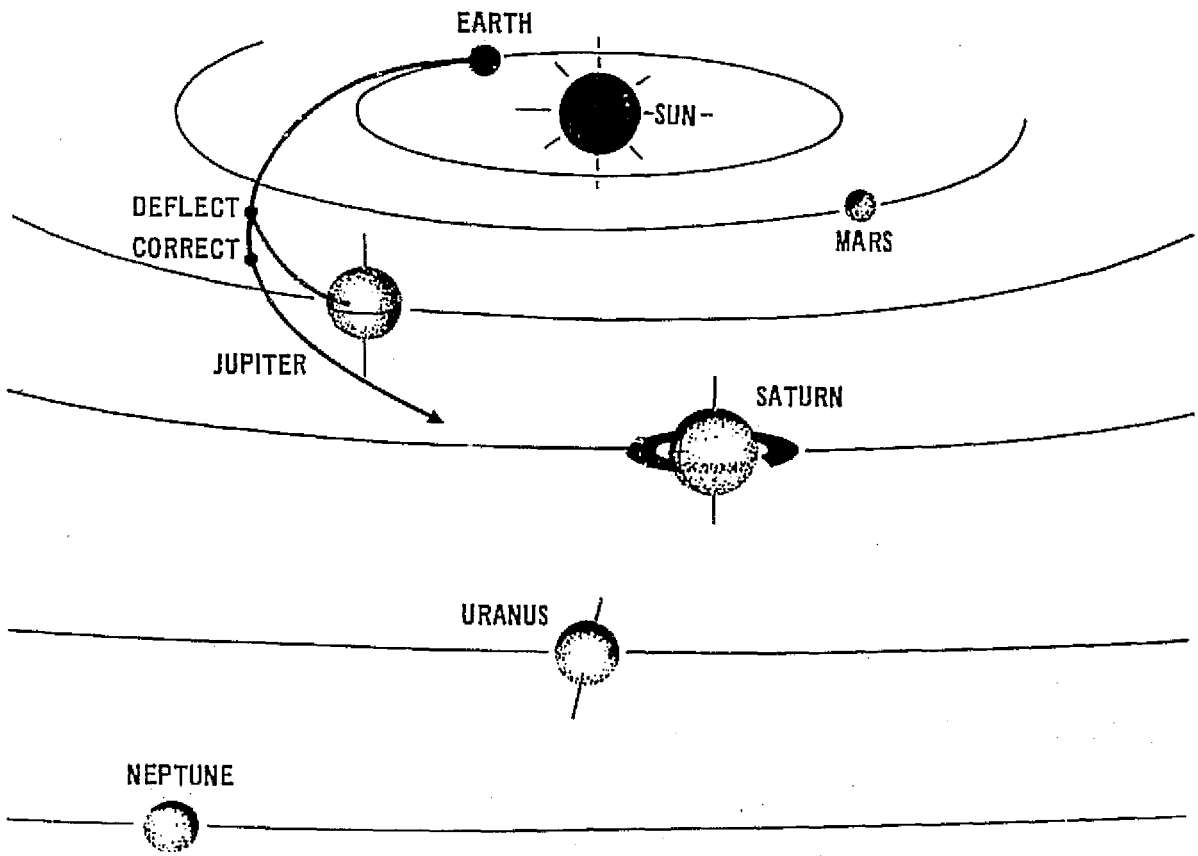

FIGURE 5

DEFINITIONS

Periapsis Radius refers to the trajectory periapsis of the spacecraft after the deflection and any correction maneuvers. Its origin is the center of the planet.

Phasing Time is the time past entry when the spacecraft is phased to pass through the probe zenith.

Spacecraft Aspect Angle - The angle, measured at the spacecraft, between the probe line-of-sight and the spacecraft spin-axis (i.e., the Earth Direction).

Probe Aspect Angle - The angle, measured at the probe, between the spacecraft line-of-sight and the probe spin-axis which is also Earth-line if released from Pioneer, but is oriented for zero angle of attack if Mariner borne.

Communication Range - The distance between the probe and spacecraft, the combination of range and aspect angle determine communicability.

Communication Duration - Time from probe entry until the spacecraft aspect angle reaches 105 degrees (communications cutoff) on Pioneer flights; another undetermined limit obtains for Mariner.

Entry Path Angle - The probe inertial flight path angle are conventionally taken at 450 km above the equatorial sphere and the pressure altitude of one bar. Note that 1000 km is generally used as the initiation of descent because the drag, gravity effects are significant from this latter altitude.

Probe Entry Latitude - Entry latitude of probe measured positive north from the Jovian equator. Longitude is important in final mission analyses and scientific interest but do affect probe design negligibly even light-side/dark-side entries. In general, early probe entries will occur within a few degrees of the evening terminator because minimum energy trajectories tend to direct entries to this region.

Transit Time - Interplanetary flight time from Earth injection to targeted (spacecraft with probe) periapsis passage. Local time is conventionally figured from this point in time:minus before passage, plus beyond.

FIGURE 6

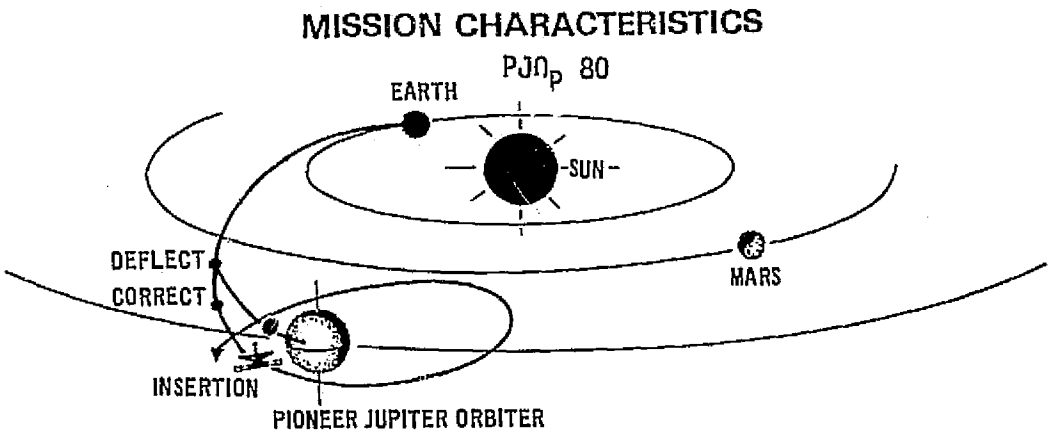

LAUNCH DATE:	6 DEC 80	PROBE ENTRY:	
ARRIVAL DATE:	14 FEB 83	ALTITUDE	450 km
SEPARATION MANEUVER:	500 R_J	PATH ANGLE	−7.5 deg
DEFLECTION ΔV	71.05 m/s	LATITUDE	4.71 deg (N)
TIME TO PROBE ENTRY	50 DAYS	VELOCITY	59.7646 km/s
CORRECTION MANEUVER	260 R_J	ANGLE OF ATTACK	16.63 deg
CORRECTION ΔV	5 m/s		
TIME TO PROBE ENTRY	23.4 DAYS		

FIGURE 7

In the cruise mode the Pioneer spacecraft is spin-stabilized along the Earth-line direction to retain communications lock with the Earth. During the probe separation and spacecraft deflection maneuvers, retention of Earth communication lock (spin-axis alignment along the Earth-line) can be retained or the spacecraft/probe can be precessed for optimum release attitude and/or optimum deflection maneuver direction application. Probe attitude and, thereby, entry angle of attack are established by the spacecraft orientation at separation. When Earth communications lock is retained, the spacecraft deflection maneuver must be implemented as two separate maneuvers; one applied along the spacecraft spin-axis and the other a pulsed maneuver applied normal to the spacecraft spin-axis. When Earth communications lock is broken (second option), a single deflection maneuver applied along the precessed spin-axis in the optimum direction is utilized. Both techniques provide acceptable entry conditions for the probe.

Orbiter Mission (PJO$_P$'80)

Another mission is described wherein the spacecraft is put into orbit immediately after the probe entry mission is completed. The entry angle,

latitude and inclination of the probe are virtually identical to that of PJ_p 79, so probe reactions are the same in both cases. The communications parameters differ so some treatment of both follows.

The spacecraft orbit is to be nearly coincident with the equatorial plane, so a nominal separation/deflection radius of 500 R_J, the spacecraft Jovian latitude is oriented to +0.02 degrees (North). Thus, probe injection is into a low angle inclination trajectory with the spacecraft inserted into a near-zero inclination orbit. This is achieved as part of the deflection maneuver implementation as seen from the equatorial plane depicted in Figure 8.

Following separation from the Pioneer spacecraft, the probe passively descends to a shallow angle entry into the Jovian atmosphere while the spacecraft is deflected for a near overfly of the probe and insertion into a low periapsis (taken at 1.8 R_J), low inclination (0.07 degree) Jovian orbit.

PROBE AND SPACECRAFT APPROACH TRAJECTORIES

PJO_p 80 MISSION

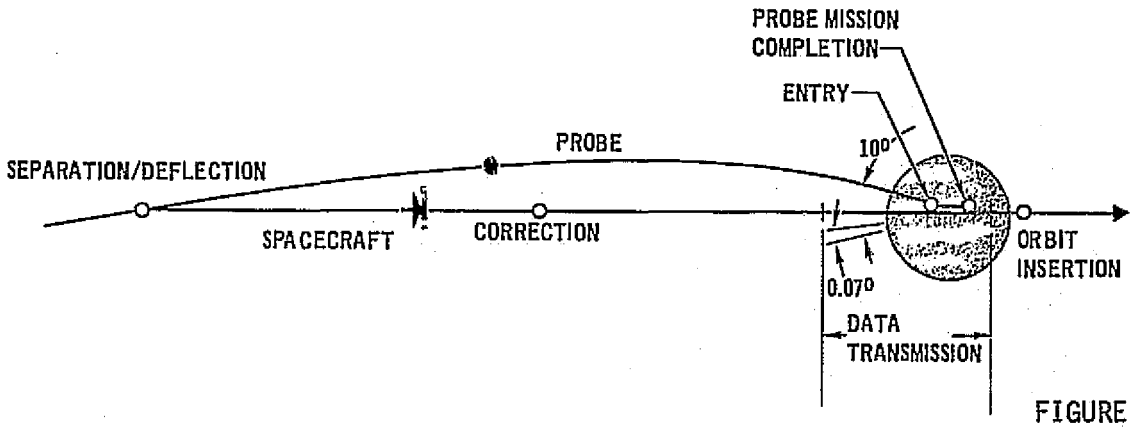

FIGURE 8

Spacecraft Phasing Time and Periapsis Radius

The variation of entry spacecraft and entry probe aspect angle with phasing time is presented in Figure 9 for three values of spacecraft periapsis radius; other values have been omitted for simplicity of presentation. Typical (in this instance, desired) limits are indicated by feathered lines. Limit angles for the probe and spacecraft are 33 degrees and 105 degrees, respectively, for a Pioneer-type spacecraft. In the case of the former, adequate probe com-

munications transmission is maintained when the probe aspect angle is held to values less than 33 degrees. Moderate excesses in probe aspect angle can be tolerated at entry but not later. On the other hand, the limit value of 105 degrees for the spacecraft aspect angle represents a hard constraint. When this angularity is reached, communications link between the spacecraft and probe is broken because of shadowing by the big dish (9 ft diameter) of the spacecraft. The preferred value for spacecraft aspect angle is approximately 65 degrees which is the center of the spacecraft beamwidth.

VARIATION OF ENTRY ASPECT ANGLES WITH SPACECRAFT PHASING & PERIAPSIS

PJ_P '79 FLYBY MISSION

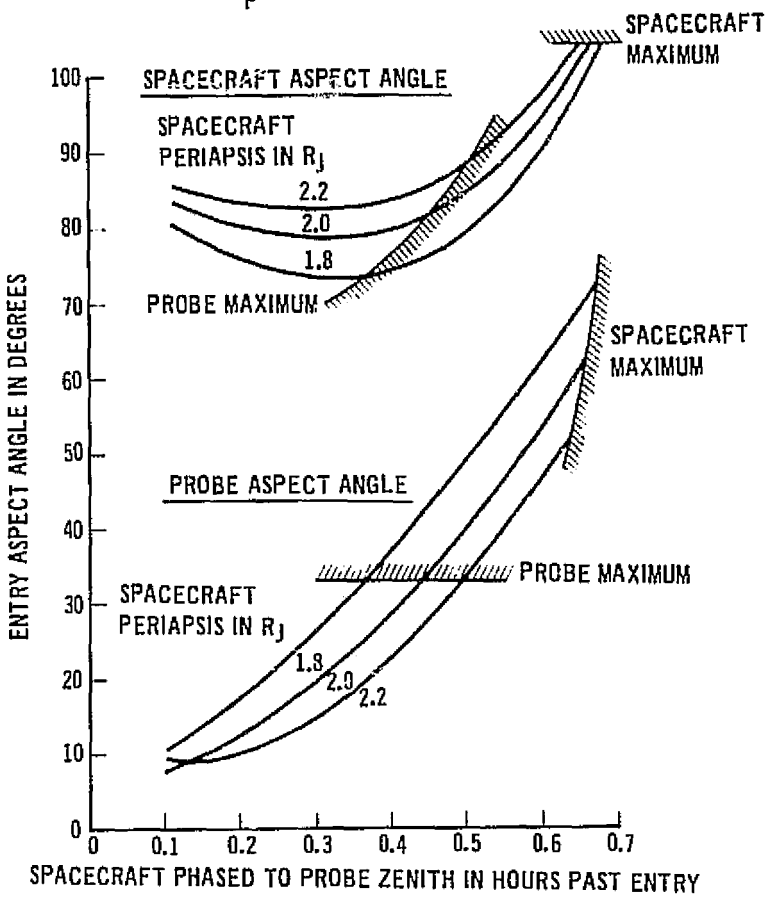

FIGURE 9

Aside from the inverse variational nature of the aspect angle with periapsis radius, inspection of Figure 10 shows that minimum values of spacecraft aspect angle occur in the vicinity of 0.3 hour phasing time. Acceptable values of probe aspect angle are also obtained in this time region. Clearly, the larger values of spacecraft phasing time (greater than 0.5 hour) are difficult to obtain even with the spacecraft orbit inclined to Jupiter's equator.

VARIATION OF ENTRY COMMUNICATION RANGE WITH SPACECRAFT PHASING AND PERIAPSIS

PJ_p'79 FLYBY MISSION

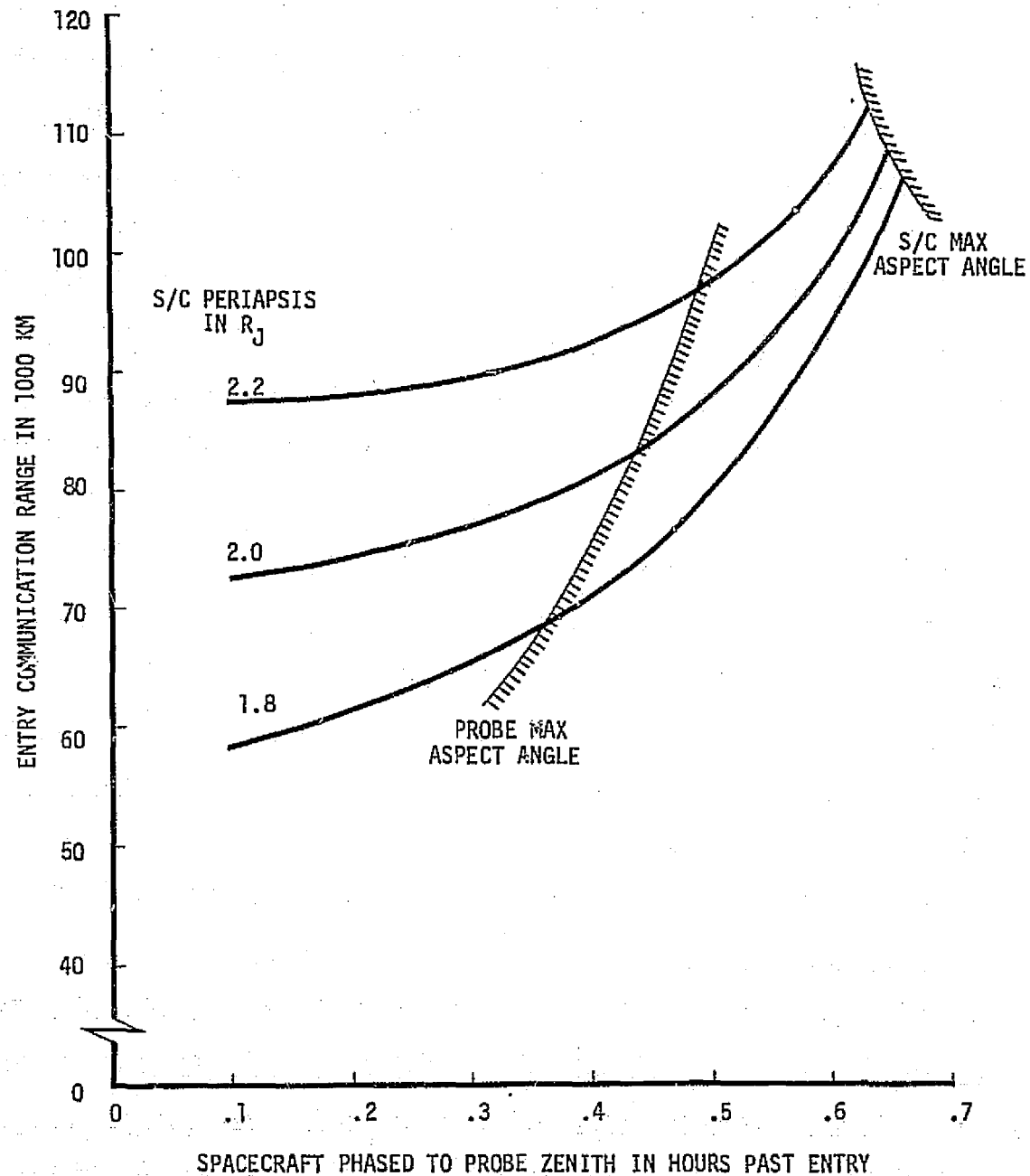

FIGURE 10

Corresponding communication angles at entry are presented in Figure 11. As expected, communication range increases rapidly with increasing phasing time as well as spacecraft periapsis radius. Except for increased deflection maneuver requirements, the study communication ranges are within acceptable bounds. Communications ranges up to the vicinity of 110,000 km (typical SUAEP value) present no major problem to communication system designers. The majority of results fall within this range limit. Also, communication range tends toward a minimum as the spacecraft approaches its specified phasing time.

The effect of post-entry geometrical change is demonstrated in Figure 11. Here curves of constant communication duration are superimposed on the parametric grid of entry aspect angle and spacecraft phasing time. Again, communications duration is taken as the time between probe entry and when the spacecraft reaches an aspect angle of 105 degrees. Note that probe aspect angle will decrease through zero as the phasing time is reached, but since spacecraft aspect angle reaches limit values near phasing times, post-entry probe aspect angle variations do not affect communication duration.

Communications durations of the order of 0.5 hour can be achieved by careful selection of phasing time and periapsis radius but not exceeded appreciably. When the requirement for maximum probe aspect angle is retained, a spacecraft periapsis radius greater than approximately 2.1 R_J is needed to obtain these durations. As will be shown later, adoption of such a radius happens to impose a severe penalty on deflection maneuver requirements.

The variation of communication duration with spacecraft phasing and periapsis radius is shown in Figure 12. Maximum achievable values are just slightly greater than 0.5 hour. These maxima are reached at phasing times in the vicinity of 0.5 hours. As phasing time is increased further, communication duration falls off very rapidly to zero (limit spacecraft aspect angle at entry). This characteristic is therefore classified as a hard constraint on trajectory trading. Unfortunately, maximum durations are achieved at the expense of excessive probe aspect angles or a large spacecraft periapsis radius.

ACHIEVABLE COMMUNICATION DURATIONS
PJ_P '79 FLYBY MISSION

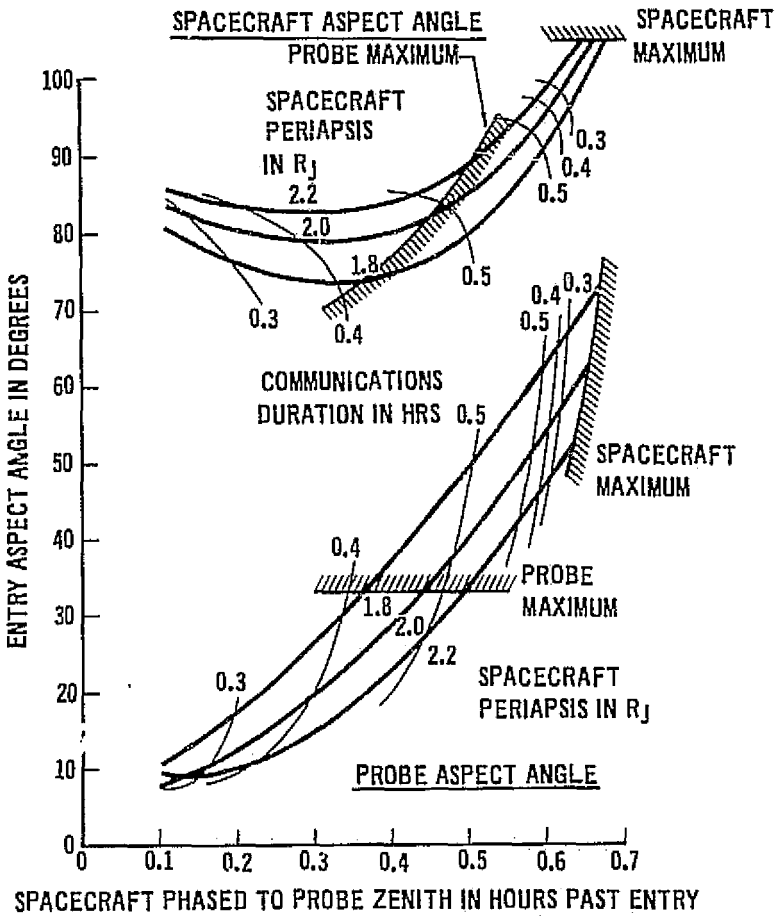

FIGURE 11

VARIATION OF COMMUNICATION DURATION WITH SPACECRAFT PHASING AND PERIAPSIS

PJ_P'79 FLYBY MISSION

CUTOFF AT MAXIMUM SPACECRAFT ASPECT ANGLE OF 105 DEG

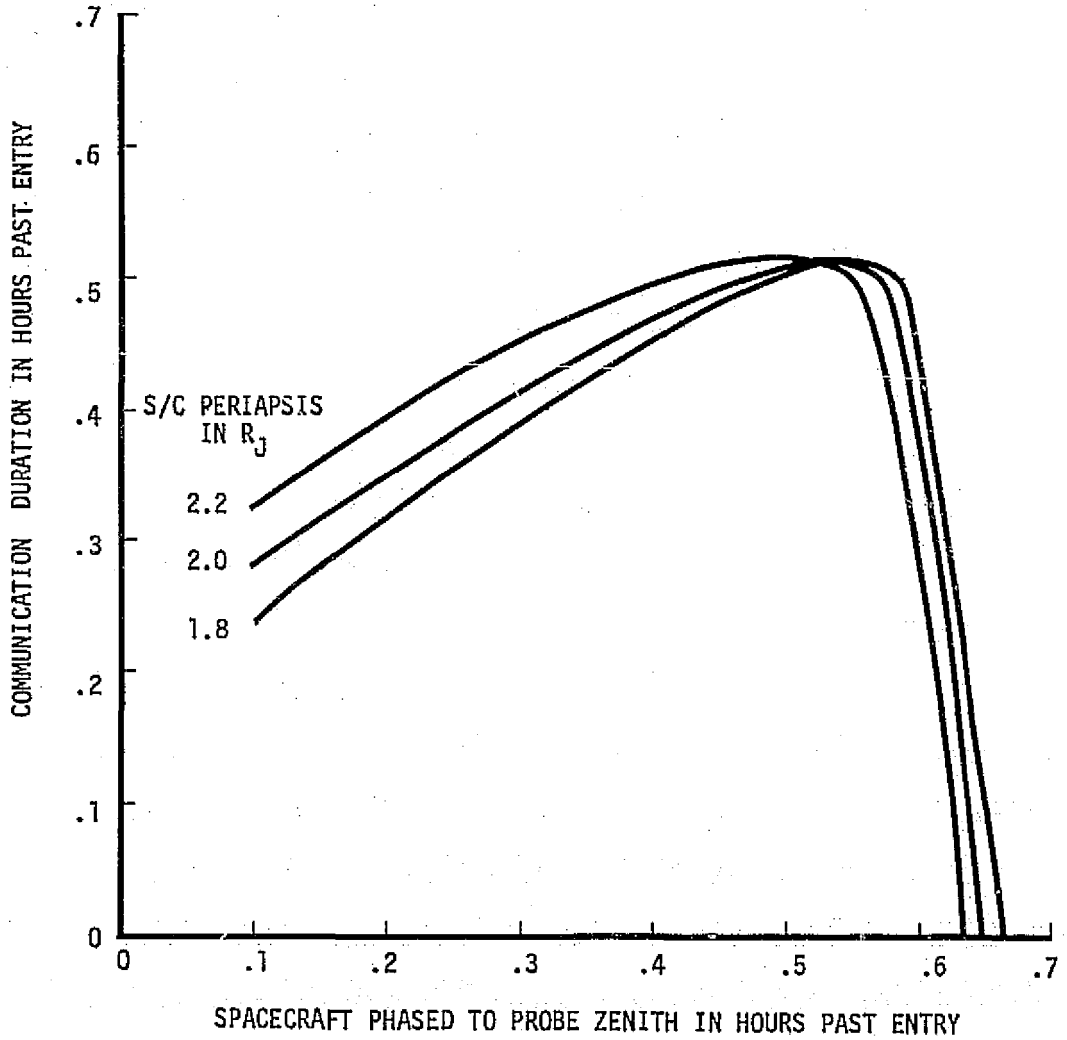

FIGURE 12

Impact of Deflection Maneuver Requirements

Results of the parametric study in spacecraft phasing time and spacecraft periapsis radius presented in the preceding discussion suggests selection of the largest possible spacecraft periapsis radius (r_p = 2.2 R_J) and a spacecraft phasing time of 0.5 hour past entry. This combination tends to maximize communication duration ($\geq$0.5 hour). Unfortunately, such a combination requires total deflection maneuver ΔV's greater than 112 m/sec (about 53 lb on a Pioneer-probe flight). In Figure 13 maneuver requirements were held to SUAEP values of less than 80 m/sec (or 36 lb). If these SUAEP values must be retained, the spacecraft periapsis radius must be no larger than 2.0 R_J with spacecraft phasing times of about 0.43 hour. Again, the spacecraft deflection maneuver is implemented as two separate maneuvers where one is applied axially along the Earth-line (i.e., along the spacecraft spin-axis) and the other is applied normal to the spin-axis in a pulsed manner. Herein, the two maneuvers (called total) are summed as an indicator of gross deflection maneuver requirements. Notice that the break in the total curves is attributed to a nulling effect on the Earth-line maneuver. It is important to recognize that positive values of the Earth-line component represents a thrust application along the spin-axis but away from the Earth indicating acceleration required; negative or Earth directed for the flyby PJ_P '79 mission considered (deceleration).

One way to alleviate the problem of excessive ΔV requirements is to perform the deflection maneuver farther from Jupiter (i.e., earlier) than the 500 R_J utilized. This effect is shown in Figure 14. The variation of deflection maneuver ΔV requirements with deflection radius is given for a spacecraft periapsis of 2.2 R_J and a phasing time of 0.5 hour. Some reduction in deflection ΔV is apparent, but with the sphere of influence at 674 R_J improvement prospects are limited. In addition, reduced accuracies could be expected with a greater deflection radius.

Parameter Influences on Communications Geometry

Several other mission and trajectory parameters can influence communication geometry. Of these, the variations in entry path angle, entry latitude,

DEFLECTION MANEUVER REQUIREMENTS

PJ_P '79 MISSION

DEFLECTION MANEUVER AT 500 R_J

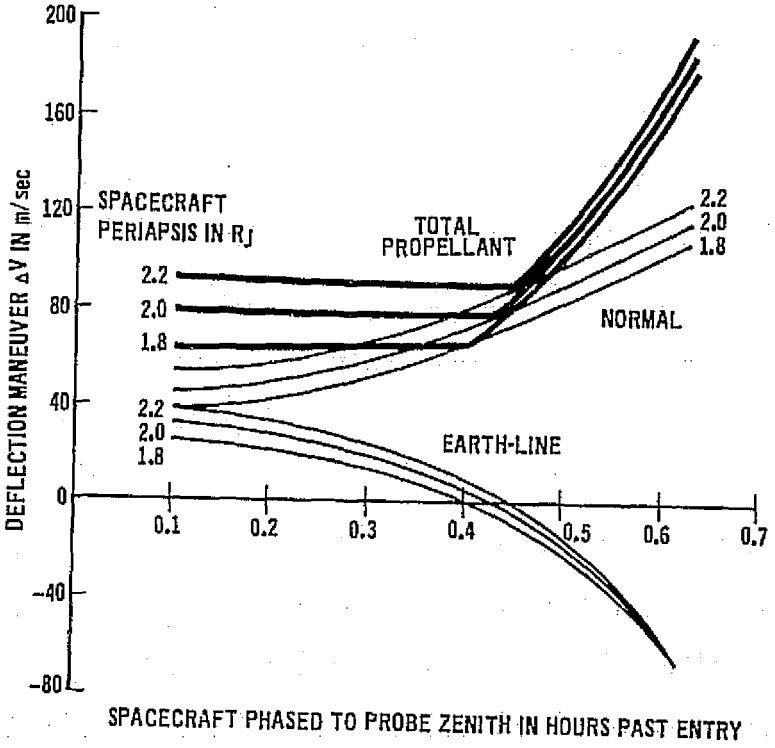

FIGURE 13

VARIATION OF DEFLECTION MANEUVER ΔV WITH DEFLECTION RADIUS

SPACECRAFT PERIAPSIS = 2.2 R_J
PHASING TIME = .5 HOURS PAST ENTRY
PJ_P '79 FLYBY MISSION

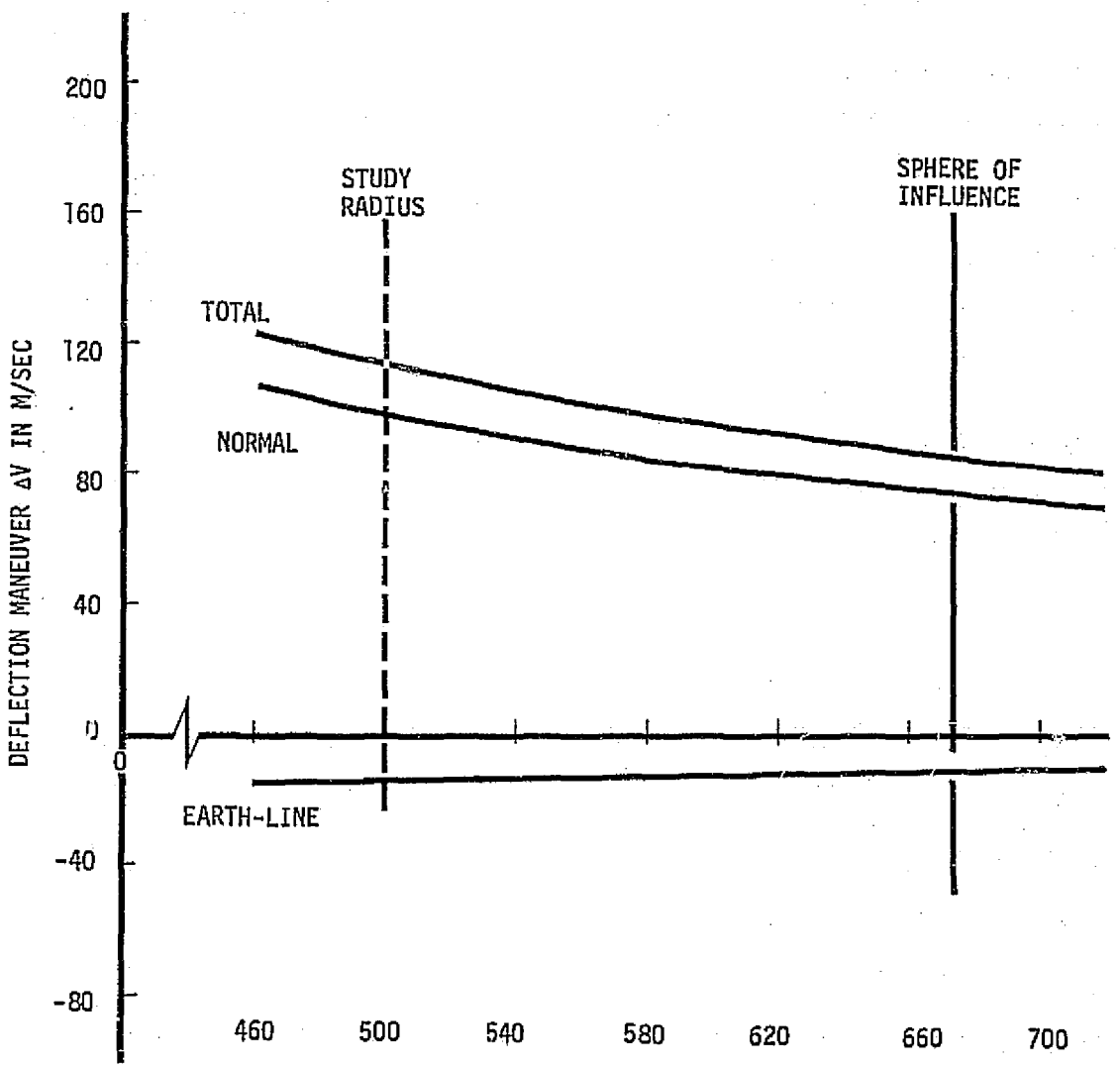

FIGURE 14

and interplanetary transit time have been checked for impact on communication geometry, especially communication duration. The relationships for entry from an orbiter mission are illustrated in Figure 15. The sequencing involves a detection and a correction maneuver to minimize entry dispersions.

The influence of entry path angle on communications geometry is shown in Figure 16. The variation of entry aspect angle and communication duration is shown as a function of entry (inertial) flight path angle for a typical spacecraft periapsis-phasing time combination. As entry path angle is increased (in negative direction), a very notable improvement in spacecraft and probe aspect angle (reduction) and communication duration (increase) occurs. In fact, if an entry path angle of -10 degrees or higher could be tolerated by the forward heat shield, a preferred spacecraft aspect angle (65 degrees), and probe aspect angle (less than 33 degrees) is achievable with communication durations approaching 0.5 hour with the illustrated periapsis-phasing combination. Duration improvement is 0.07 hour over a nominal value of 7.5 degrees. Further, the relatively low periapsis radius of 1.8 R_J for this example imposes rather low deflection maneuver requirements on the spacecraft as seen in Figure 13 for a flyby mission. (Note that they are comparable for orbiter missions.)

Probe entry latitude is also an influence on communication geometry. As seen in Figure 17, both spacecraft and probe aspect angles vary with entry latitude of the probe, but latitude has little effect on mission duration. Entry latitudes less than +1 degree will give desirable aspect angles. However, these lesser entry latitudes require lower trajectory inclinations for both spacecraft and probe (Figure 18), but the lower inclinations do increase the radiation hazard for both vehicles. The effect of latitude is illustrated for several latitudes north and south in Appendix I.

Since the baseline interplanetary transit time for this study was preset at 854 days, it is apparent from Figure 19 that little improvement in communication duration can be achieved by a variation in transit time. It is obvious that the selected value was chosen with maximum communication duration as a criterion by ARC personnel.

MISSION PROFILE FOR JUPITER PROBE

PJOP'80 ORBITER-PROBE MISSION

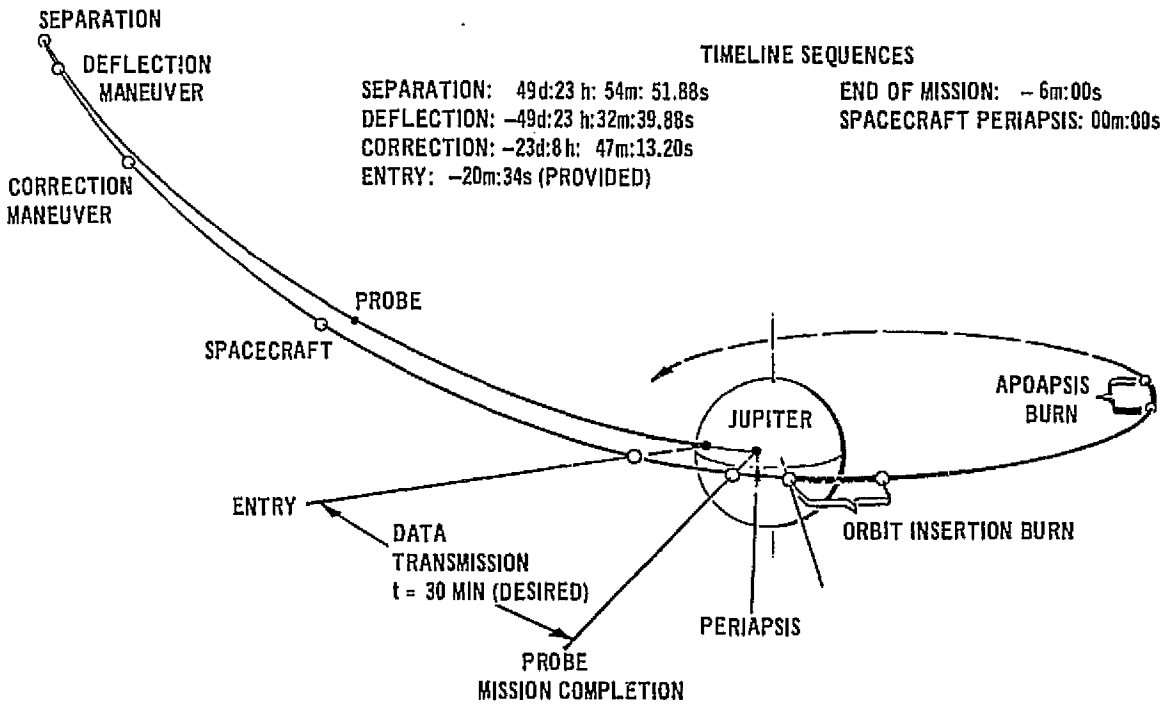

FIGURE 15

INFLUENCE OF ENTRY PATH ANGLE ON COMMUNICATIONS GEOMETRY

PJ_P'79 FLYBY MISSION

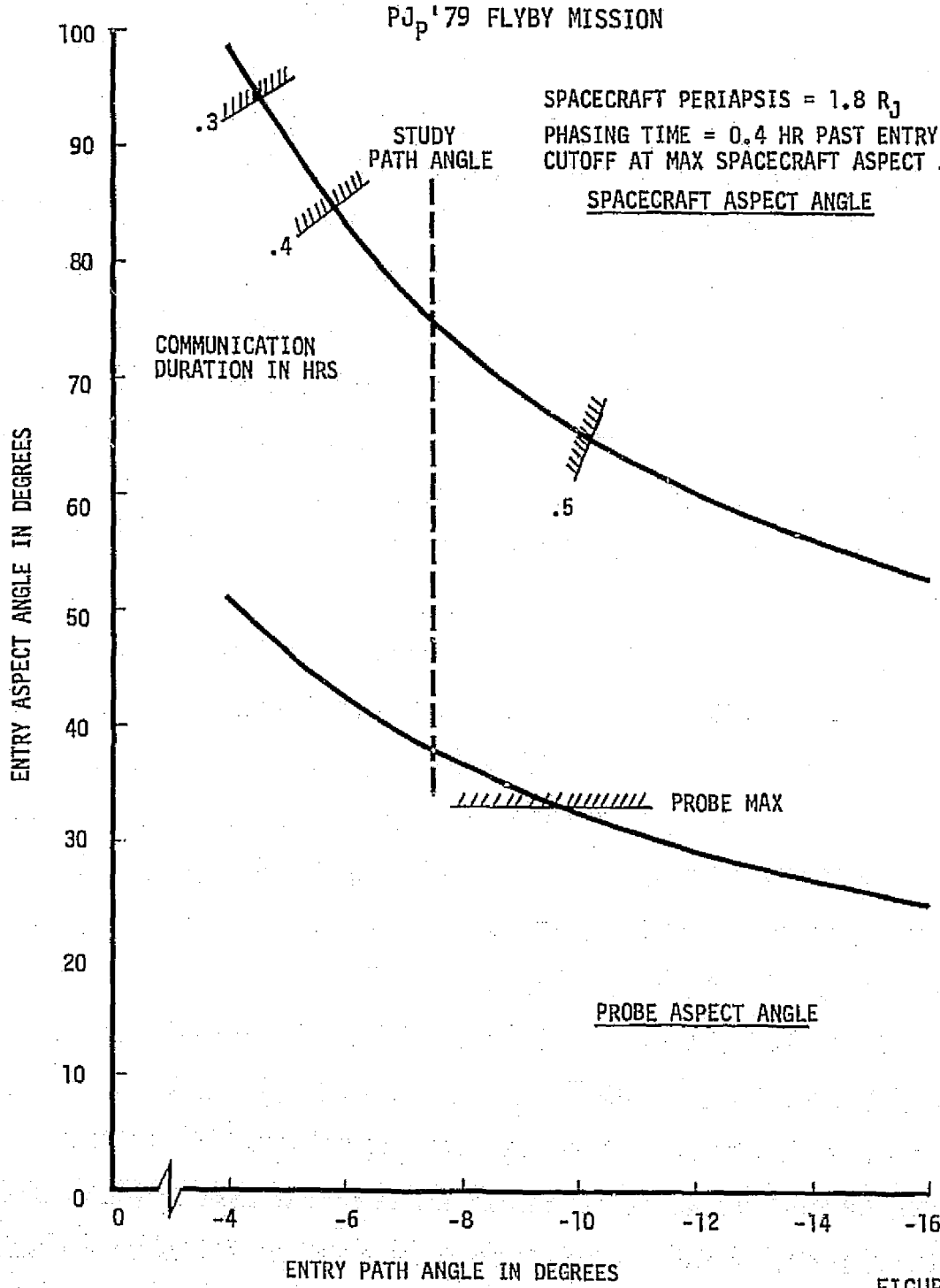

FIGURE 16

INFLUENCE OF ENTRY LATITUDE ON COMMUNICATION GEOMETRY

PJ_P '79 FLYBY MISSION

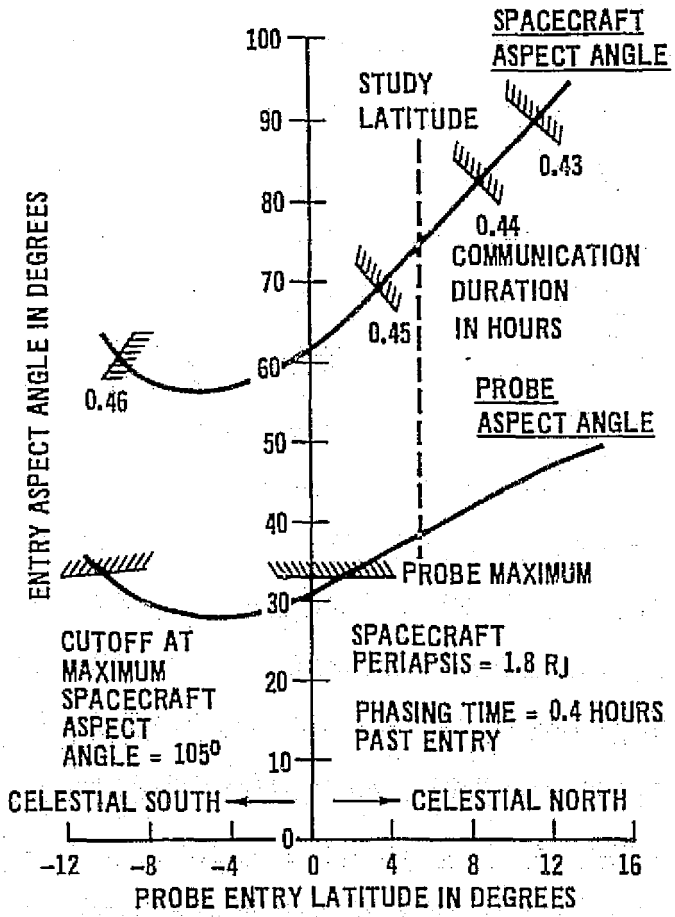

FIGURE 17

VARIATION OF TRAJECTORY INCLINATION WITH ENTRY LATITUDE
PJ_P '79 FLYBY MISSION

SPACECRAFT PERIAPSIS IS 1.8 R_J

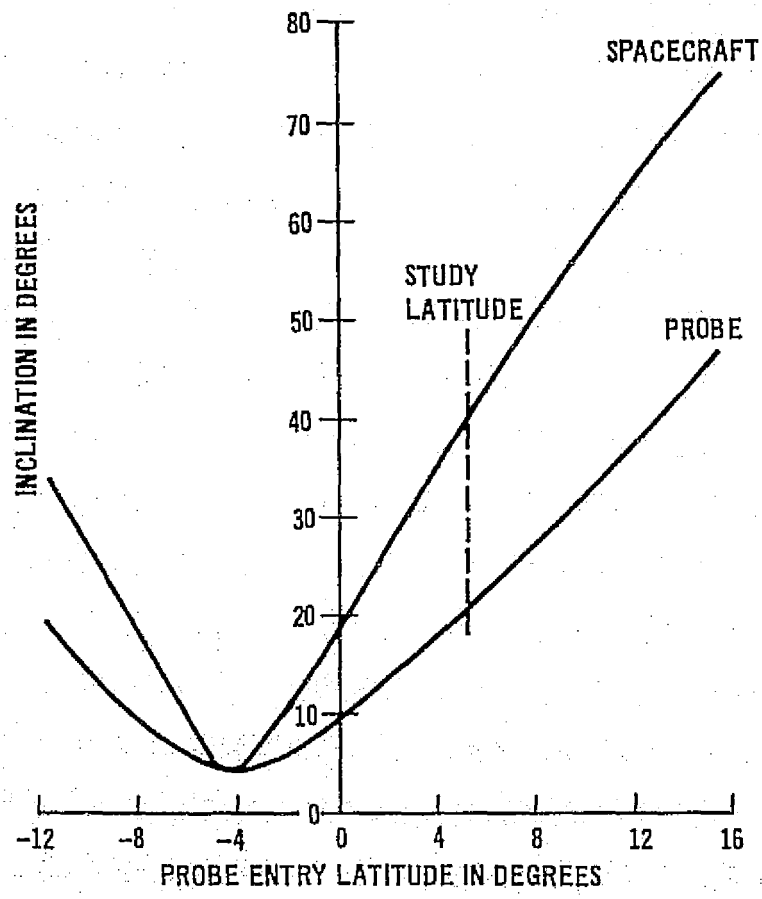

FIGURE 18

INFLUENCE OF TRANSIT TIME ON COMMUNICATION DURATION
PJ_P '79 FLYBY MISSION

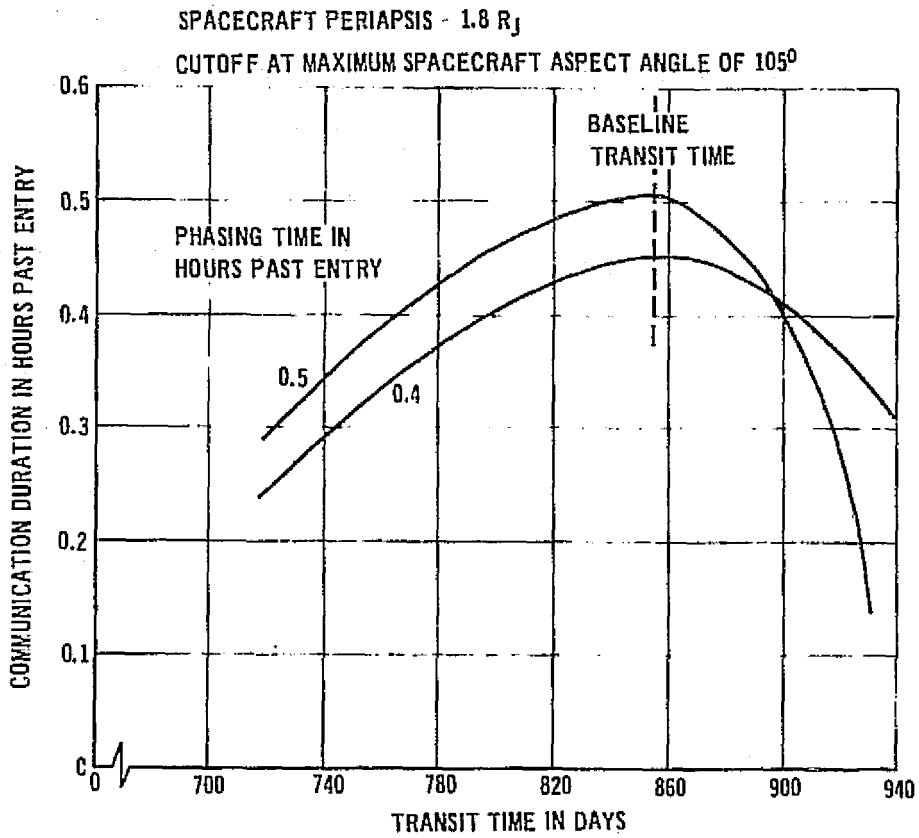

FIGURE 19

Separation Maneuvers (Pioneer/Mariner)

At roughly 500 R_J from Jupiter the probe is released and the spacecraft is retargeted for a phased overfly of the probe during the probe's data gathering descent into the Jovian atmosphere. Probe gathered data is transmitted to the spacecraft for relay to Earth. The following text discusses the probe as carried by a Pioneer spacecraft primarily. At points where significant variations occur, if the probe is carried by a Mariner, the nature of the variations is included for illustrative purposes. This study was not scoped to include a complete solution of both variants but noting the points of difference will aid any study of Mariner accommodations by this focusing of attention. Thus, spacecraft as used herein generally refers to Pioneers, but, where both are discussed in a paragraph, the generic label is inserted to distinguish between them. A typical separation to entry trajectory for a Jupiter flyby with probe mission is shown in Figure 20 but relationships are similar for orbiter missions.

DEFLECTION AND CORRECTION MANEUVERS

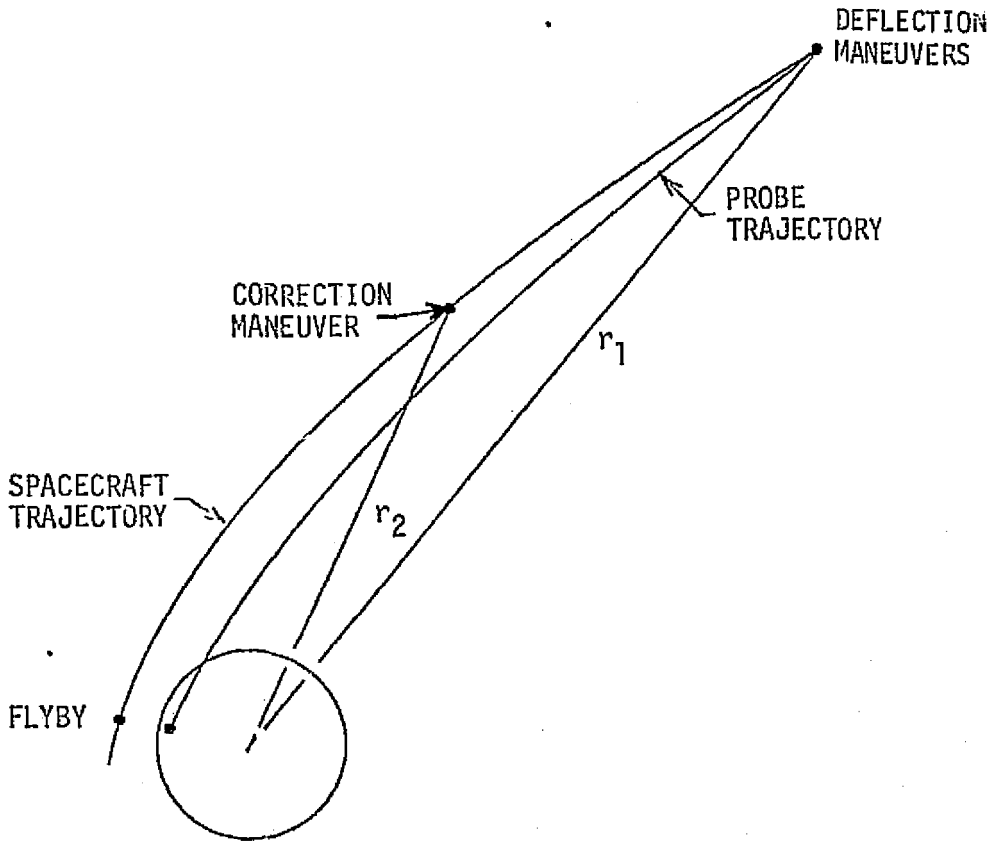

FIGURE 20

Spacecraft and probe attitudes throughout the planetary encounter phase are established by the requirement for spin-axis alignment along the Earth-line for the retention of Earth-lock by the Pioneer spacecraft. This requirement results in the implementation of the spacecraft deflection maneuver as two separate maneuvers - one is applied along the Earth-line (Pioneer spacecraft spin-axis) and the other is a pulsed maneuver applied normal to the spin-axis. The numerical sum of these two separate maneuvers is about 70 m/sec for this mission - applied at 500 R_J with a spacecraft periapsis of 1.8 R_J. The technique for a Mariner transported probe varies in two steps: (1) Earth-line orientation is broken prior to probe release with the spacecraft stepped about its three axes to place the probe into a zero angle of attack attitude at the apex of peak deceleration, and (2) the deflection maneuver need not be a pulsed normal component because of the three axis stabilization capability. To effect a $\gamma = 0$ at peak deceleration, the angle at 1000 km (or beginning of gravity turn phenomenon) the entry angle, γ, would be approximately -3 or -4 degrees. Note that a probe spin up is also required for Mariner bus carries.

Since errors accrued during the spacecraft deflection maneuver can result in intolerable dispersions in communications geometrical parameters (especially, spacecraft and probe aspect angles with values in the vicinity of $\pm$20 degrees, 3σ having been encountered), a spacecraft correction maneuver has been incorporated into the mission profile to bring these dispersions within manageable bounds. This correction maneuver has been rather arbitrarily applied at 260 R_J (24.6 days before probe entry). Such a mid-descent maneuver permits adequate time for post-deflection trajectory determination while retaining minimal ΔV requirements for correcting the spacecraft to the desired periapsis radius. It is of course recognized that the retention of Earth-lock is incumbent on this maneuver. Although rigorous study of this correction maneuver is still to be made, both the ΔV size of the maneuver (approximately 5 m/sec) and the resulting dispersions in communications parameters have been estimated. The maneuver(s) is considered to be beneficial whether Pioneer or Mariner borne.

Dispersions Following Deflection and Correction Maneuvers

The deflection and correction maneuvers are executed at a radius of r_1 ($\sim$500 R_J) and r_2 ($\sim$200 R_J) as illustrated in Figure 20. The method of estimating dispersions at flyby due to errors in the correction maneuver is given in

Figure 21. The rationale is that the deflection maneuver will be executed with zero error along the Earth-line (because of Earth tracking) but with a 6% error (3σ) in the component normal to the Earth line. Effects of ephemeris errors of the spacecraft and the planet are not changed by the deflection maneuver. Also, the correction maneuver is assumed to have the same error characteristics, or a 6% (3σ) error normal to the Earth line. Referring to Figure 21, it is assumed that flyby dispersions due to the deflection maneuver errors will be reduced to 6% of the values calculated. This improvement is dramatically illustrated in Figure 22.

ESTIMATE OF DISPERSIONS FOLLOWING A DEFLECTION AND A CORRECTION MANEUVER

DISPERSIONS FOLLOWING DEFLECTION MANEUVER:

$$\Delta S = \left[\Delta S_1^2{}_{\substack{\text{EPHEMERIS} \\ \text{ERRORS}}} + \Delta S_2^2{}_{\substack{\Delta V \text{ MANEUVER} \\ \text{ERRORS}}} \right]^{1/2}$$

DISPERSIONS FOLLOWING DEFLECTION/CORRECTION MANEUVER:

$$\Delta S = \left[\Delta S_1^2{}_{\substack{\text{EPHEMERIS} \\ \text{ERRORS}}} + (.06)^2 \, \Delta S_2^2{}_{\substack{\Delta V \text{ MANEUVER} \\ \text{ERRORS}}} \right]^{1/2}$$

RATIONALE:

a) Error (3σ) in executing deflection maneuver is 6%

b) Residual error following correction maneuver is 6% of deflection maneuver error.

c) Ephemeris errors unaffected by correction maneuver.

FIGURE 21

Accurate assessment of the flyby dispersions following the correction maneuver(s) requires a new analysis tool to calculate the dispersions by a Monte Carlo or other probabilistic technique. Monte Carlo means that a random variable (flyby position) is generated by repeated simulations of a random

DOPPLER AND DOPPLER RATE HISTORIES
PJ_P 80 ORBITER-PROBE MISSION

RELEASE RADIUS = 260 R_J PERIAPSIS RADIUS = 1.8 R_J PHASING TIME = 0.4 HR

——— 3 σ DISPERSIONS, NO CORRECTION MANEUVER

— — — 3 σ DISPERSIONS, CORRECTION MANEUVER 24.6 DAYS BEFORE PROBE ENTRY

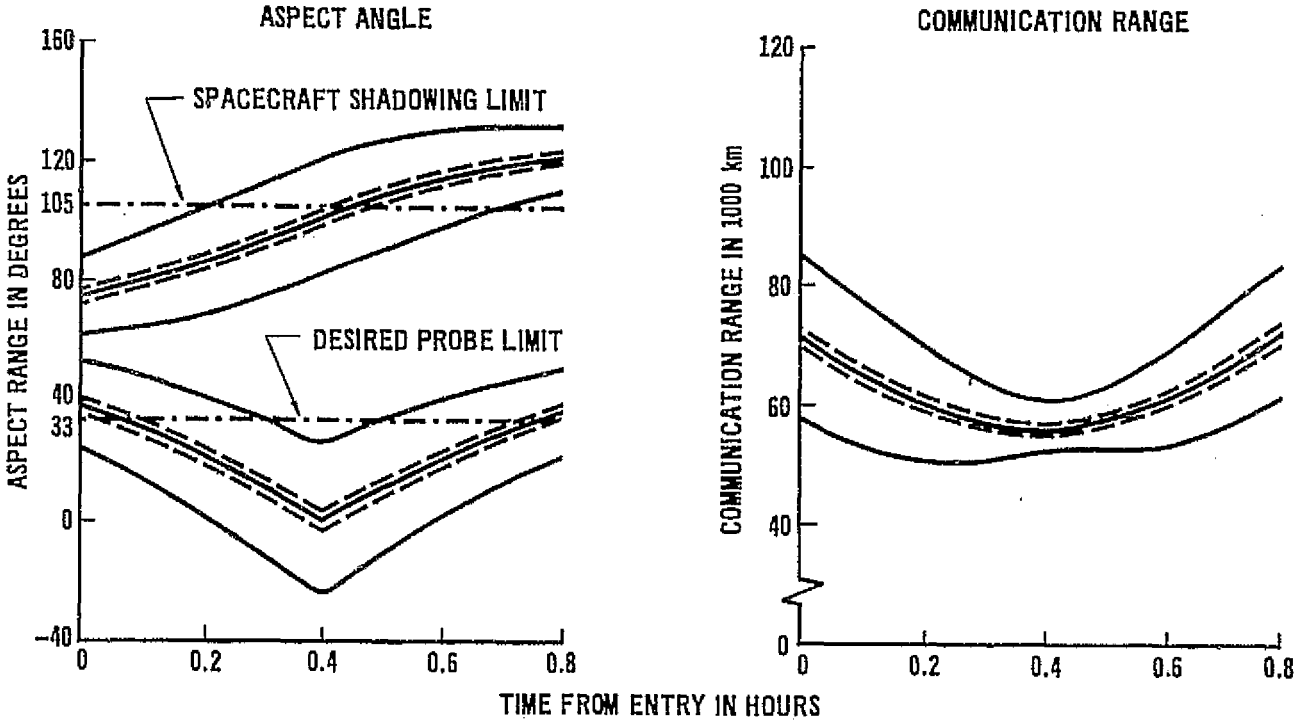

ENTRY DISPERSIONS (3 σ)

γ_E = $-7.5^0 \pm 0.536^0$ $LONG_E$ = $1.51^0 \pm 0.987^0$ REFERENCE TO SUB-EARTH AT 0^0 LATITUDE

α_T = $29.06^0 \pm 0.006^0$ V_E = $59.7 \pm 1.43^{/-6}$ km/sec

LAT_E = $4.8^0 \pm 0.366^0$ t_E = 43 d 4h 46 m 49.0895 ± 74.35 s

FIGURE 22

process and the standard deviations calculated based on actual occurrences. This analytical approach is required because the flyby dispersions are a function of the product of two random variables. The computer program used describes dispersions by a linearized covariance technique which is applicable because the dispersions following the deflection maneuver are linear combinations of random variables and constants, not products of random variables. For example, the Jet Propulsion Laboratory estimates the second and subsequent mid-course correction maneuvers by Monte Carlo techniques since dispersions after the second maneuver are functions of random errors in the second maneuver which, in turn, are a function of random errors in the first maneuver. The same is true for any maneuvers that follow the second one.

To illustrate the calculation of the correction maneuver and flyby dispersions, consider the flyby dispersions following deflection assuming no correction maneuvers;

$$\Delta P = F_1 \quad \bar{\varepsilon}_{\Delta V_1} \text{ (error vector)}$$

$$Sp = F_1 \quad S_{\varepsilon \Delta V_1} \; F_1^{T} \text{ (covariance)},$$

where the overline $(-)$ denotes a random variable.

The required correction velocity change is:

$$\Delta V_2 = (F_2^{-1})(F_1)(\bar{\varepsilon}_{\Delta V_1}) \quad (\Delta V_2 \text{ vector})$$

$$S\Delta_{V_2} = (F_2^{-1})(F_1)(S_{\varepsilon \Delta V_1})(F_1^{T})(F_2^{-1^{T}})(\Delta V_2 \text{ covariance}).$$

Now, the error in ΔV_2 is a random function of ΔV_2,

$$\varepsilon_{\Delta V_2} = \overline{K \Delta V_2} = \bar{K}(F_2^{-1})(F_1 \; \overline{\varepsilon_{\Delta V_1}}).$$

Flyby position error following ΔV_2 is

$$\Delta P = F_2 \bar{K} \; F_2^{-1} \; F_1 \quad \overline{\varepsilon_{\Delta V_1}}.$$

The covariance of ΔV_2 can be estimated by linearized covariance techniques since it is a function of constants $(F_2^{-1} F_1)$ and a Gaussian random variable $\overline{\varepsilon_{\Delta V_1}}$. However, flyby dispersions after the correction maneuver are functions of the product of two random variables $\bar{K}$ and $\overline{\varepsilon_{\Delta V_1}}$ and can only be estimated (practically) by a Monte Carlo analysis.

Communications Geometry

Flybys of Jupiter by Pioneer 10/11 have proven two important points. First, that hardened electronics can survive the Jovian radiation belt. Second, that interplanetary guidance is accurate enough to assure shallow entry angles. It is the latter point which is of paramount interest here, although without the former, the entry question would hardly have arisen.

Given that the interplanetary guidance is sufficiently accurate to allow shallow (cool) entries into Jupiter, rather than steep (hot) entries, the overriding thermal protection problem abates significantly. Hence, other questions of mission feasibility can be explored; namely, communications.

The study begins with the interplanetary trajectory previously discussed. This defines the arrival date (angle to the Earth from the hyperbolic asymptote) and hyperbolic excess velocity. From this, the deorbit conditions can be applied to the probe, and subsequent hyperbolic orbit corrections applied to the spacecraft.

The communications studies fall into two categories: the early studies of varying the communication system characteristics while leaving the spacecraft trajectory fixed (periapsis at 2 radii), and the later studies leaving the communication system characteristics essentially fixed and varying the post-separation spacecraft trajectories. The first or parametric studies are documented in the following subsection titled, "Spacecraft Relationships"; the later, more tailored studies are documented in the subsection titled, "Orbit Variations" starting on page 56.

Spacecraft Relationships

The spacecraft is aimed at the entry point of the planet up until probe release. As the probe descends, the spacecraft is deflected to a predetermined periapsis passage altitude. By adjusting the spacecraft deflection velocities, different geometries, that affect communications range and aspect angles can be achieved. Physically, slowing the spacecraft parallel to outbound asymptote (phasing) results in changed range and angles. Actual design of the link is preceded by an examination of these parameters as given in a previous section. The process provides a preliminary estimate of link capability. The relationships are given in Figure 23.

COMMUNICATIONS GEOMETRY

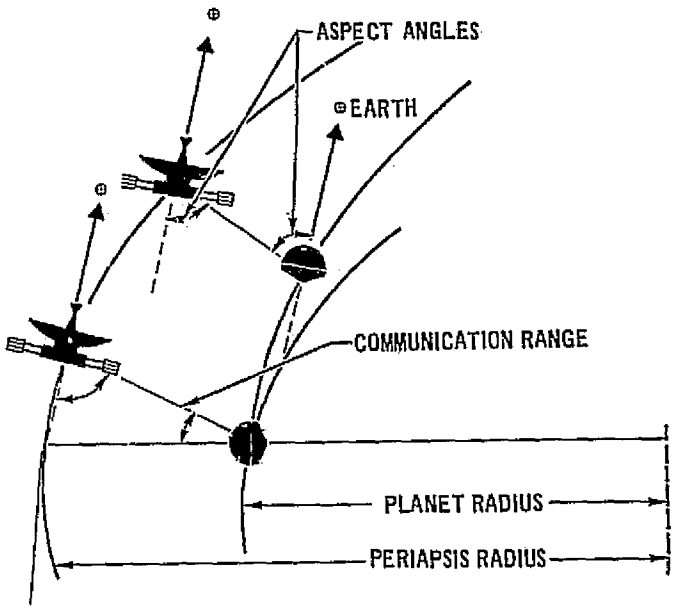

FIGURE 23

Initial investigation of the link for Jovian entry indicated that for an entry angle, γ = -10 and -7.5 degrees a link was feasible under best conditions though inadequate under the worst and some of the nominal descent conditions. The analysis was expanded to consider design variations in mission profile, probe parameters, and spacecraft equipment in a Jupiter flyby (PJ_p'79) environment.

Refined Link

From the analysis of the interplanetary trajectory, histories are calculated of the antenna look angles and communication range; typical outputs are shown in "Probe Description". The next step is to employ this geometric data together with the electrical characteristics of the link to establish the relative link performance, herein called link margin. For this study the latter step has been automated.

The communication geometry history data used in the following paragraphs describing approaches is derived from Figures 10-12 and 16-19. In summary, the communication range for a 0.4 hr phasing is 72,000 km, the spacecraft aspect angle, defined pictorially in Figure 23, is 73 deg and the probe aspect angle is 28 deg at entry. These parameters all change in value until communication termination at the time that spacecraft shadowing occurs. Physically, the receiving antenna for probe data is cut-off by the shadow cast

by the 9 ft diameter S-band antenna effectively at an aspect angle of 105 deg. This occurs in the 3σ dispersion case (with a correction of spacecraft positioning and orientation) at just over 0.4 hr after entry. At that time the probe aspect angle is down to 0 deg $\pm$ 3σuncertainties and range is down to 58,000 km. Hence, probe aspect angle and range improve as the spacecraft overtakes the probes radial position, but, as the spacecraft passes the probe's zenith (assuming identical planetary tracks), the spacecraft tends to cut-off communication by self-shadowing the receiver antenna.

Seven approaches to communications were studied:

Approach 1 - The initial investigation centered on varying the communications parameters and holding the trajectory fixed. The first approach is then to directly try Saturn/Uranus link parameters on the Jovian trajectory. Briefly, this link is a 400 megahertz, 40 watt, 44 bit per second transmission over a microstrip antenna which has a 66 degree beamwidth and is centered along the probe's roll axis to a loop vee antenna which has a 50 degree beamwidth and is axially symmetric with the peak gain 65 degrees off the roll axis. Figures 24 and 25 show the link margins for two entry angles for the Saturn/Uranus link parameters. The data for these, and succeeding probe variations is documented in Appendix II. The 10 degree entry provides slightly better communications performance than a 7.5 degree entry, however, the latter has lower heat protection requirements so it was selected as the baseline entry condition. Note that for a nominal exoatmospheric trajectory, the margin in a 7.5 degree entry trajectory never exceeds the sum of the adverse tolerances which is completely unacceptable.

Approach 2 - Some improvement in performance seemed to lie in increasing the carrier frequency since background noise (both cosmic and synchrotron) decreases with increasing frequency. The increased noise is one of the major differences between the Jupiter mission and the Saturn/Uranus missions. Figures 26 shows these noise effects, Figure 27 shows the atmospheric and ionospheric absorption, and Figure 28 illustrates the margin. It is seen that even though the environment becomes less severe with increasing frequency, the margin is still lower with increasing frequency. This lowering is caused by the increased free space loss with

fixed beamwidths which more than offsets the gain in noise reduction. Just increasing the frequency does not of itself improve performance.

COMMUNICATIONS SYSTEM MARGIN FOR
A -10 DEGREE ENTRY

- o SUAEP UNMODIFIED LINK
- o PJ_p '79 FLYBY MISSION
- o APPROACH 1

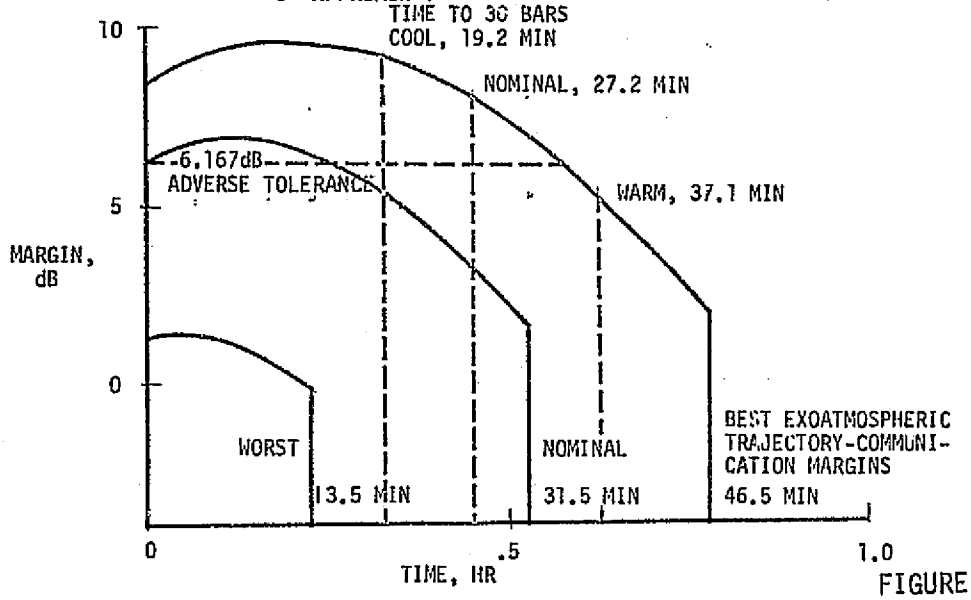

FIGURE 24

COMMUNICATIONS MARGIN HISTORY FOR
A -7.5 DEGREE ENTRY

- o SUAEP LINK (UNMODIFIED)
- o PJ_p '79 FLYBY MISSION
- o APPROACH 1

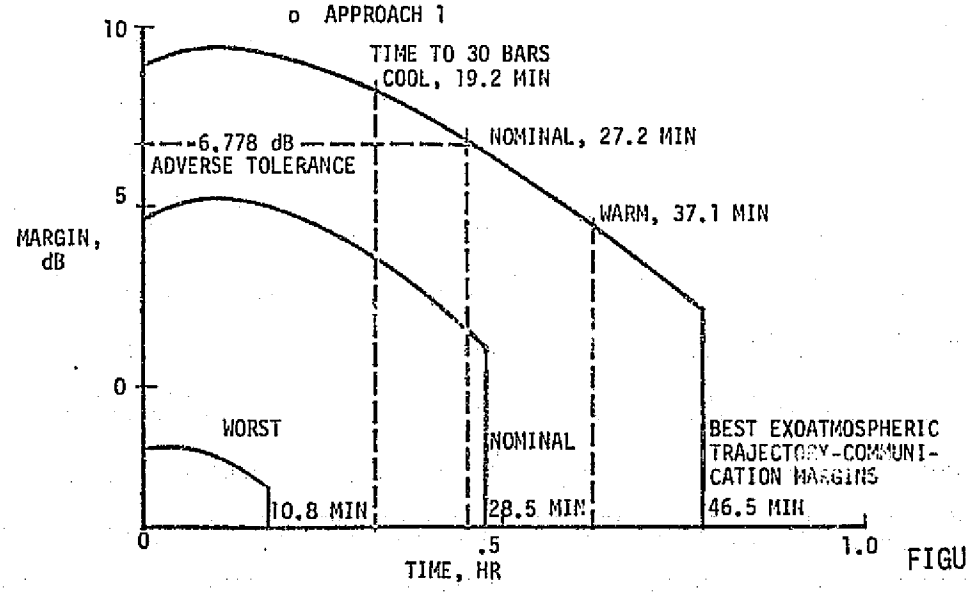

FIGURE 25

NOISE TEMPERATURE

o APPROACH 2

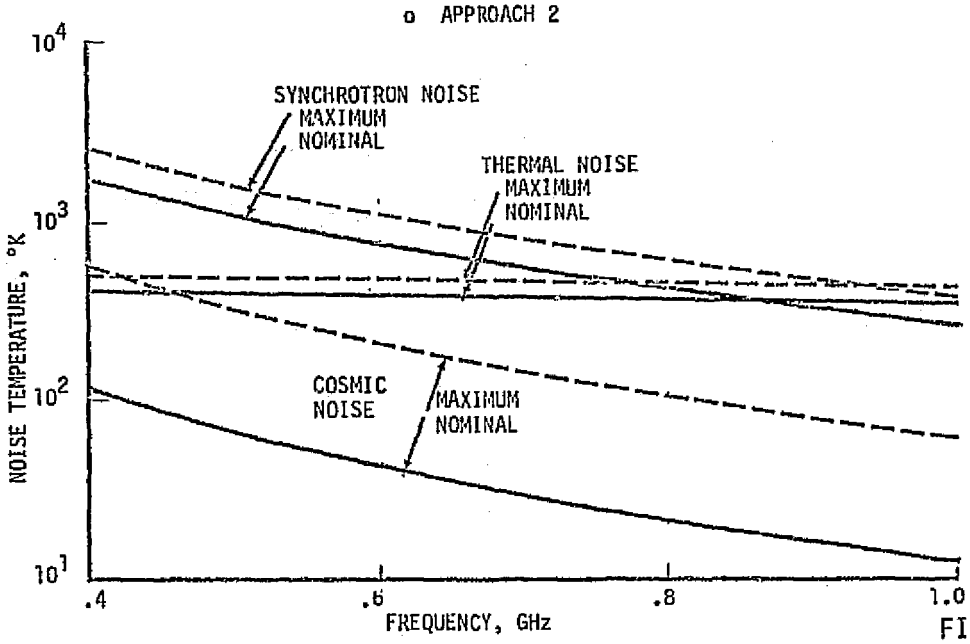

FIGURE 26

ATMOSPHERIC EFFECTS ON LOSSES

o APPROACH 2

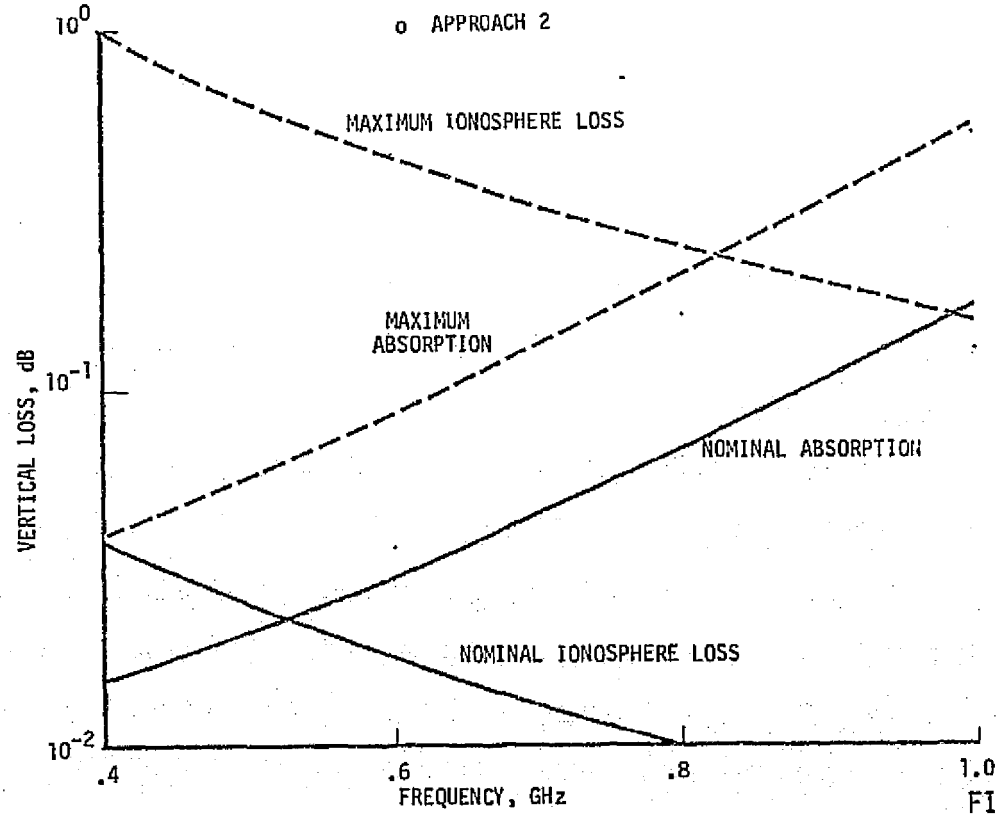

FIGURE 27

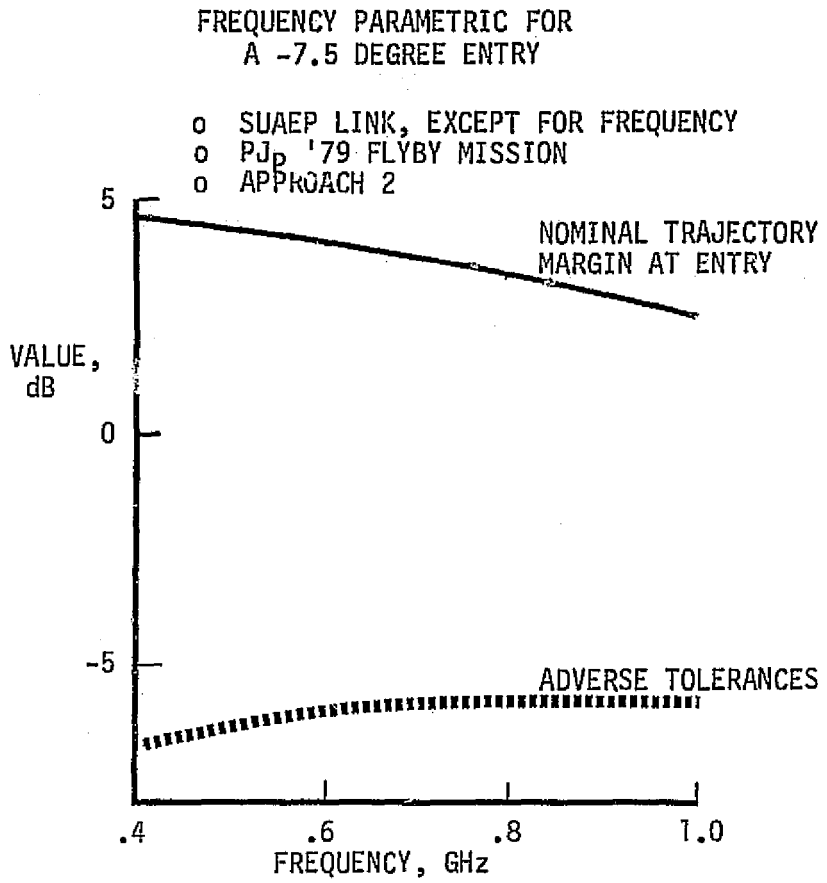

FIGURE 28

Approach 3 - The next approach is to "improve the probe" as much as feasible. That is, one could increase the transmitter to the limit-of-the art, 50 or 60 watts. Margin can also be gained by reducing the data rate. Figure 29 shows two possible ways to decrease the rate to 21 bits per second. One way is to simply cut the neutral mass spectrometer rate in half (taking either less samples or eliminating one of the two read-outs) and interleaves the memory dump 1:2 with the real-time. The other way cuts the neutral mass spectrometer to 1 bit per second (inferring data processing) and interleaves the memory dump 2:1. Although neither approach may be satisfactory as a final solution from the data handling viewpoint, the former has the advantage of minimal impact on the neutral mass spectrometer, and the latter has the advantage of the quicker dump of the memory. The total impact of memory dump time will be considered when varying the spacecraft trajectory. Herein, only the rate is of concern.

Questions of memory dumping rate and neutral mass spectrometer data processing depend upon the science strategy selected by the NASA.

Figure 30 shows the margin history for this link configuration. The margin for a nominal trajectory is above the adverse tolerance for nearly 0.4 hour. Except for worst case dispersions, this could be acceptable.

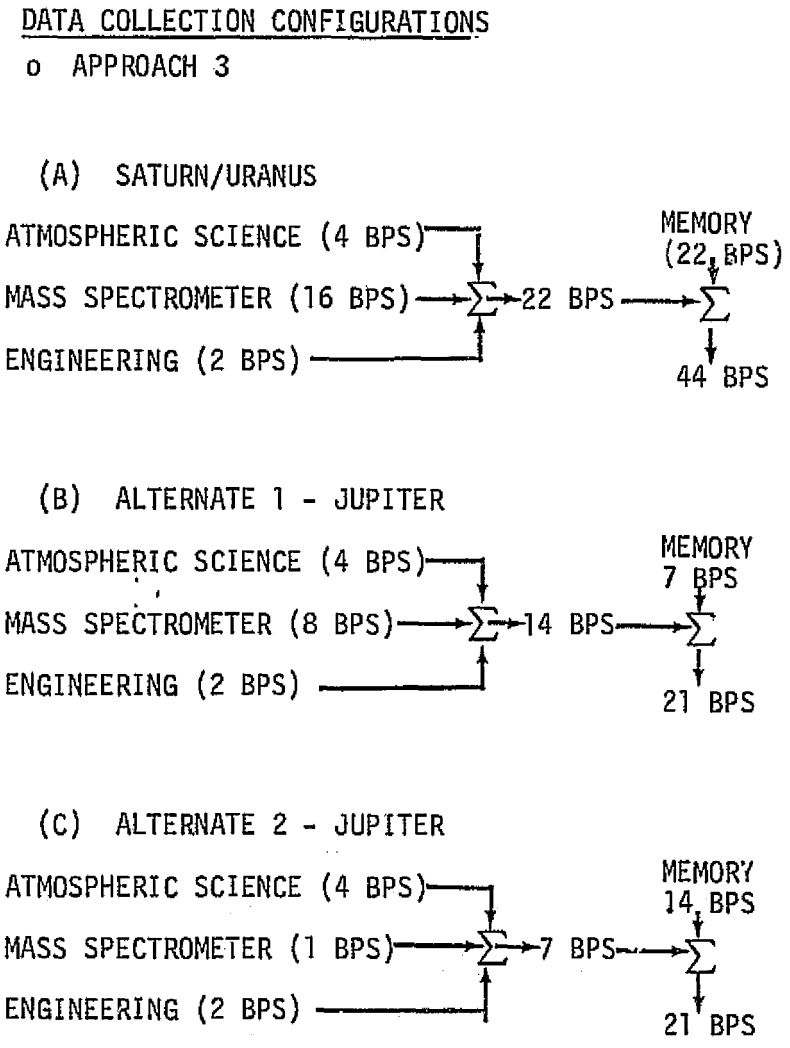

FIGURE 29

COMMUNICATIONS MARGIN HISTORY FOR
A -7.5 DEGREE ENTRY

- o SUAEP LINK, EXCEPT FOR 50 WATTS 21 BPS
- o PJ_P '74 FLYBY MISSION
- o APPROACH 3

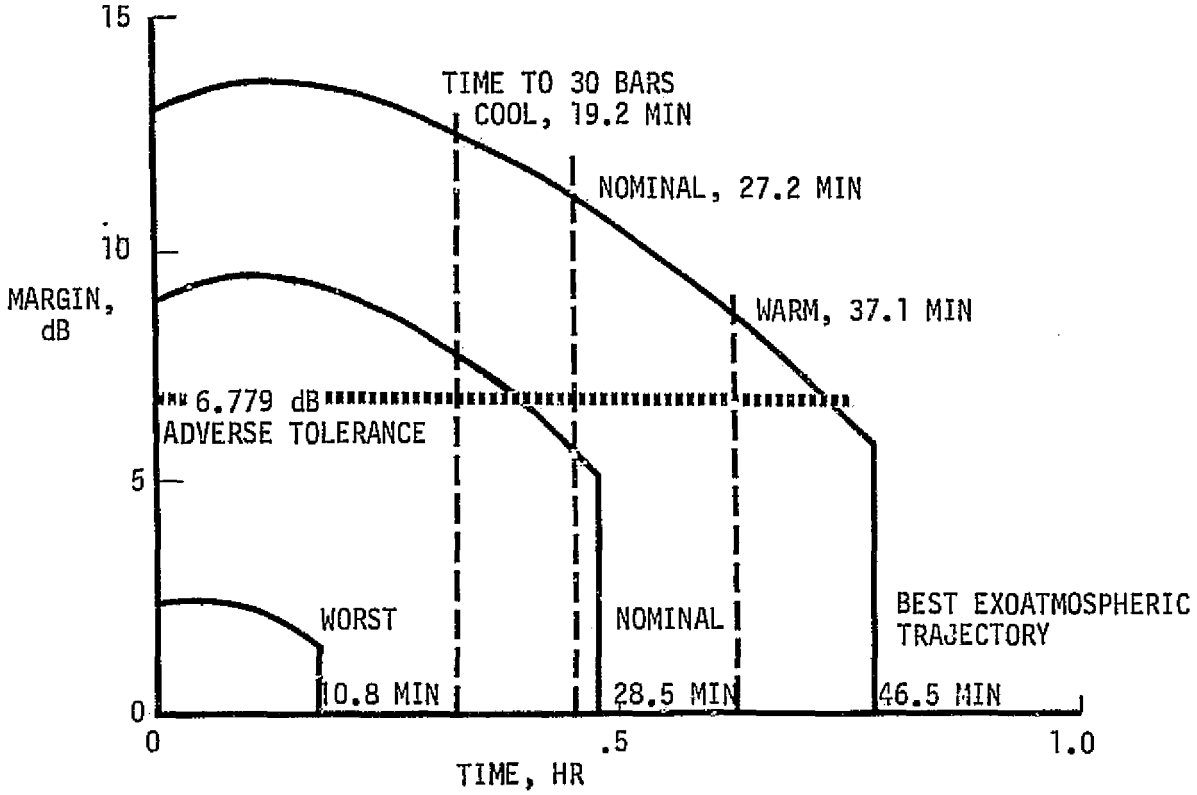

FIGURE 30

Approach 4 - The fourth approach is not so much a full variation as simply answering the question of how a 50 watt, 21 bit per second system performs as a function of frequency. Figure 31 shows the same trend as approach 2.

Approach 5 - As seen from the preceding margin histories, all of the links terminate fairly early and very abruptly. This shutdown is caused by the assumption of zero receiving gain at angles where it is shadowed by the 9 foot diameter dish of the spacecraft. An obvious option then is to add an additional antenna on the side of the spacecraft which faces the

Earth. To maintain gain, of course, this antenna is electrically separate from the rear or outbound antenna, with a separate receiver, and a decision device between the two antennae/receivers to select the output with the "best" (greatest automatic-gain-control) signal. Figure 32 illustrates the margin history. As seen, the nominal trajectory has nearly one hour above the adverse tolerances of the link table. If a deep penetration is required, then the second receiving subsystem is needed to obtain full receipt of the data.

FREQUENCY PARAMETRIC FOR
A -7.5 DEGREE ENTRY

- SUAEP LINK, EXCEPT FOR 50 WATTS
  21 BPS AND FREQUENCY CHANGE
- APPROACH 4

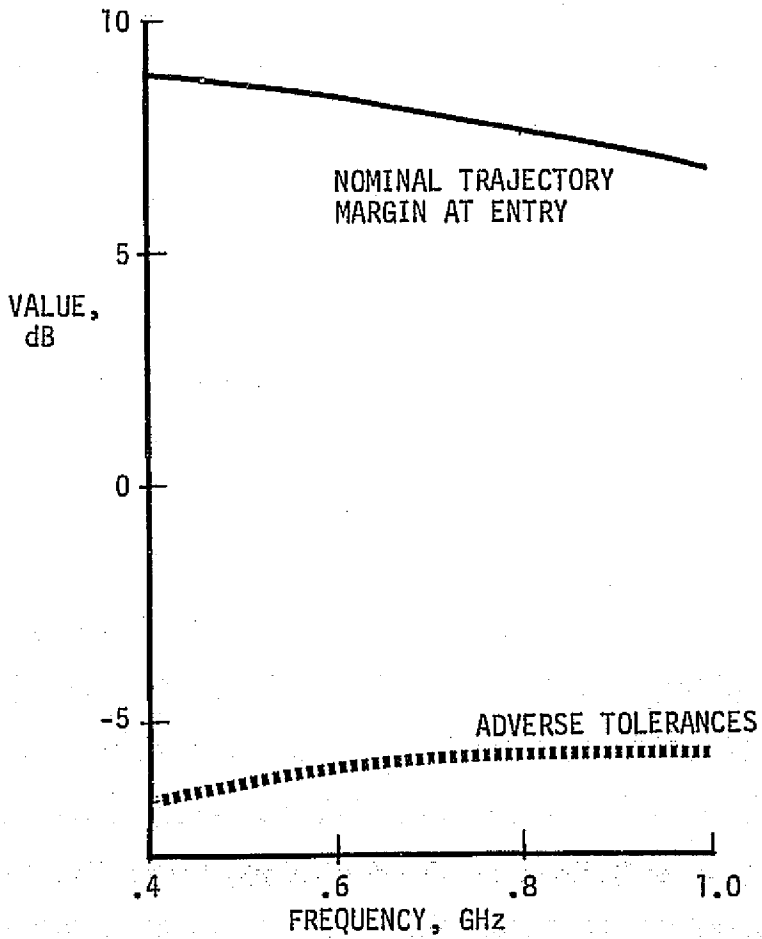

FIGURE 31

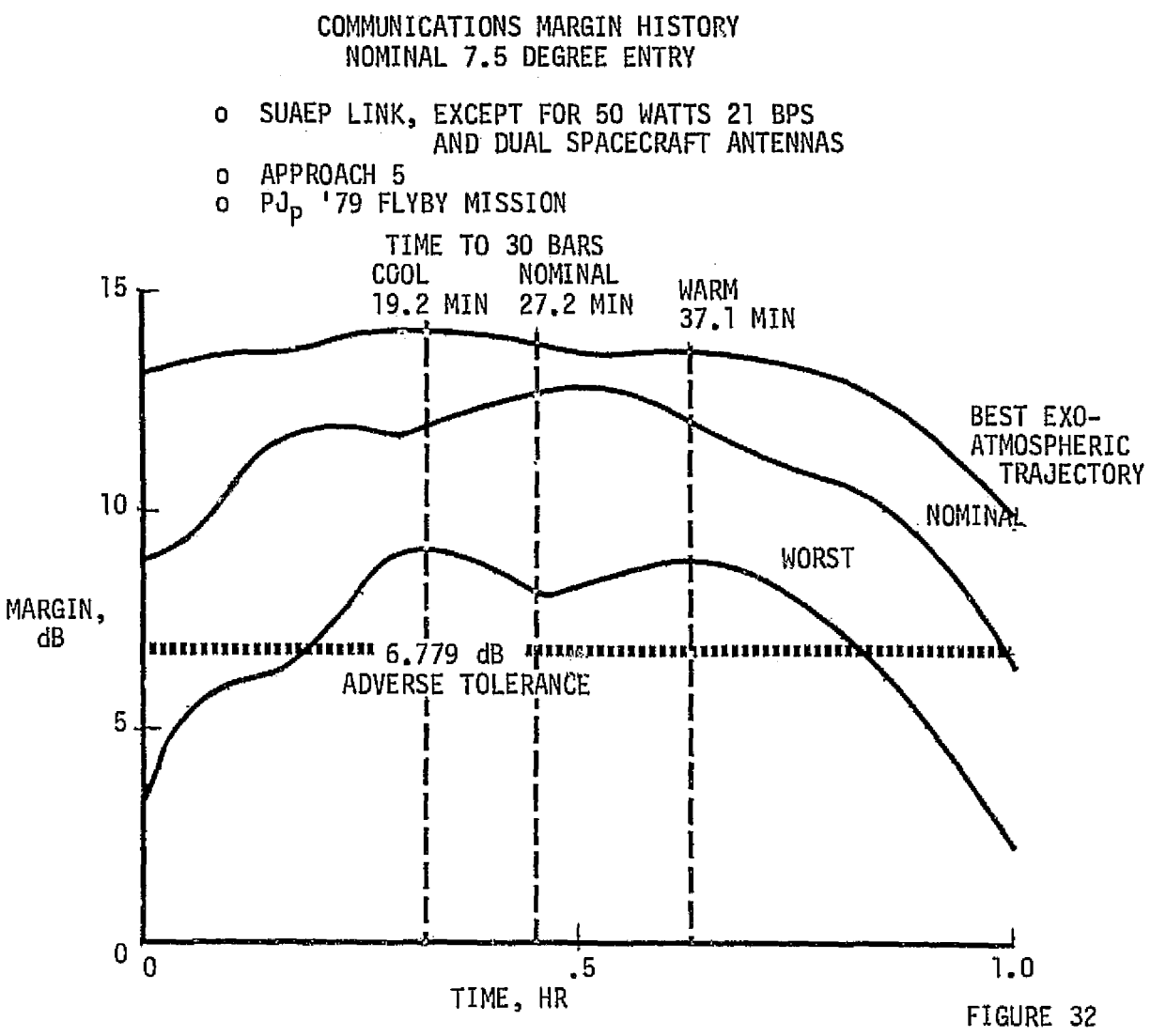

FIGURE 32

Approach 6 - Any structure in front of the big spacecraft dish could also cause some blockage of that dish antenna, thus the size and location of the probe receiving antenna is important. For a loop vee receiving antenna, the circumference is approximately a wavelength, or at 400 megahertz the diameter is about 9.4 inches. A big dish feed structure has been sized as 11 to 16 inches, thus minimizing the likelihood of blocking the main antenna. If blockage became a question, higher frequencies could be employed. Figure 33 illustrates the effect of higher frequencies. The frequency trend is the same as in Approach 2. Herein,

for twice the baseline frequency, 800 megahertz, or a 4.7 inch diameter loop vee, the margin drops from 8.75 dB to 7.6 dB. This may be an acceptable probe relay link degradation trade-off to preclude blockage loss to the direct-to-Earth link.

FREQUENCY PARAMETRIC FOR
A -7.5 DEGREE ENTRY

- SUAEP LINK, EXCEPT FOR 50 WATTS, 21 BPS, FREQUENCY CHANGE AND DUAL SPACECRAFT ANTENNAS
- APPROACH 6
- PJ_p '79 FLYBY MISSION

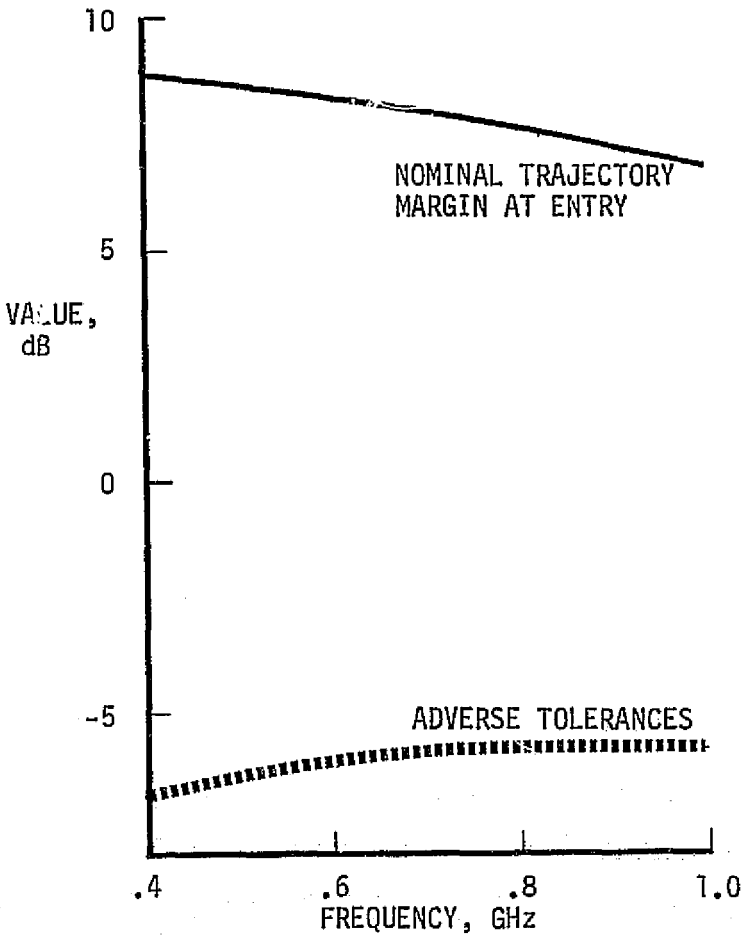

FIGURE 33

Approach 7 - As a final approach, if no blockage is allowable, and the short view times of one rear antenna are unacceptable, the margin can be increased by despinning the spacecraft receiving antenna. As noted at the beginning of this section, the receiving antenna is taken as being axially symmetric, i.e., having its (rotating) beam center a fixed angle off the spacecraft roll axis. This is the simplest implementation for a spinning spacecraft, which is a tacit assumption. However, if the spacecraft were not spinning, at least electrically from the relay link viewpoint, the effect of increased gain with fixed aperture and with increasing frequency could be employed to increase link margin. Figure 34 illustrates the effect. Because of the finite efficiency of devices with high frequency, an optimal frequency in the vicinity of 800 megahertz does occur.

An unmodified Saturn/Uranus relay communications link is not acceptable for a Jupiter mission as the link does not have adequate margin to overcome the probable adverse tolerances. Simply increasing the frequency degrades the performance. Increasing probe transmission power and decreasing probe data rate also create a marginally acceptable subsystem. The nominal mission is above adverse tolerances for a short time, but the worst case exoatmospheric trajectory case is always below the adverse tolerances. A viable alternative is a dual switchable system (antenna/receiver) aboard the spacecraft. Increasing frequency for this approach, to decrease possible big dish blockage effects, is acceptable relay geometry. If a despun antenna is developed and the short view times associated with one antenna are acceptable, a pointed spacecraft receiving antenna can dramatically increase the relay link margin.

Orbit Variations

In the preceding section the perturbations were limited to electrical variations of the communication system. The effects of varying the spacecraft's trajectory with a periapsis of 2 Jovian radii with a phasing (time from probe entry to the spacecraft passing overhead) of 0.4 hour was not varied. It can be seen that in all cases the dispersions in the relative trajectories of the probe and the spacecraft created large variations in the margin histories. Most of these dispersions are shown to be due to the angle/burn errors associated with changing the spacecraft trajectory after probe release. As postulated there, if these angle/burn errors are eliminated by a second or

DESPUN SPACECRAFT ANTENNA

- o EQUIVALENT 3 FOOT PARABOLA
- o -7.5 DEGREE ENTRY
- o SUAEP LINK EXCEPT FOR 21 BPS
- o APPROACH 7
- o PJ_p '79 FLYBY MISSION

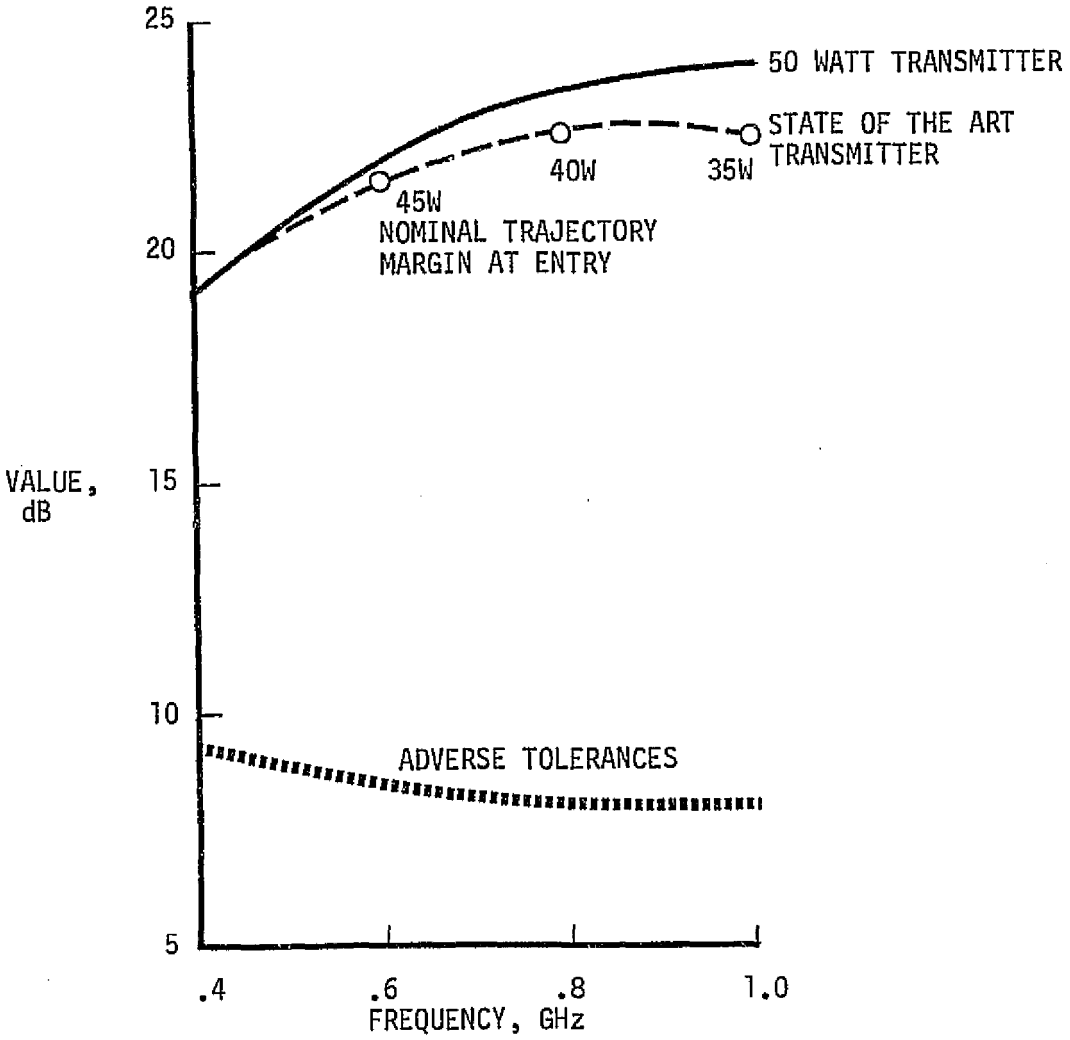

FIGURE 34

"correction" burn, the variations in communications range and antennna look angles would be significantly reduced. Accordingly, in this section, the influence of several spacecraft nominal orbits is explored on two different antenna configurations. The probe transmission parameters are assumed to be the same as for the spacecraft link.

Two principal spacecraft receiving antennas were evaluated on the Saturn/Uranus links. The loop vee is a relatively small antenna having a 50 degree beamwidth in revolution and a beam center 65 degrees off the outbound roll axis. The Lindenblad is a 3 element array with a 40 degree beamwidth in revolution and a beam center which is electronically steerable fore and aft along the roll axis. The loop vee was selected in the Saturn/Uranus study because of its small size, relative simplicity and acceptable margin by mutual agreement of the spacecraft and probe contractors and by Ames Research Center. First, the spacecraft orbit effects are determined for the loop vee (A) and then for the Lindenblad (B) antenna.

(A) Loop Vee Antenna

Figure 35 depicts the margin histories for the spacecraft periapsis from 2.2 to 1.7 radii and spacecraft phasings from 0.2 to 0.5 hour. The data for these histories is given in Appendix II. The abrupt termination of the margin histories is due to shadowing by the big spacecraft dish. It is somewhat difficult to assess this mass of data. For example, taking a 1.8 R_J periapsis case, it is seen that as the phasing time is increased, the initial margin drops, while increasing the viewing time. At a phasing of 0.4 hour, the link starts out just above the adverse tolerance limit, increases to a peak of 7.1 dB, then drops below the adverse tolerance line at .375 hour after entry, then abruptly ends at .44 hour. A phasing of 0.5 hour, never brings the margin above the sum of the adverse link table tolerances.

In order to determine the optimal performance a new parameter is defined. This parameter is the total received energy, i.e., the integral of the margin curve. Figure 36 shows these data. As far as the analysis went, the closer in the spacecraft, the higher the parametric value, with the best phasing being near 0.26 hour. However, for this entry case only 0.3 hour of transmission time is available. For the nominal and warm atmosphere models 0.3 hr does permit

COMMUNICATIONS MARGIN-TRANSMISSION TIME RELATIONSHIP AS A FUNCTION OF SPACECRAFT PERIAPSIS

- o LOOP VEE ANTENNA
- o SUAEP UNMODIFIED DESIGN
- o PJ_p '79 FLYBY MISSION

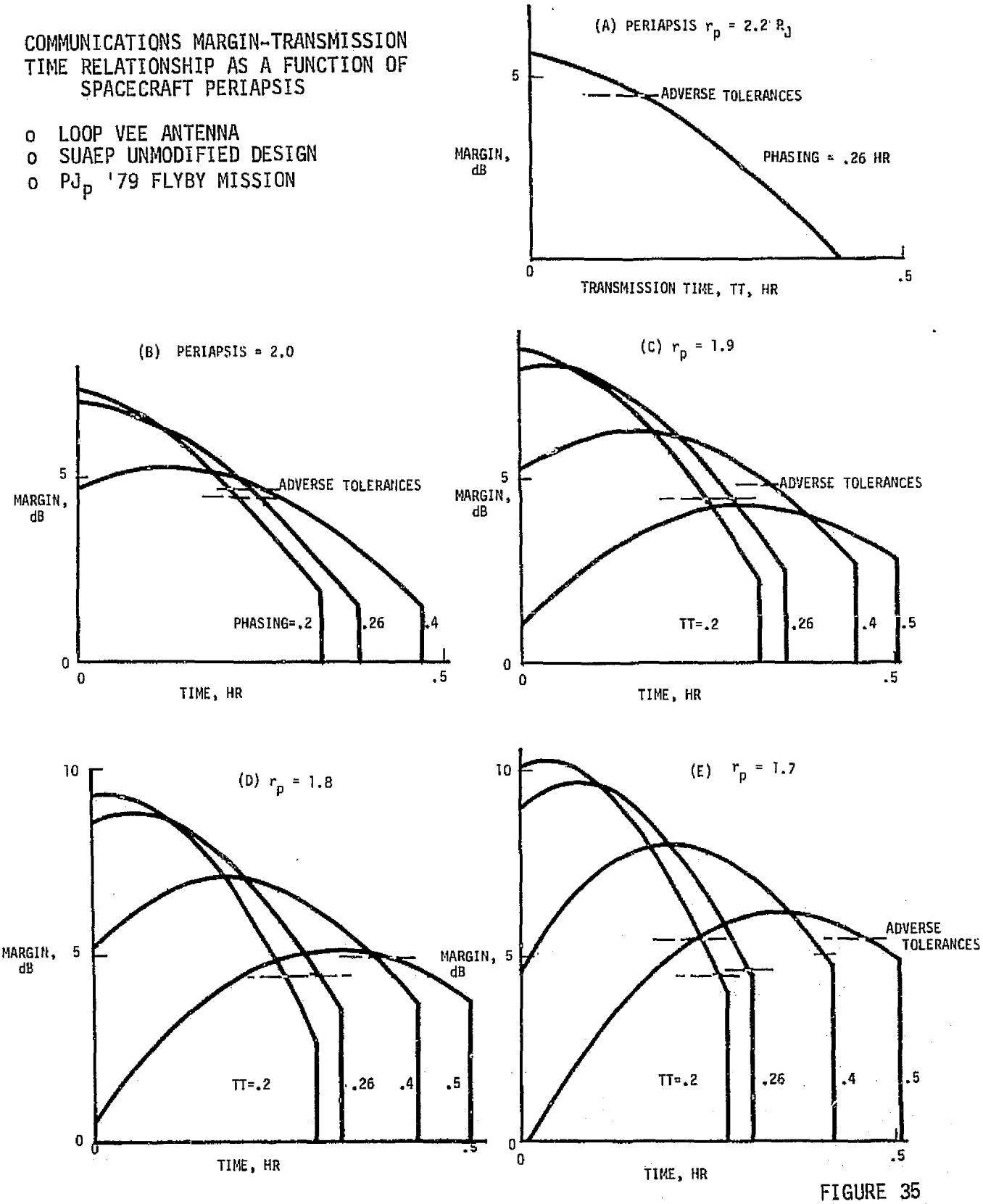

FIGURE 35

probe data transmissions down to the maximum desired pressures, thus fulfilling mission requirements. It does however restrict the time available for read out of stored data. Nominally more than one data store dump is desired in order to verify that acquisition has been achieved.

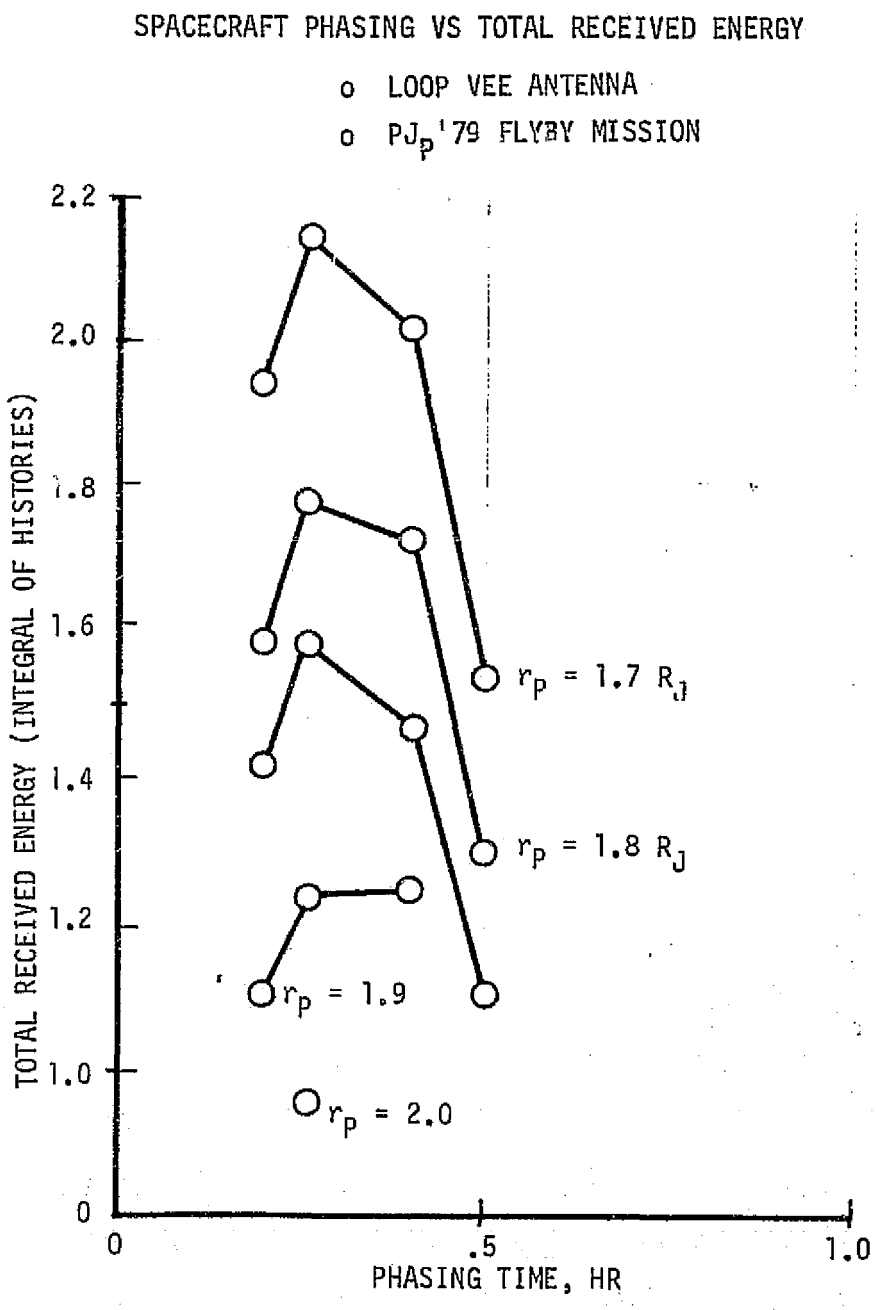

FIGURE 36

The table below summarizes the mission times over which storage is required in a typical flyby mission (PJ_p'79) using the same data handling assumptions as for SUAEP.

ACCELEROMETER STORAGE TIME REQUIREMENTS

		Time (seconds)		
Atmosphere	Entry Angle	$-.0004\uparrow$ to $-.01g_E\downarrow$	$-.01\uparrow$ to $-3g_E\downarrow$	$-.0004\uparrow$ to $-3g_E\downarrow$
Warm	-5	40	247	287
	-7.5	24.4	134.6	164
Nominal	-7.5	10.7	97.2	107.9
Cool	-7.5	7	67.4	74.4
	-10	28	50.5	53.3

In the worst case atmosphere and worst case entry angle situation (5 deg), 287 seconds of storage is required. At the Saturn/Uranus design rate of 180 bits per second, this corresponds to 51,660 bits of storage. When dumped at 22 bits per second, .65 hour is required. If the entry angle is limited to 7.5 degree, a maximum of 164 seconds is required, resulting in a total of 29,520 bits of storage for a .37 hour dump time. The dump time is still in excess of the optimal time defined by a total received energy parametric, even without considering the receiver acquisition time. Acquisition time precedes scientific data transmission time and is of the order of two minutes. Refinements may cut its duration somewhat but halving the time doesn't help overall transmission time significantly.

Another interesting cross-plot of the margin histories is shown in Figure 37. Herein, the transmission time is shown, both the "total" (to zero decibel margin or blockage), and that above adverse tolerances. It is seen that as the periapsis is lowered, the time above 0 db margin decreases while the time above adverse tolerances increases. This trend continues until the trends cross, when both design periods decrease with further lowering of the periapsis. The "break" away to lower transmission times shown for the time above adverse tolerances is due to the initial portion of the trajectory being below the adverse tolerance limit, e.g. in the margin history of the periapsis of 1.7 with a 0.5 hour phasing. As seen from the figure, the optimal spacecraft orbit to maximize

the communications for this antenna configuration is a 1.7 periapsis with a 0.4 hour phasing yielding a coincidental 0.4 hour transmission time.

SPACECRAFT PHASING VS TRANSMISSION TIME

- o LOOP VEE ANTENNA
- o PJ_p'79 FLYBY MISSION

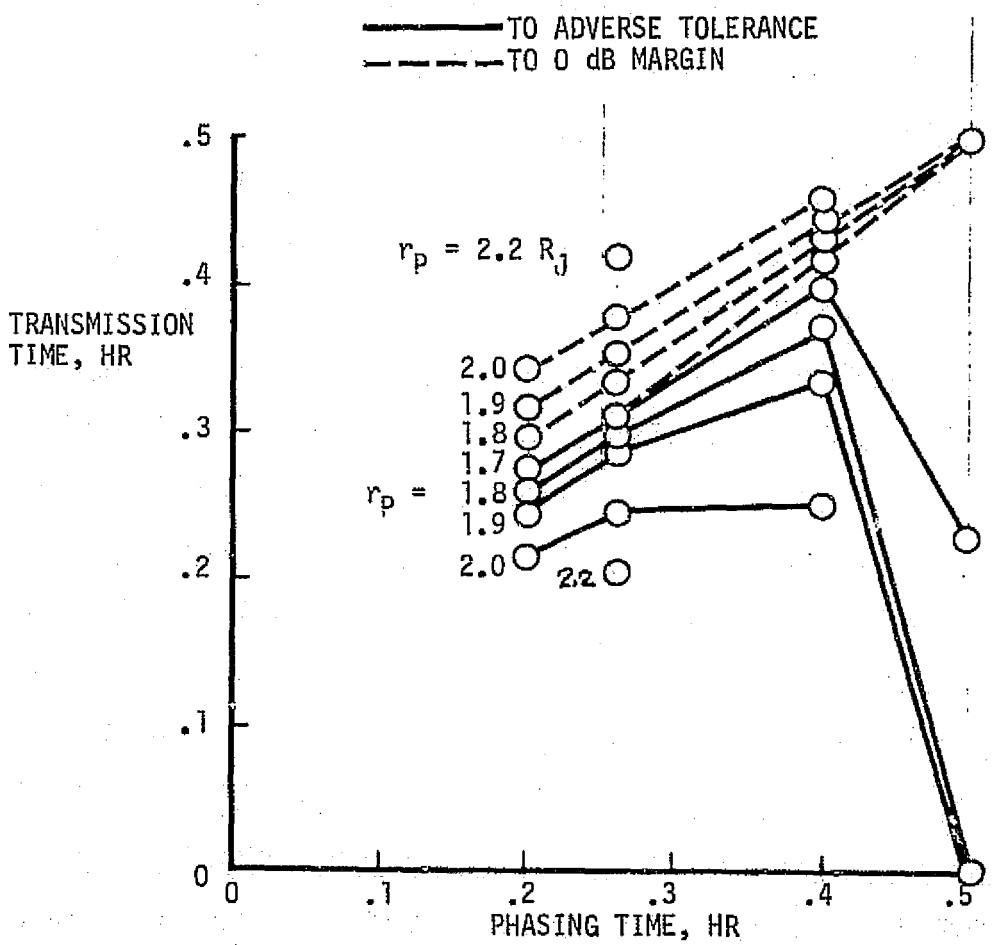

FIGURE 37

Figure 38 illustrates several alternatives for dumping the stores, given a 24 minute (0.4 hour) transmission. In (A) the Saturn/Uranus design is shown to aid comparison. Briefly reviewing the design, (1) the preentry store is a first in-last out which is initiated prior to the least resolvable g-value ($-.0004g_E\uparrow$),(2) at $-.01g_E$ (a reliable g-point) the 2700 bit store has trapped $-.0004$ to $-.01g_E\uparrow$and the remaining store filled, (3) at some point (typically -2 or $-3g_E\uparrow$after maximum deceleration) transmission can begin and the preentry store is capped off, (4) 2 minutes are allowed for acquisition followed by a redundant dump of the acquisition store, and finally, (5) the preentry store is dumped twice for redundancy. For the Jupiter Warm, $\gamma = -5$ degree entry with a 51,660 bit store it is obvious, from (B) that dual store dumps cannot be accommodated in 24 minutes, or for that matter not even a single dump fully. If only the -7.5 degree entry design of 29,520 bit preentry store is to be accommodated, as in (C), a single dump time is still in excess of 24 minutes.

STORAGE/PLAYBACK ALTERNATES

o PJ_p 79 FLYBY MISSION

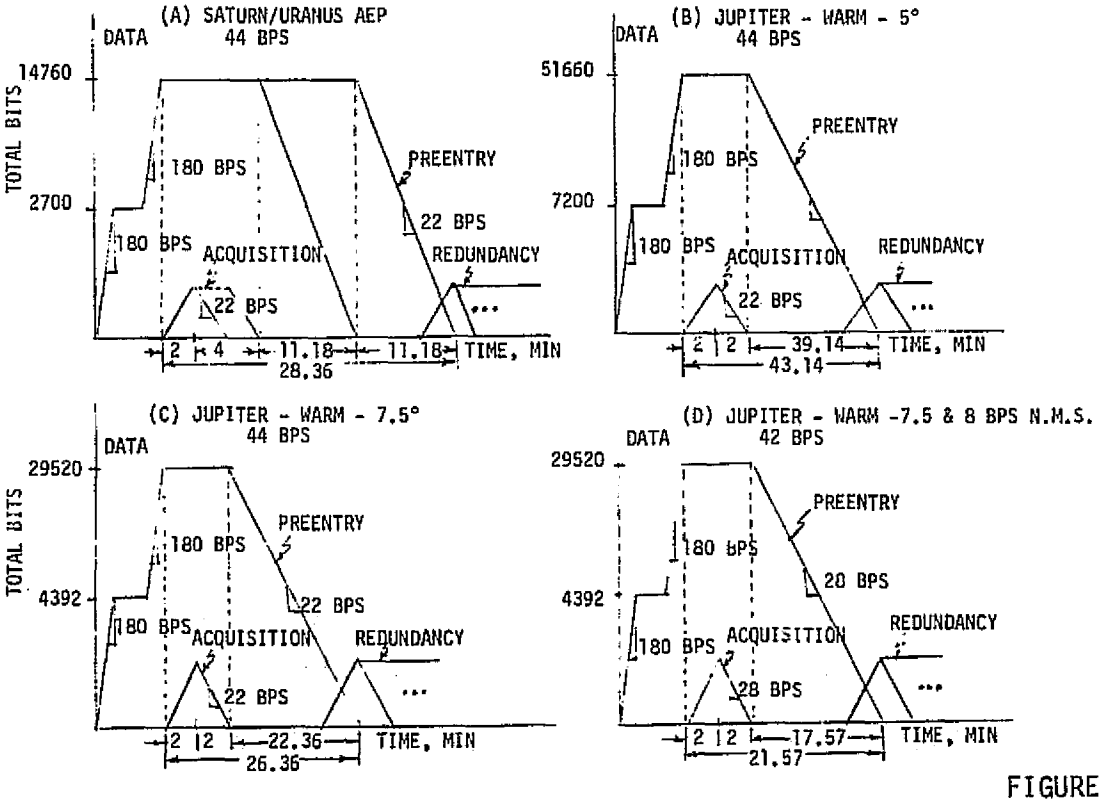

FIGURE 38

A possible solution is dropping the neutral mass spectrometer to 8 bits per second, resulting in a 14 bit per second real-time rate and 2:1 interleaving of the stores, see (D), which results in a transmission rate of 42 bits per second. This gives a 2.5 minute margin which is barely adequate.

A possible variation in the preentry store to reduce the dump time is to reduce the amount of data collected. The data is currently collected at a constant 5 samples per second. Given that the atmosphere above some level, say $-3g_E\uparrow$, is essentially exponential, the $-.0004g_E\uparrow$ to $-3g_E\uparrow$ data could be collected at a lower rate, say once per second. The $-3g_E\uparrow$ (up the deceleration curve) occurs at 42 seconds in the worst (Warm -7.5 degree entry) case. The store is then (27 + 42) x 180/5 + (137 - 42) x 180 = 19,584 bits. This could be dumped in 18.84 minutes with the acquisition store, or well within the 24 minute communications time. In all cases, triggering or cueing occurs by the data handling equipment reading the uninterrupted accelerometer data flow.

(B) Lindenblad Antenna

The advantages of Lindenblad equipped spacecraft are the narrower beamwidth (additional gain) and the ability to electronically present the beam center. For this analysis the half-power beamwidth is constrained to graze the shadow of the 9 ft dish, which places the maximum beam center at 85 degrees. Figure 39 shows the margin histories for the same range of spacecraft periapsis and phasings as for the loop vee antenna. The data for these plots is given in Appendix II. The increased gain of this antenna is apparent in the histories, not only for the increased absolute margins, but because the transmission cut-off due to adverse tolerances generally coincides with the cut-off caused by shadowing of the big dish.

Figure 40 illustrates the total received energy versus the phasing for the Lindenblad antenna. Compared to the loop vee case, the maximum energy occurs at 0.4 hour phasing, rather than 0.26 hour.

The transmission times versus phasing are shown in Figure 41. Except for the break at 0.5 hour phasing, which is caused by the initial portion of the mission being below adverse tolerances, the shadowing and adverse tolerance view-times coincide. The optimal spacecraft trajectory for the Lindenblad for the range of trajectories investigated is a periapsis of 2.0 Jovian radii and

a 0.4 hour phasing; resulting in a view time of 0.46 hour. This is 3.6 minutes longer than the optimal loop vee capability. For this trajectory/antenna combination, the Jupiter Warm -7.5 degrees data handling approach of Figure 38(C) would be acceptable, i.e., the neutral mass spectrometer could be kept at 16 bits per second.

Conclusions

Using an unmodified Saturn/Uranus relay link with a variety of probe data rate, transmitter power, receiving antenna combinations with a fixed spacecraft trajectory led to the conclusion that none of these combinations were totally satisfactory. Dispersions in the relative trajectories of the spacecraft and probe resulted in large margin variances which cannot be adequately accommodated.

By correcting the spacecraft trajectory to minimize the dispersions, optimal spacecraft periapsis (1.7 R_J)/phasings (0.4 hour) become apparent. The Saturn/Uranus communications link design (40 watt, 400 megahertz microstrip to loop vee) can then accommodate a Jupiter mission if minor variations in the data handling system are made. Typically, these variations include the amount of storage (from 17,400 to 31,200 bits at most), the number of memory dumps (from 2 to 1.27), and revised neutral mass spectrometer sampling rates (from 16 to 8 bps). Selection among these variations must be made while simultaneously considering science data gathering strategy (instrument value as a function of altitude), heat protection requirements, thermal histories, probe stability, and spacecraft deflection errors. Jovian ephemerides will be adequately in hand after Pioneers 10 and 11 and two Mariner Jupiter/Saturn flybys to assure manageable position error sources at probe release, but the other factors do affect transmission capability.

COMMUNICATIONS MARGIN - TRANSMISSION TIME RELATIONSHIP AS A FUNCTION OF SPACECRAFT PERIAPSIS - LINDENBLAD ANTENNA

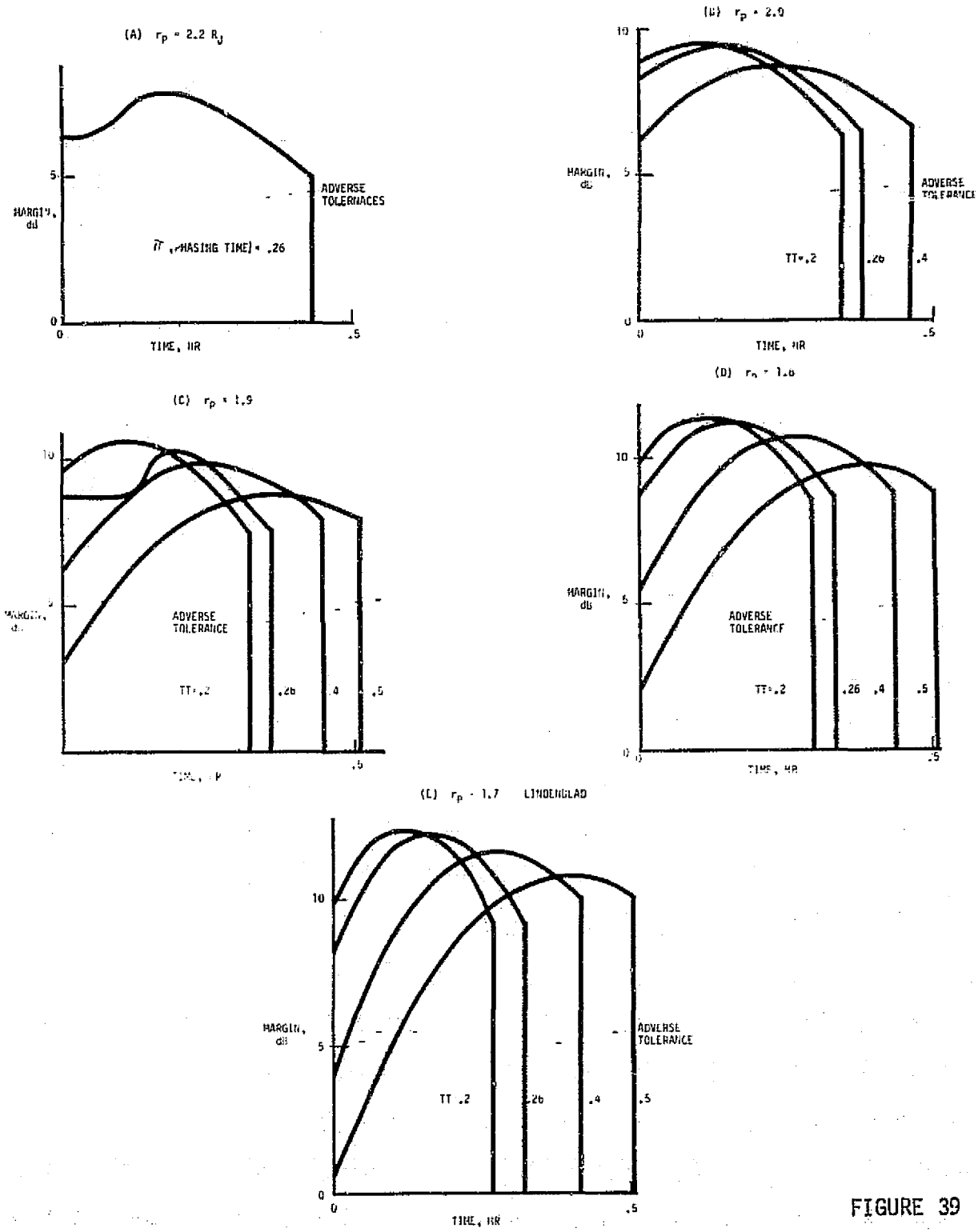

FIGURE 39

SPACECRAFT PHASING VS TOTAL RECEIVED ENERGY

- o LINDENBLAD ANTENNA
- o PJ_p'79 FLYBY MISSION

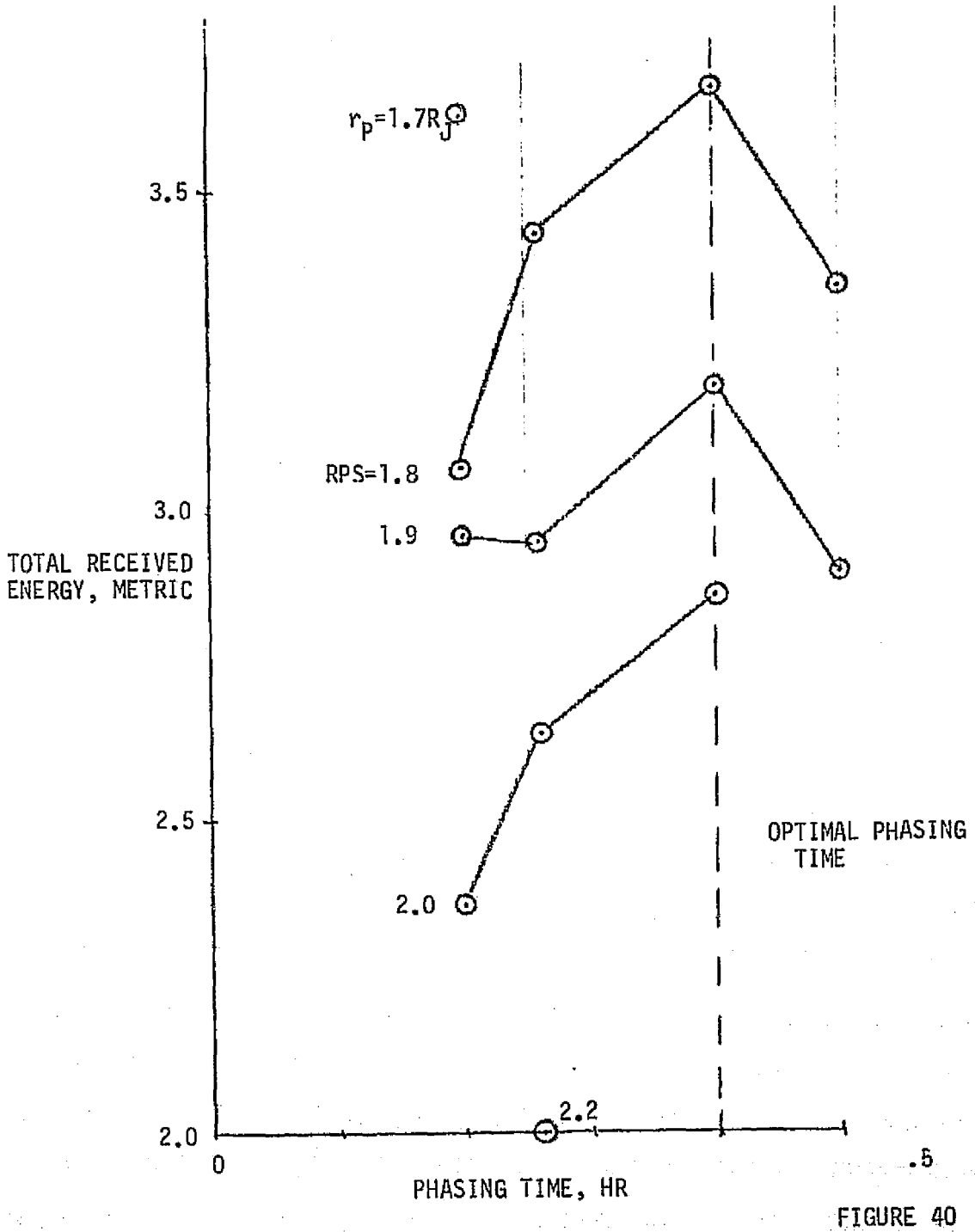

FIGURE 40

TRANSMISSION TIME PARAMETRIC ANALYSES

- o LINDENBLAD ANTENNA
- o PJ_P'79 FLYBY MISSION

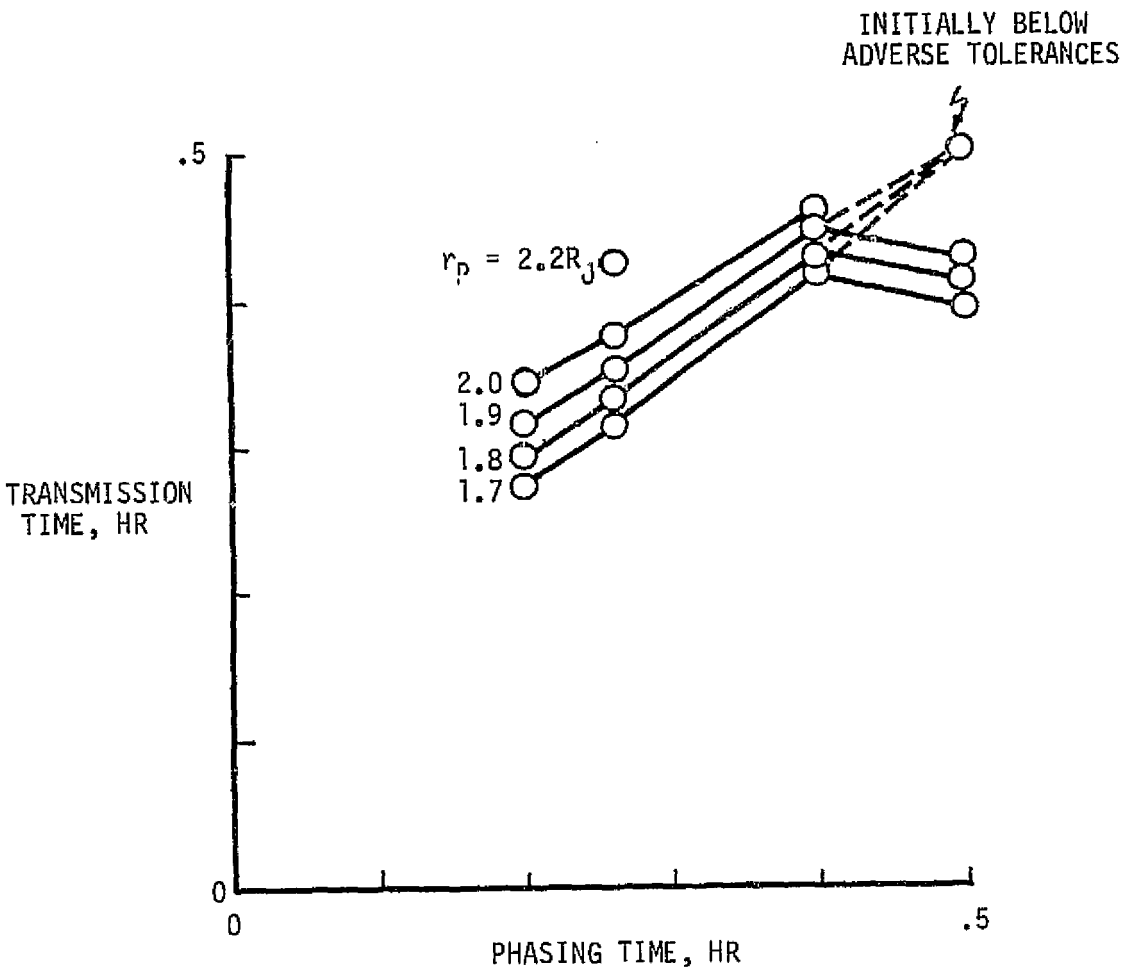

FIGURE 41

SCIENCE

A number of fundamental issues regarding the solar system can be clarified by means of atmospheric entry missions to the outer planets. Of these planets, Jupiter is the most attractive for atmospheric exploration. Jupiter has received the greatest attention from astronomers, so that new data can be fitted into a rich mosaic of previously obtained knowledge.

The specific information that we seek to know about Jupiter falls into four categories: planetary environment, energy sources, chemical composition and state of evolution. With regard to the planetary environment, ultra-violet radiation and energetic particles,which originate at the Sun, impinge on Jupiter's outermost atmosphere. The specific interaction between the planet and the incoming radiation is a function of Jupiter's particular chemical and electromagnetic properties. Due to its strong magnetic field, Jupiter is surrounded by an intense belt of highly energetic protons and electrons.

With the identification of hydrogen as the major chemical component of Jupiter's atmosphere has come a verification of the theory that this planet is very similar to the Sun in composition, but existing at much lower temperatures. Direct, accurate identification of the chemical compounds present in the atmosphere and measurement of their relative abundance and isotopic ratios can elucidate the chemical history of Jupiter from the time of its formation out of the primordial solar nebula.

Jupiter, Saturn and Neptune have the unique characteristics of emitting much more thermal energy than they receive from the Sun. The data from the infrared radiometry experiment on Pioneer 10 indicate that Jupiter emits over twice the incident solar radiation. The identification of the sources of this emission and the radiative mechanism by which it is generated may prove that Jupiter is a stillborn star or one in the last stages of decay.

A strong case for Jupiter atmospheric entry missions can be made in terms of the questions that will remain unresolved even after the Pioneer 10 & 11 flyby missions. On the basis of the Principal Investigators' analyses of Pioneer 10 Jupiter data, it appears that the infrared photometry and radio occultation experiments are unable to provide a precise description of Jupiter's

atmosphere. The obstacles to defining Jupiter's atmosphere by means of remote flyby experiments arise from the dense opaque nature of the atmosphere. In the case of optical spectroscopy, the spectra of the atmosphere has proved to be very difficult to interpret, especially in the infrared. There are an enormous number of weak lines in the spectra for which we cannot ascertain a corresponding quantum state. The presence of aerosols in the atmosphere compounds the difficulty of interpreting the spectrum. These particles tend to scatter the incoming solar light, causing the path of an incident photon to be quite complex. Also, the scattering power of the aerosols exhibit a wavelength dependence. Therefore abundance estimates require measurements of lines of comparable intensity in the same region of the spectrum and result in relative rather than absolute abundances.

Radio occultation is also of limited usefulness. In very dense atmospheres, such as Jupiter's, extinction of the radio signal is caused by excessive defocusing attenuation within the atmosphere. In the case of Jupiter extinction, this occurs at a pressure level for S-band of 2.8 bar. Below this level no further tangential penetration by radio rays is possible.

Science Objectives

The probe is designed to fulfill these four scientific objectives:

Near Planetary Radiation -

The energetic particle detector provides an integrated measurement of high-energy protons and electrons from 2 R_J to 1 R_J, in order to complete the mapping of the Jupiter radiation environment.

Atmospheric Structure -

The accelerometer experiment measures the aerodynamically - induced accelerations of the entry probe by the planetary atmosphere. The ambient atmospheric density is derived directly from the aerodynamic deceleration. In the lower atmosphere the data on atmospheric structure from the accelerometer are supplemented by direct measurements of atmospheric temperature and pressure.

The location of cloud layers within the atmosphere is determined with the backscatter nephelometer. Information on the density of the layers and their optical opacity is obtained by combining a comparison of the nephelometer and visible-IR flux meter data.

Atmospheric Composition

The chemical composition of the atmosphere is determined primarily by the mass spectrometer. A supplementary measurement of the hydrogen/helium ratio is provided by an explicitly designed gas chromatograph.

Visible-IR Spectra Radiations-

The thermal energy emitted into the atmosphere is measured by the visible - infrared flux meter. These measurements are correlatable with those obtained on the orbiter.

The design rate of sampling related to altitude is depicted in Figure 42.

The Atmosphere of Jupiter

The definition of the atmosphere of Jupiter is the reason for the mission, but a good postulation is required in order to design a probe that has adequate margins for success. The sources available for postulation are earth-based sensing, flyover spectroscopy and occultation data. Currently, the results of all three do not correlate. The S-band occultation data obtained by Arvydas J. Kliore's team, the JPL Principal Investigator, during the Pioneer 10 flyby are used to bound several design aspects because it is more diffuse that the monograph values of Reference 5. Curves of the results are shown in Figures 43 through 45, however, the design is based only on Reference 5 data.

The experimentalists' data are given in Figure 43, with the altitu referenced to the local distance from Jupiter's center. The lower portion of the figure is a facsimile of Kliore's curve. As can be seen, above 70,550 km three separate temperature curves are given, for T_o = 50, 100 and 150K, respectively. This circumstance arises from the fact that an initial value for the temperature must be assumed in converting radio frequency (rf) attenuation into atmospheric parameters. Also, above 70,575 km the atmosphere proved to be too diffuse to attenuate the rf signal; therefore, above this level theoretical considerations must be invoked to obtain complete atmospheric properties.

The most inclusive analysis of the upper atmosphere of Jupiter is by D. F. Strobel and G. R. Smith (Reference 6), who includes the effect of hydrocarbon photochemistry on atmospheric properties. Strobel predicts a constant thermospheric temperature of 155K for a Jupiter atmospheric composition similar to that assumed by Kliore. Therefore, it is reasonable to fair in a thermopause temperature of 155K into the 150K branch of the radio occultation curve.

DATA SAMPLING RATES

JUPITER NOMINAL ATMOSPHERE

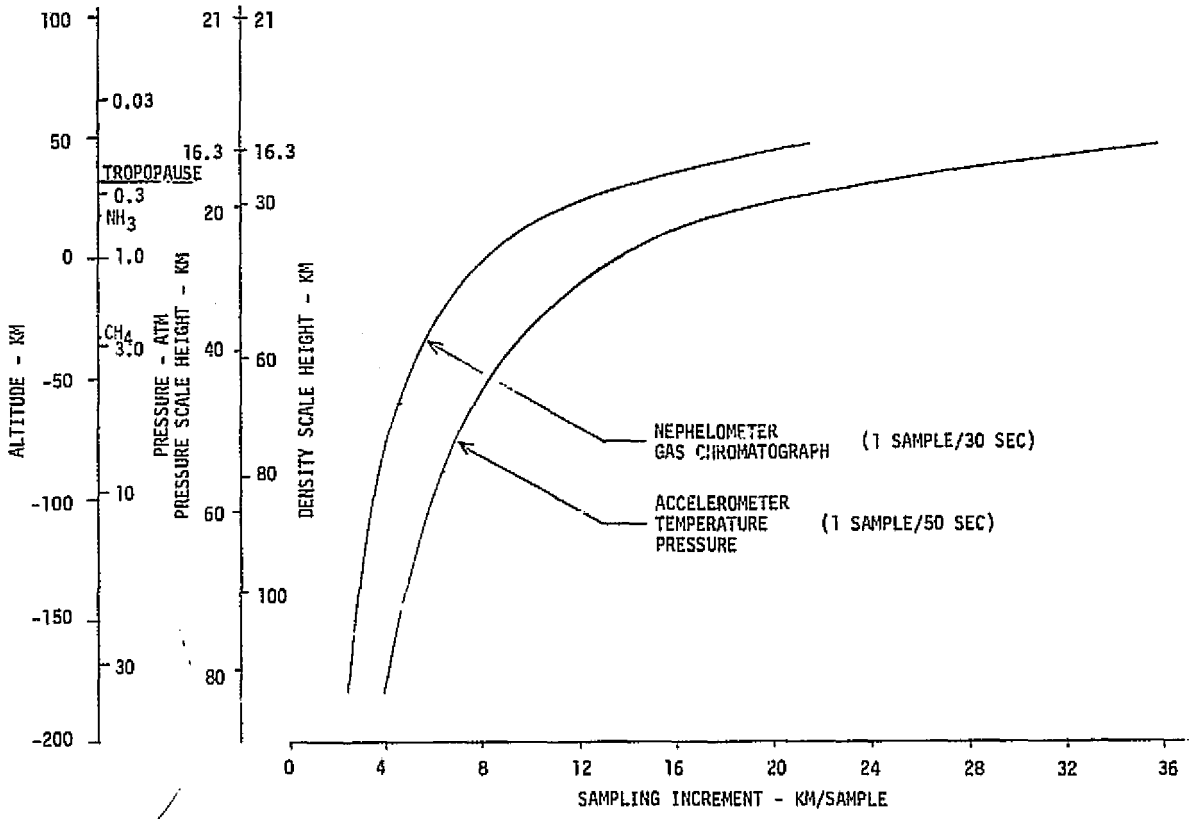

FIGURE 42

JUPITER ATMOSPHERE TEMPERATURE
PIONEER 10 OCCULTATION DATA

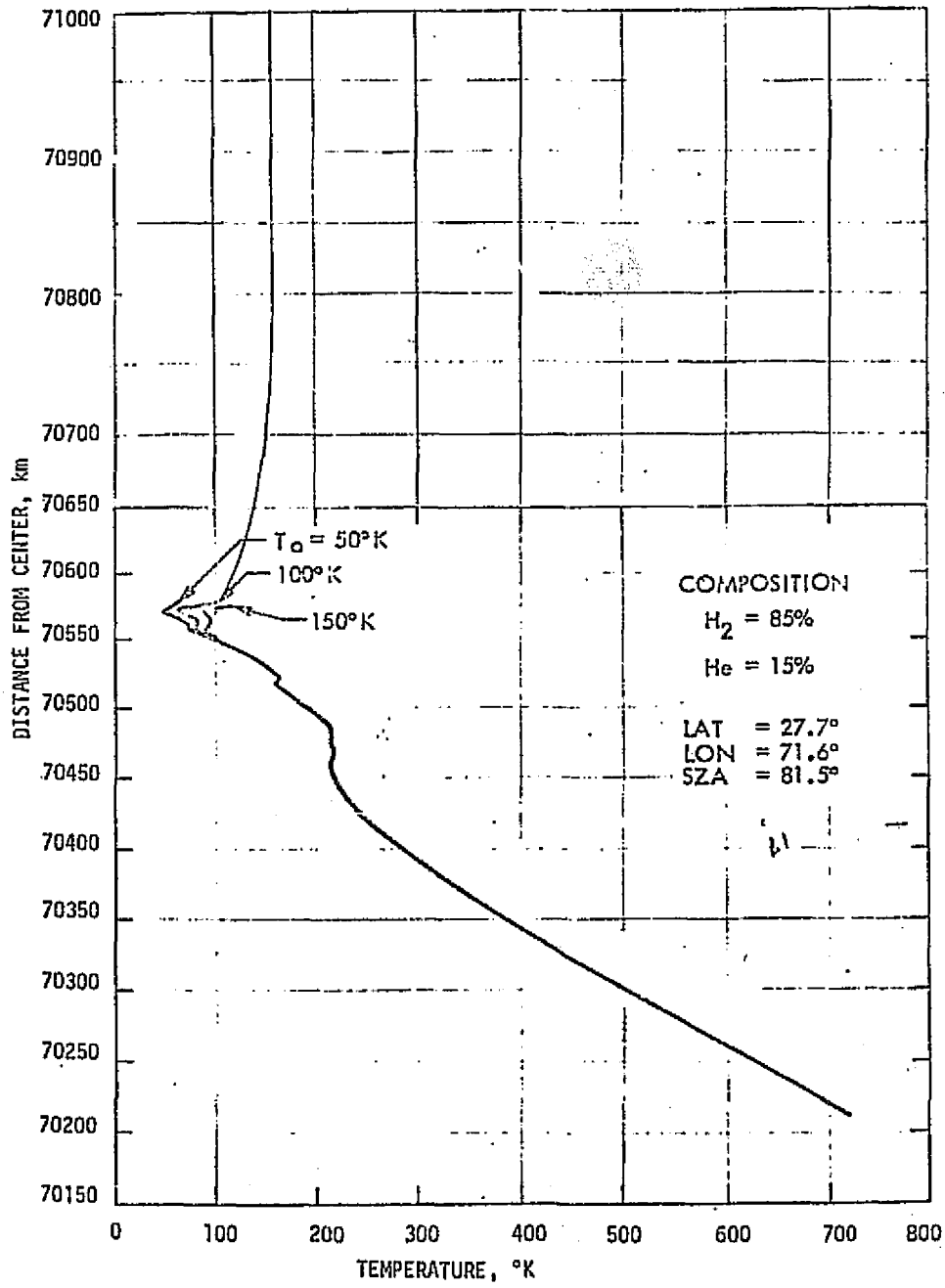

FIGURE 43

JUPITER ATMOSPHERE

$h, p, \rho = f(T)$

- 85% H_2; 15% He

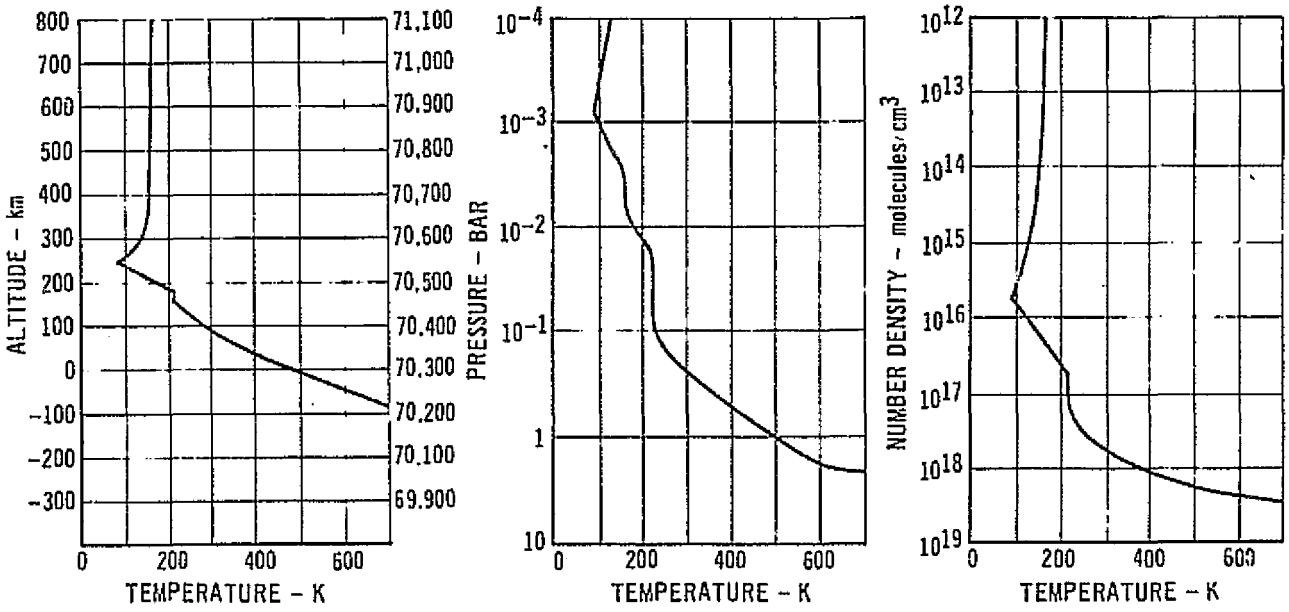

(A) (B) (C)

FIGURE 44

JUPITER ATMOSPHERE DEFINITIONS

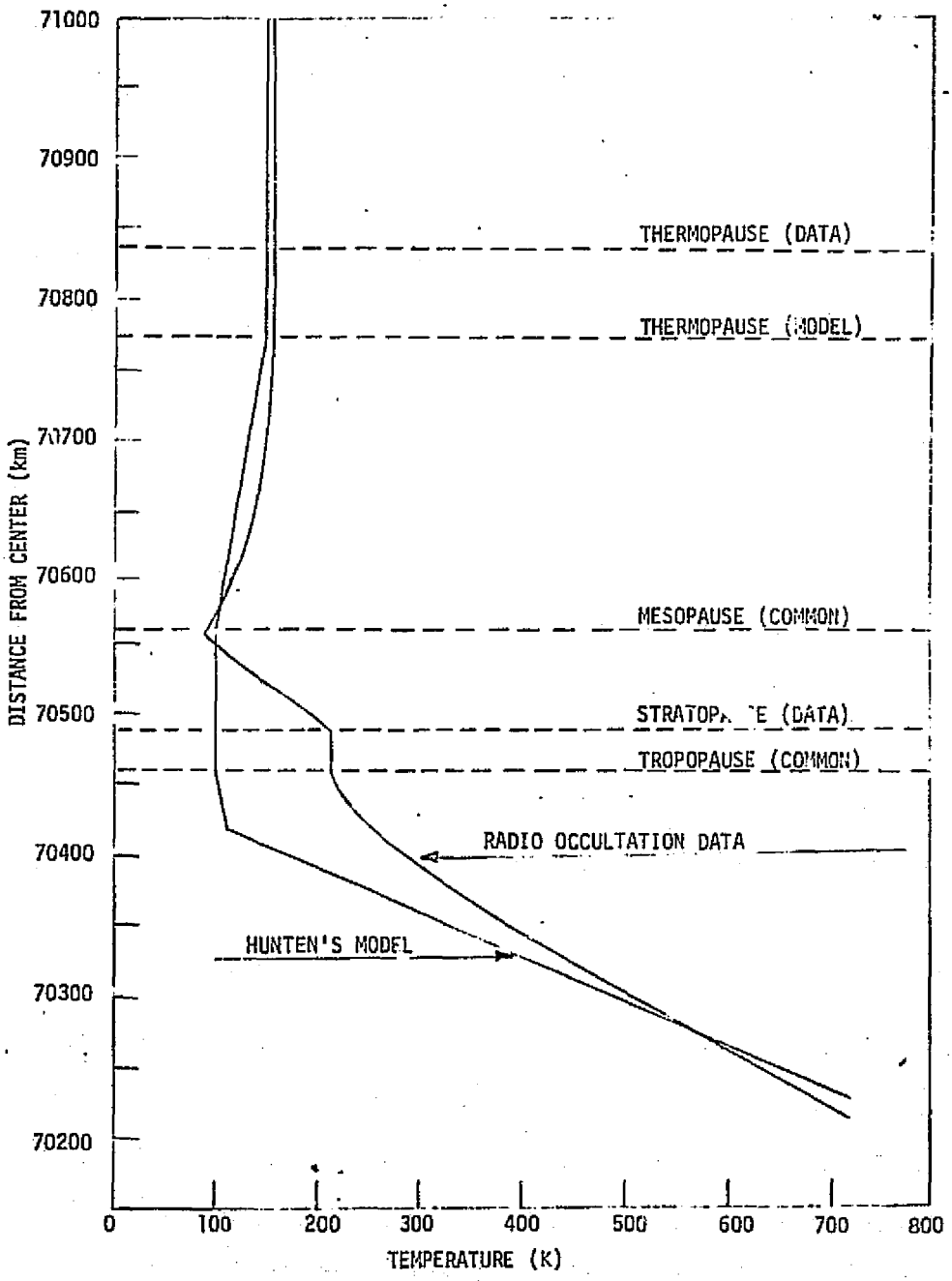

FIGURE 45

By use of the radio occultation data in Figure 43 and the ideal gas law, the properties of Jupiter's atmosphere can be derived. The results of this process are given in Figures 44 and 45, namely plots that interrelate altitude, pressure and number density. Two altitude references are used, distance from Jupiter's center and distance from the 1 bar pressure level. The 1 bar level occurs at 70305 km, 490K and a number density of 1.52×10^{18} molecules/cm^3 for the latitude of occultation.

Prior to acquisition of the Pioneer 10 data, various Jupiter temperature profiles had been proposed. Of these the one by D. M. Hunten (Reference 7) has received wide currency. It is instructive to compare the Pioneer 10 altitude-temperature curve with Hunten's model. This comparison is made in Figure 45. In order to make the comparison, the altitude of the tropopause in Hunten's model is placed at the indicated tropopause observable in the radio occultation data, 70460 km. The altitudes of the other atmospheric boundaries in Hunten's model are then referenced from their distance from the tropopause. The mesopause altitude predicted by Hunten coincides with that detectable in the Pioneer 10 data. That Hunten's model reflects the existence of a distinct mesosphere is the consequence of a deliberate choice on his part. He intentionally constructed a simplified model that neglected the effects of photochemical reactions that result in ultraviolet cooling in the mesosphere. Strobel's work was undertaken to assess these photochemical effects.

The differences between theory and experiment in the lower atmosphere, below the mesopause, are very vivid, and have incited considerable discussion. Conventional wisdom has predicted a tropopause temperature of about 115K; a value of 210K is derived from the radio occultation data. Temperatures this high in this region of the atmosphere are not anticipated based on Earth-based infrared spectroscopy. It is hoped that the Pioneer 10/11 data force a rigorous re-examination of Jupiter atmospheric models. The influence of the internal planetary thermal source, measured by Pioneer 10 to be nearly equivalent to the incident solar heating, must now be included in any serious atmospheric modeling. As of this date no completely rigorous study of the combined effects of external and internal heating has been done, hampering the task of probe design with minimal margins of safety. Thus, overdesign and overdevelopment are recourses that are resorted to for high probability of mission success.

The chemicals that have been identified in Jupiter's atmosphere by visible and infrared spectroscopy are hydrogen, methane and ammonia. The presence of helium was strongly suspected but not directly observed. Now the Pioneer 10 ultraviolet photometry experiment has yielded a direct identification of helium in the Jovian atmosphere. In answer to a direct question as to the trend in the data with respect to the hydrogen-to-helium abundance ratio, the Pioneer Jupiter ultraviolet photometry Principal Investigators (Judge and Carlson) replied, "roughly solar" or numerically about 18, atomically.

The most prominent features in the spectrum of Jupiter are the absorption bands of methane and ammonia (Reference 8). In 1960 the diffuse quadrupole lines of molecular hydrogen were detected. The presence of helium in Jupiter's atmosphere was always strongly suspected, but never directly observed. An estimate of the abundance of helium, derived from the extent of the pressure-broadening of the 6190A methane bands, is < 34 km - amagat. This value sets a lower limit to the hydrogen-to-helium ratio:

$$H_2/He > 2.5$$

The direct detection of helium in the atmosphere of Jupiter involves the observations in the far ultraviolet. The strongest feature in the spectrum of helium is the 584A line in the ionization spectra. This line is invisible to ground-based telescopes due to the earth's ozone layer and is too weak to be detected with rocket-borne spectrographs or small earth-orbiting observatories. Hence, we had to wait for the close-up measurements from Pioneer 10 (and 11 which has not yet been deciphered).

The Pioneer ultraviolet photometry experiment (Reference 9) employs a two-channel photometer to measure the emissions from the hydrogen 1216A and helium 584A lines. The radiative processes being observed are the resonance scattering by the Jovian atmosphere of incident solar hydrogen and helium line emission. The photometer measures the photons that impinge on photocathodes from the two emissive sources. Data reduction involves converting the photoelectron current to radiative flux and thence to abundance ratios. The preliminary published report (Reference 10) presents provisional values of about 1000 rayleighs and 10-20 rayleighs for hydrogen and helium, respectively. As noted above, the PI's preliminary estimate of H_2/He is that corresponding to the solar atmosphere.

Prior to having the ultraviolet photometric measurements, the presence of helium was inferred from its identification in the sun's atmosphere and the assumption that Jupiter's composition closely resembles the sun's. Measurements of the solar corona indicate an atomic hydrogen-to-helium ratio:

$$H/He = 16. \qquad \text{(Ref 11)}$$

In Jupiter's atmosphere, the hydrogen is in the molecular state, H_2, Therefore, the assumption that the hydrogen to helium in Jupiter's atmosphere corresponds to the solar abundance ratio yields a molecular abundance ratio:

$$H_2/He = 8.$$

The abundance ratios for CH_4 and NH_3 as derived from the visible and infrared spectra are:

$$H_2/CH_4 = 1.4 \times 10^3$$

and

$$H_2/NH_3 = 6.0 \times 10^3$$

There is close agreement between the measured values for the sun and Jupiter.

The conclusion reached is to assume as the nominal composition model for Jupiter the following (solar) abundance ratios.

$$H_2/He = 8$$

$$H_2/CH_4 = 1.4 \times 10^3$$

$$H_2/NH_3 = 6.0 \times 10^3$$

Instrument Implementation

To characterize the atmosphere, the probe must carry a complement of instruments that can obtain a variety of data that permits correlation of Earth-bound and spacecraft-borne measurements. The complement of instruments is designed to supply the information to meet the objectives previously listed.

Figure 46 lists the science instruments and measurement characteristics of each of these instruments for the Pioneer Jupiter Orbiter Probe mission. Some of the material in this report was done prior to inclusion of the gas chromatograph, visible IR flux meter, and energetic particle detector, e.g., the Pioneer Jupiter Probe for 1979.

SCIENCE PAYLOAD

PJO_p'80 ORBITER MISSION

INSTRUMENT	OBJECTIVES	RANGE	SAMPLE RATE
• ACCELEROMETER	DENSITY PROFILE	0 TO 0.1 g_E	1 sps DURING – 0.004 g_E TO –0.01 g_E
LONGITUDINAL		0 TO 10 g_E	
		0 TO 800 g_E	4 sps DURING – 0.01 g_E TO –3 g_E
LATERAL		0 TO 10 g_E	0.05 sps
• PRESSURE GAGE	PRESSURE PROFILE	0 TO 0.1 atm 0 TO 5 atm 0 TO 10 atm 0 TO 25 atm 0 TO 50 atm	0.05 sps (LOWER ATMOSPHERE)
• TEMPERATURE GAGE	TEMPERATURE PROFILE	50 TO 550°K	0.05 sps (LOWER ATMOSPHERE)
• NEUTRAL MASS SPECTROMETER	COMPOSITION	0 TO 40 AMU	CONTINUOUS SAMPLING WITHIN THE LOWER ATMOSPHERE (12 bps)
• GAS CHROMATOGRAPH*	H_2/He RATIO	N/A	3 GAS SAMPLES (0.5 bps)
• VISIBLE/IR FLUX* METER	TEMPERATURE VARIATIONS	0.5 TO 55 μm	3.0 bps
• NEPHELOMETER	CLOUD LAYERS	N/A	1.5 bps
• ENERGETIC PARTICLE*	ENERGETIC PROTONS	PROTONS > 60 MeV	2000 bits

N/A = NOT APPLICABLE

* NOT INCLUDED IN PJ_p'79 MISSION

FIGURE 46

Accelerometer - The accelerometer unit is a self-contained package that consists of three orthogonally mounted mass-rebalancing accelerometers along with their supporting electronics. It is a modified version of one used on the PAET vehicle (Reference 12) and Pioneer Venus. The package is mounted with the longitudinal accelerometer aligned with the centerline of the probe and with the proof mass as close as possible to the probe's center of gravity. A compromise location longitudinally is planned between fore-and-aft c.g. extremes.

Pressure Gage - The pressure gage is a single unit that contains four pressure transducers and a common electronics package. The inlet ports of the pressure gage is collocated within the atmospheric sampling inlet tube assembly. The four transducers successively provide readings in the ever-increasing pressure domains.

Temperature Gage - The temperature gage consists of two components, the deployable sensor unit and the electronics package. It is typical of platinum wire sensors used in many space probes except for its deployment. A mechanism is needed which must eject a carbon-phenolic plug as well as extend the sensor. It is located outward on the forward cone to assure high velocity flow over the dual platinum wires.

Neutral Mass Spectrometer - The neutral mass spectrometer is a double focusing magnetic deflection instrument similar to one used on the Atmospheric Explorer Satellite. Atmospheric gas samples are obtained through a 0.48 cm diameter tube which is concentrically housed within a deployable tube of 1.7 cm diameter. Deployment is initiated by a pyrotechnic pin-puller which releases a preloaded metal bellows. A continuous sample of the atmosphere is tapped off a manifold via a sampling tube. As the probe descends through the atmosphere, data is obtained at all pressure levels once the tube is deployed. The continuous sampling spectrometer being considered requires repackaging to a toroidal planform.

Gas Chromatograph (H_2/He Ratio) - The gas chromatograph shown is a modified version of the one being developed for the Pioneer Venus. This is a dedicated instrument which explicitly measures the H_2/He ratio during the probe descent. It also taps off of the manifold; it is a single column instrument.

Visible Infrared Flux Meter - The visible-IR flux meter is an adaptation of the Pioneer Venus net flux radiometer. The instrument is deployed by a spring-loaded,four-bar mechanism through a jettisonable port in the aft heat shield. The detector looks down at the planet to measure variation in radiant energy levels as the probe descends into the atmosphere. An upward measurement is of little value as the baseline entry longitude is 15-20 degrees beyond the evening terminator.

Nephelometer - The nephelometer is a Ames Research Center design for the Pioneer Venus probe. The instrument consists of a light source, lenses and an optical detector. These components together with the power supply and data processing electronics are packaged into a single unit. The unit is located aft of the foam equipment cover and looks out radially after porthole cover removal. The incident light on a particle produces backscattered light which is simply tallied for transmission. No sizing of particles is accomplished.

Energetic Particle Detector - The concept of the energetic particle detector is based on the Aerospace Corporation detector used on ATS 1. Modifications to the packaging are required to fit it into probe. The detector looks aft through the probe aft heat shield with a 40° cone-angle field of view. The detector measures energetic protons above 60 MeV and a spectrum of electrons. The instrument will function during the 45 minute period of descent that precedes entry. It is energized on a signal from the x-day clock, which also energizes the data handling system and the pre-entry store.

Instrument Accommodation

Each of the instruments are accommodated within the probe as shown in Figure 47. Addition of a gas chromatograph and an energetic particle to the science payload necessitated a rearrangement of some toroidal segments and relocation of some connectors within the baseline design. The visible- infrared flux meter is located in the aft hemisphere. It requires the incorporation of another porthole in the aft heat shield, but little else besides thermal insulation. Two science instrument changes also resulted from the rearrangements: the temperature sensor is mounted radially farther out as are the pressure sensor capsules.

INSTRUMENT ACCOMMODATION

o PJO_P'80 ORBITER MISSION

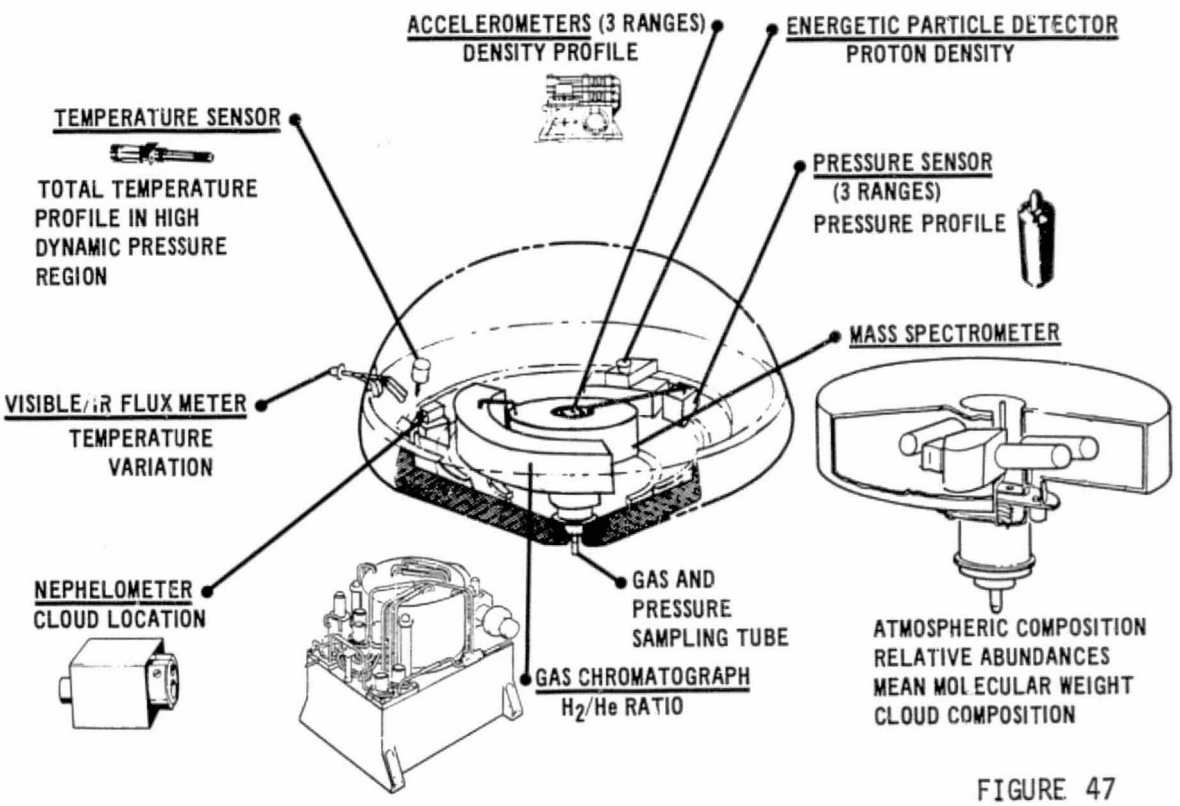

FIGURE 47

Instrument Installation

The location of science instruments in the probe considered packaging for survival of high deceleration entry loads and c.g./balance constraints, primarily.

Of the five science instruments three viewing instruments (visible-IR flux meter, nephelometer and the energetic particle detector) are installed aft of the equipment cover. In the aft hemisphere instruments require thermal insulation wraps to maintain in-transit temperatures (nonoperating) between -40°F to +20°F. The remaining instruments inside the equipment cover are maintained within their temperature limits.

The accelerometer package is attached to a rigid structure in the hub section of the mass spectrometer analyzer section. This positions the longitudinal accelerometer axes along the centerline of the probe with the proof mass as close as possible to the probe's center of gravity.

The pressure gage is located between the two outer rings of the probe at 330.2 mm (13 in.) radius from the probe longitudinal centerline. Pressure sampling is obtained from a tube with the inlet collocated with the gas sampling inlet tube.

The temperature gage consists of two components, the deployable sensor unit and the electronics package. Before deployment the sensor unit is positioned behind the forward heat shield in the vicinity of the probe maximum diameter. Upon deployment the sensor unit is located in a region of high local dynamic pressure within the flow field. The sensor is extended approximately two centimeters beyond the probe boundary layer.

The temperature amplifier electronics package is mounted to the two outer rings at a 330.2 mm (13 in.) radius from the probe longitudinal centerline near the deployable sensor.

The neutral mass spectrometer analyzer and sampling system is a self-contained unit located symmetrically on the probe centerline. Attachment to the probe is accomplished by three fittings extending from the structural rings. The forward sampling section butts against the conical apex of the probe structure for deceleration and side-head restraint. This mounting arrangement provides for thermal expansion and high deceleration loads.

The gas chromatograph is packaged in a toroidal structural box, attached to adjacent probe structural rings. It is located next to the mass spectrometer to maintain a minimum-length sampling tube from the manifold.

The visible-IR flux meter is mounted to the aft equipment cover at the probe maximum diameter. A door in the aft heat shield is jettisoned to allow sensor deployment when subsonic speed is attained. A spring-loaded, four-bar mechanism extends the sensor outside the probe mold line into the free stream.

The nephelometer is located in the aft hemisphere of the probe near the maximum diameter, its view angle is perpendicular to the spin axis of the probe. The instrument is recessed within the probe to prevent the accumulation of atmospheric condensation or dust particles on an exterior window. A viewing port is opened in the heat shield at -3 $g_E \downarrow$just prior to the initiation of nephelometer measurements.

The energetic particle detector is housed in two packages. The detector with a directed aperture is mounted on the aft equipment cover at the probe maximum diameter. The electronics are packaged in the probe equipment section just forward of and adjacent to the energetic particle detector (aperture) package.

PROBE DESCRIPTION

The Jupiter probe design emphasizes use of current technology and flight-proven materials, hardware, subsystems, and components. The development phase is based on exploitation of existing testing and research facilities, established fabrication processes, and proven aerospace methods. The probe's size, shape and internal arrangement is not optimized for minimum weight; instead it is designed for minimum development risk. The goal is to achieve low technical risk through conservatism and moderate overdesign. Development confidence is increased which assures minimum cost through fabrication simplifications which preclude sophisticated validation testing.

Most of the structure, mechanisms, internal support, and other components (see Figure 48) have already been fabricated in Ames Research Center machine shops. A full-size engineering model, complete with installed ballast equipments, simulated heat loads, wire bundles, and insulation will be completed and available for structural, vibration, and thermal test validation early in 1975. A quarter size carbon-phenolic forward heat shield has been fabricated, and a full-size heat shield is scheduled for fabrication next year. This heat shield will be used on the engineering model. Many design tests, including sample inlet and contamination tests, mechanical systems tests, heat shield specimen characterizations, insulation characterizations, structural tests, vibration and shock tests, thermal tests, aerodynamic stability validations, antenna patterns, and communication simulations are also underway.

Probe Development

The feasibility of an entry probe into Jupiter's atmosphere combined with an orbiter based on the Pioneer spacecraft is the subject of considerable interest. Definition of a different mission imposes new uncertainties as noted in Figure 49. Based on previously gathered analytical and test data, the '79 & 80 opportunities were studied preliminarily to ascertain the adaptability of a probe designed for Saturn and Uranus entry to one for Jupiter entry. It is concluded that the latter mission's requirements are compatible with the design of the former missions (see Figure 50). Changes in the heat shield thickness and the communication power level and, perhaps, frequency are

PROBE CONFIGURATION

PJOP'80 ORBITER MISSION

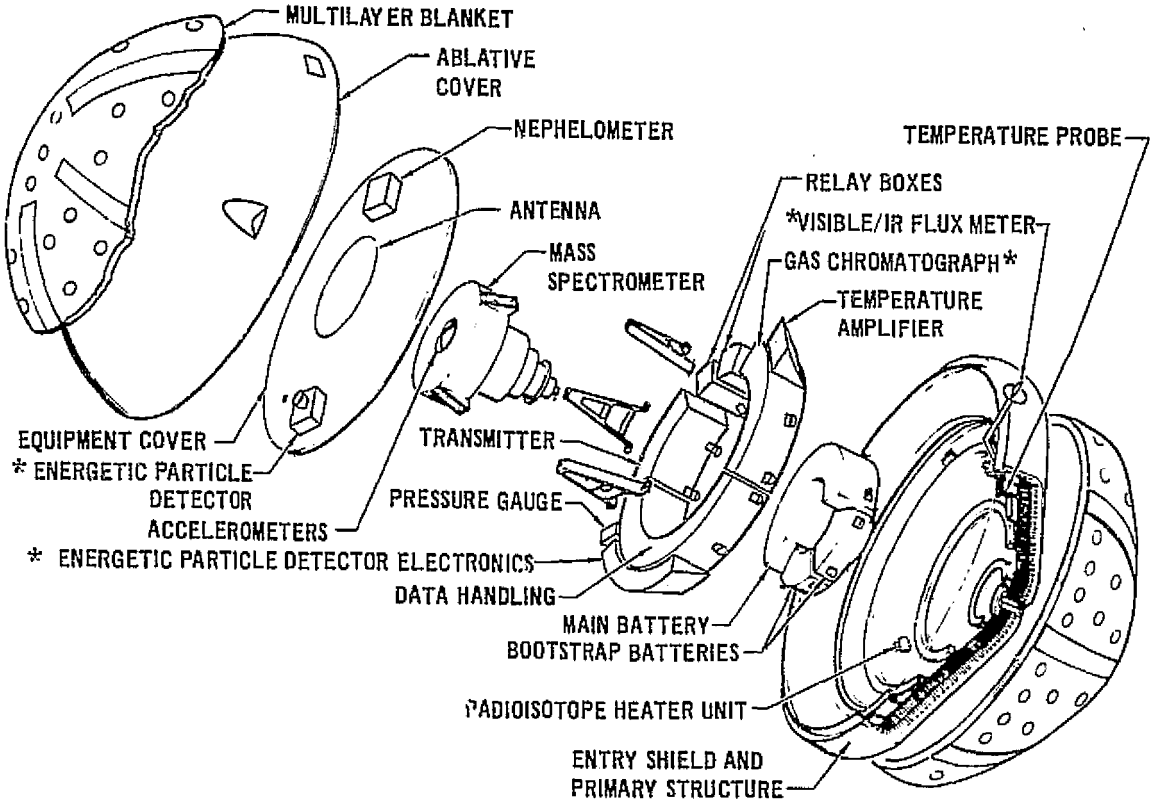

* NOT INCLUDED IN PJP'79 FLYBY MISSION STUDY

FIGURE 48

NEW MISSION UNCERTAINTIES

• TRAJECTORIES	ENTRY CONDITIONS PHASING TIME COMMUNICATIONS GEOMETRY ORBITER COMPATIBILITY
• ENVIRONMENT	TRAPPED PARTICLE MISSION DURATION
• ATMOSPHERIC DESCENT	DYNAMIC STABILITY ABLATION RATES THERMAL HISTORY
• COMMUNICATION LINK	LOSSES & TOLERANCES FREQUENCIES DATA RATES PREENTRY STORES
• SCIENCE	OBJECTIVES INSTRUMENTATION & COMMUNICATIONS
• ENERGY SOURCE	POWER PROFILE MISSION DURATION

FIGURE 49

CONCLUSIONS: PROBE DESIGN AND DEVELOPMENT

• DEVELOPMENT OF A JUPITER PROBE	34–36 MONTHS (1979 OR 1980)
• ORBIT INSERTION	6 MINUTES AFTER END OF PROBE MISSION
• TRAPPED PARTICLE RADIATION	SURVIVAL PREDICTED; HARDENING/SHIELDING REQUIRED
• ENTRY ACCURACY	$\pm 0.5^0$ OF AIMPOINT
• ENTRY HEATING PROTECTION	LAMINATED CARBON-PHENOLIC OR SILICA-SILICA
• SCIENCE PAYLOAD	PRE-ENTRY: STORED POST ENTRY: REAL-TIME AND STORE DUMPED
• STABILITY	SATISFACTORY AT $\alpha = 30^0$; IMPROVED AT $\alpha = 0^0$
• COMMUNICATIONS	GOOD WITH A 60 W, 44 BPS CONVOLUTIONALLY CODED RELAY LINK
• ELECTRICAL POWER	125 W-HOURS REQUIRED
• THERMAL CONTROL	INSULATION AND RADIOISOTOPE HEATER UNITS
• PYROTECHNICS	NASA SBASI OR EQUIVALENT
• INTERFACES – SPACECRAFT	SIMPLE; DEFINED EXCEPT FOR RECEIVER ANTENNA

FIGURE 50

required. The addition of instruments led to a reformatting of data as well as rearrangement of boxes, connectors and cabling. The net effect of these changes is an increase in power from earlier Jupiter entry studies; the increase can be accommodated. A shift aft in center of gravity also occurs which remains within acceptable dynamic stability boundaries; and an increase in heat load results which may lead to the use of heavier gages in black-box thicknesses to enhance heat sink capability.

The two primary hazards, viz., trapped particle radiation and entry heat protection require continuing study to obtain optimal solutions. The equipment section is partially shielded by the plastic and metallic structures. Any added metal for heat sinking automatically enhances particle shielding if placed on the vulnerable side. Care in timing of the entry can reduce the environment encountered by a factor of 4 or more. Entry heat protection can be provided by using either current state-of-the-art laminated carbon phenolic or by near-term silica-silica heat shield materials.

A probe development schedule of three years or less (Figure 51) is well balanced in terms of solving the important design problems early, validating all aspects of the spacecraft-probe combination prior to completion of flight hardware, and progressive fabrication of successive probes or modified models by a single probe team. A program free from single-point bottlenecks and multiple back-ups is thereby achieved.

Aerodynamics Analysis

The probe enters the atmosphere at a total angle of attack which is dependent upon the spacecraft/probe separation conditions. Upon entry into the planet's sensible atmosphere, the descent trajectory and aerodynamic properties will determine the probe's motion characteristics. Clearly, the motion-time history during hypersonic descent must be well established for the mission to ensure small angles of attack during peak heating and subsonic motion characteristics which are consistent with communications and science constraints. A six-degree-of-freedom trajectory analysis (which incorporates aerodynamic force-moment and stability test data) was used to predict the motion-time history for the Jupiter mission. Figure 52 presents the results obtained for two different initial angles of attack; the 29° entry is

OUTER PLANET PROBE

SUMMARY MILESTONE SCHEDULE - 1980 LAUNCH

o MINIMUM DEVELOPMENT TIME = 34 MONTHS

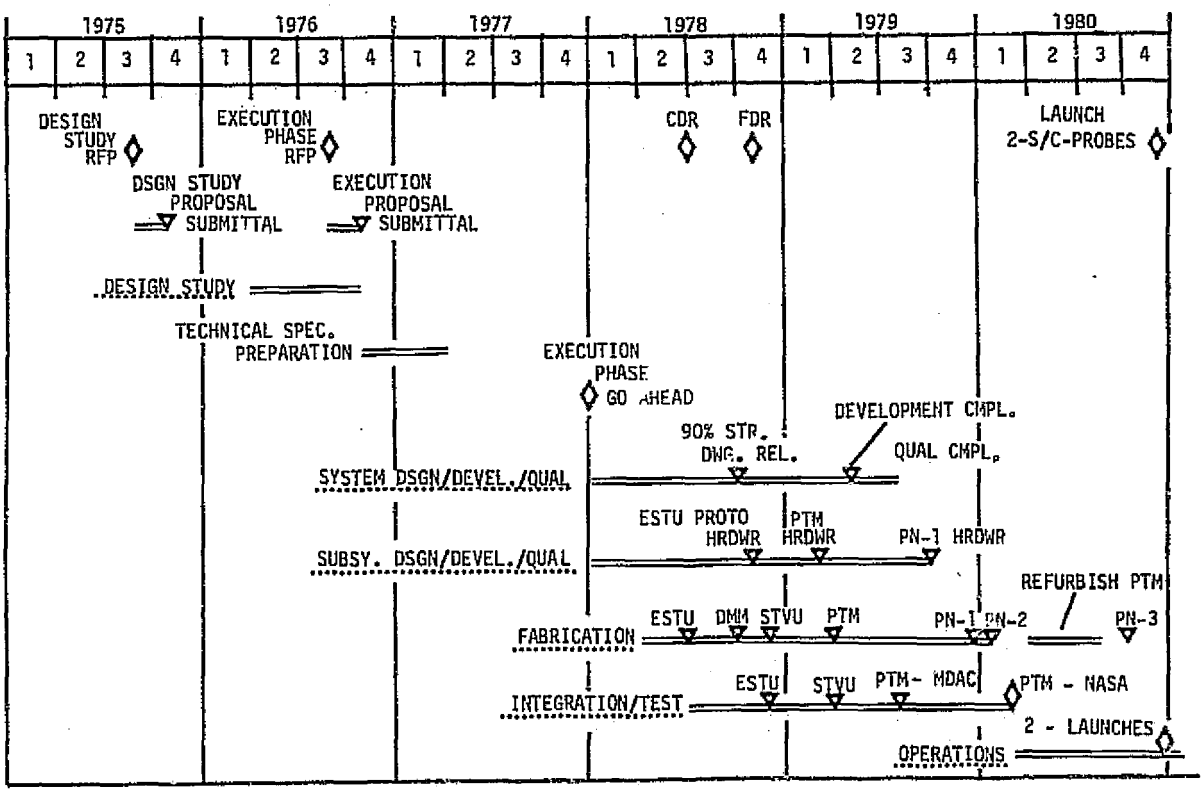

FIGURE 51

JUPITER ENTRY TIME HISTORY

(NOMINAL ATMOSPHERE MODEL)

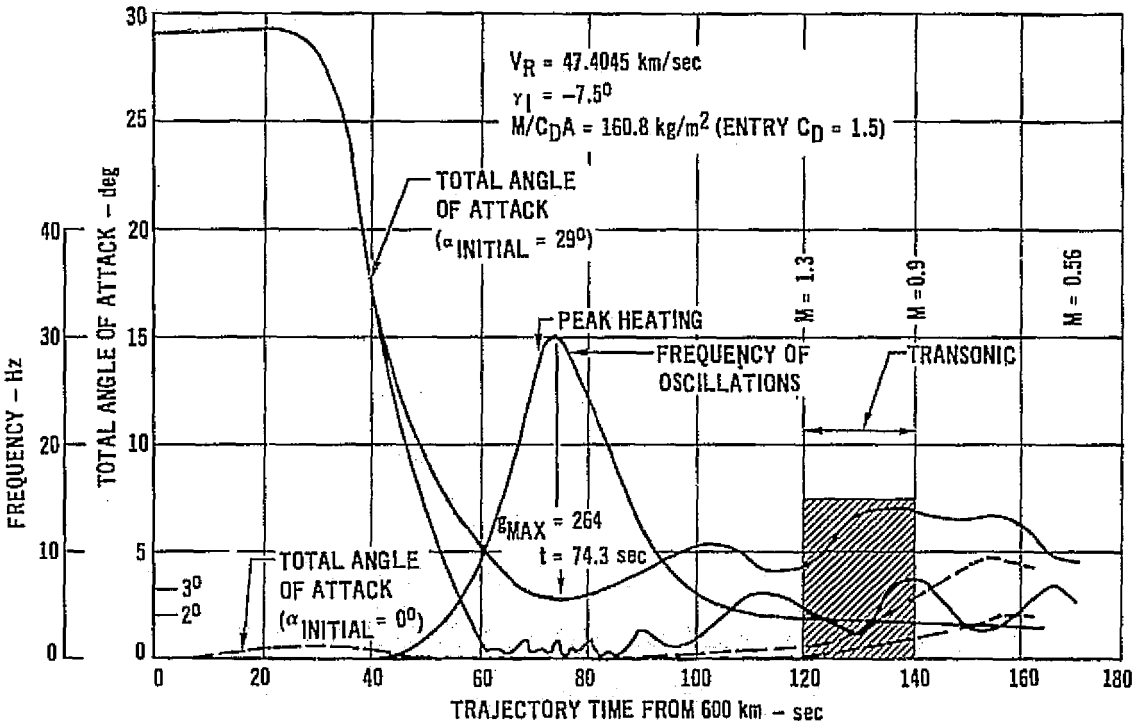

FIGURE 52

associated with a Pioneer mission which maintains Earth-lock during probe separation while the zero degree case reflects the entry angle of attack if the spacecraft breaks Earth-lock. Both calculations indicate low subsonic limit cycle oscillations (less than 7 deg) which are satisfactory for providing a solid platform for science measurements and which do not significantly degrade the communications subsystem. Entry at zero degree angle of attack results in a near zero degree angle at peak heating while the Earth-lock case exhibits a maximum angle of attack of 2.75 degrees at peak heating. The higher angle of attack at peak heating results in asymmetrical ablation and a lateral shift in the probe's center of gravity. Neither the severity nor the effects of the nonsymmetrical ablation have been assessed, as yet; but subscale tests of ablation are underway at Ames Research Center and at the McDonnell Douglas Astronautics Company.

The descent time history of a point mass is extended in Figure 53 to the end of tip-over. The entry flight path angle of -7.5 degrees limits entry decelerations to the $-300g_E$ level which is well within the original design value. The tip-over condition is completed by 5 minutes after entry.

Configuration

The major features of the Jupiter entry probe are illustrated in Figures 48 and 54. The probe is a compact, blunted 60 degree half-angle cone forebody and a hemispherical afterbody. The forebody is a single piece, machined carbon-phenolic sphere-cone 889mm (35 in.) in diameter. The afterbody is a fiberglass-phenolic honeycomb hemisphere (45 cm spherical radius) filled with a low density elastomeric ablation material. The forward ablator is a 5.35 cm (2.1 in.) thick carbon phenolic of 1441 kg/m^3(90 lb/ft^3) density. The billet for this heat shield is made by layering carbon-phenolic cloth and forming it under heat and pressure up to 690 N/mm^2 (1000 psi). The heat shield is sized to dissipate the Jupiter entry heat load (primarily by ablation) that is calculated for a Jupiter Nominal atmosphere at an entry angle of -7.5 degrees.

Two ejectable plugs are fitted into the heat shield. One is located at the center of the sphere-cone and accommodates the extension of the atmospheric sampling tube for the mass spectrometer, the gas chromatograph and the total pressure gage. The other plug allows the extension of the atmospheric total

DESCENT TIME HISTORY
JUPITER NOMINAL ATMOSPHERE

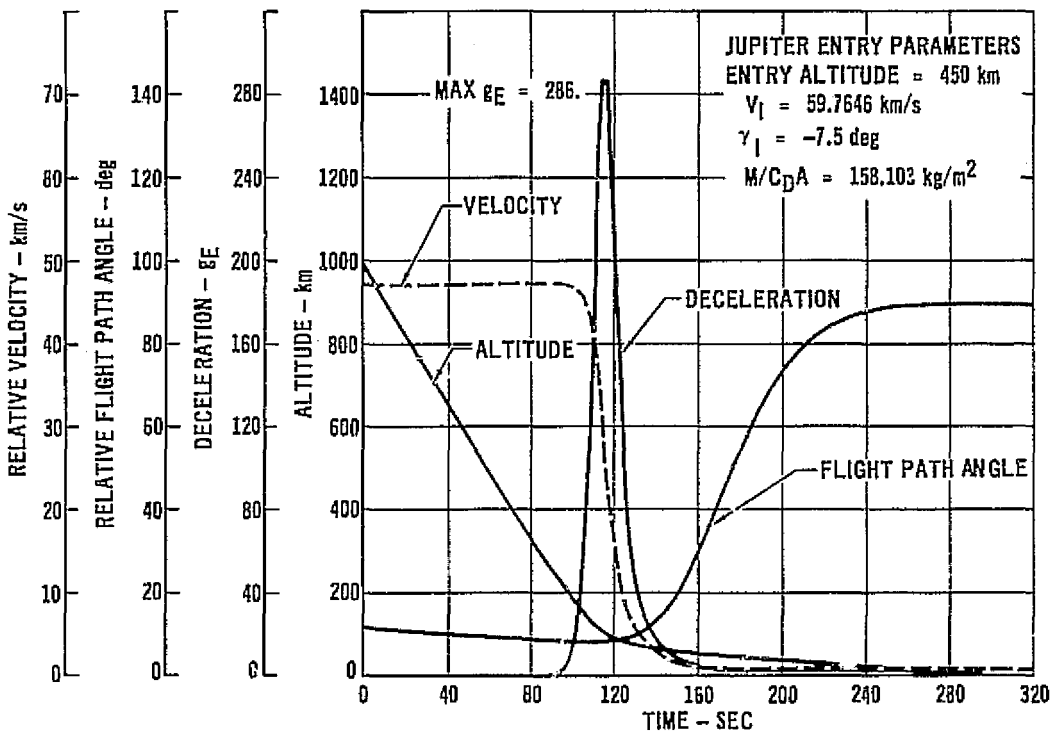

FIGURE 53

PROBE LAYOUT

PJOP'80 ORBITER MISSION

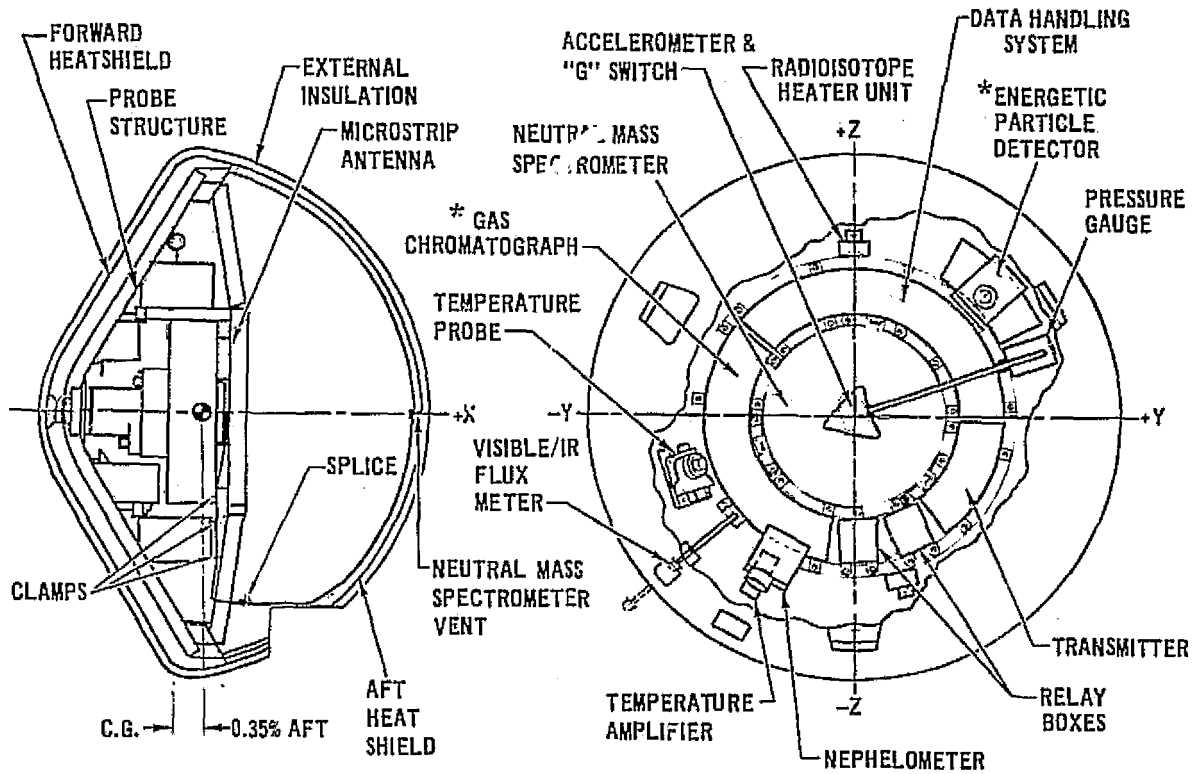

* NOT INCORPORATED IN PJP'79 FLYBY MISSION

FIGURE 54

temperature sensor and is located on the conical section. When initiated by the appropriate accelerometer readout, both plugs are ejected after maximum entry heating and at subsonic free-fall velocity.

The probe's primary structure is a 1.52 mm (.060 in.) aluminum (7075-T351) cone (coolie hat) with 5 integrally machined concentric rings. This structural cone is machined from a formed conical billet 5.1 cm (2 in.) thick. The two outer most rings are closed to form a box ring section by mechanically attaching a pressed "L" ring of 7075-T351 aluminum sheet stock (.063 in.). This outer box ring is the major structure to which the afterbody is attached by 31 circumferential bolts. All fasteners used in the probe are titanium. Attachment to the Pioneer spacecraft is at 3 stainless steel attach fittings located 120° apart around the afterbody. The recessed attach fittings are bolted to the fiberglass honeycomb afterbody dome. Launch loads are transmitted through the 3 attach fittings, and the loads are distributed to the primary structure at the outermost box ring. The three inner machined rings support the bulk of all the probe's support equipment and the instruments. A 2.15 cm (.85 in.) thick 1/4 8.5 fiberglass honeycomb core is bonded by a high temperature adhesive to the outer surface of the machined aluminum cone. The fiberglass-phenolic honeycomb core has an outer fiberglass facesheet 1.27 mm (.050 in.) thick. The machined one piece carbon-phenolic heat shield is bonded to this face.

The primary structure described above is designed for entry decelerations of 800 g_E with a safety factor of 1.25. This level, though not required in a low angle entry into a Jovian atmosphere is retained in the interest of commonality. A 28% weight reduction potential exists in the structural components for a dedicated Jupiter low angle entry (-7.5 deg) probe. The bonded attachment of the heat shield to this structure is not considered additive to the structural strength. The nearly circumferential arrangement of the component containers distributes the individual inertia loads to the conical honeycomb structure almost uniformly. These individual loads are uniformly balanced by the atmospheric pressure loads that impinge on the heat shield face during entry, so that a minimum of bending is present on either the carbon-phenolic heat shield or on the primary sandwich-type structure.

The aft heat shield is non-structural except for its own inertia loads. It consists of a hemispherical fiberglass honeycomb sandwich 0.6 cm (.25 in.) thick (two .012 in. fiberglass facesheets) to which is bonded a 0.6 cm (0.25 in.) thick open honeycomb core. The core is filled with a low density elastomeric ablator by a vacuum injection technique. The external appearance of the assembled probe is striking. The forward cone section is smooth dull black, while the aft dome is flat white finely detailed by the 0.25 in. honeycomb cell pattern. The afterbody is transparent to radio frequency energy for data transmission and is below 2.5 gm/cm^2 equivalent mass density to facilitate sensing of trapped particle radiation internally.

Mass Properties

The probe mass properties requirements are:

- The center of gravity (c.g.) should be as far forward as possible and on the roll axis. Tests indicate c.g. positions progressively greater than two percent aft of the theoretical diameter, i.e., aft of the intercept plane formed by extending the forebody/afterbody surfaces causes an increasingly unstable aerodynamic configuration.
- The roll inertia must be large relative to the pitch or yaw inertia; ratios greater than 1.2:1 are acceptable.
- The principal axis must coincide with the roll axis. All cross-products and c.g. eccentricities must be nulled to provide a known attitude at the beginning of entry.

A goal of the design activity has been to make a Jupiter entry probe that is of the order of 150 kg (330.75 lb). The data of Figure 55 and 56 demonstrate that such a goal is realizeable in both an orbiter and a flyby mission to Jupiter. Of particular significance is the fact that the science payload represents 14 percent of the take-off weight (20 percent of the end of the mission of a PJOP'80 mission. This has been achieved through careful design of the heat shield, restriction of the communications power level and a relatively short atmospheric descent period. The PJP'79 design has a heavy weight neutral mass spectrometer; both have reduced weight corner designs.

Estimates, based on Aerotherm nominal Jovian analyses, were made of the thickness required to fulfill the requirements of ablative recession and of mechanical erosion. An example of recession due to sublimation and erosion is

MASS PROPERTIES

PJO_P '80 ORBITER MISSION

SUBSYSTEM	MASS (kg)
STRUCTURE	13.3
HEAT SHIELDS	68.6
HEATERS & INSULATION	6.9
COMMUNICATIONS & DATA HANDLING	10.3
ELECTRICAL POWER	9.3
PYROTECHNICS	3.7
SCIENCE PAYLOAD	20.4
INSTRUMENTATION	0.7
WEIGHT MARGIN (10%)	13.3
PROBE WEIGHT	146.5
LESS:	
INTERFACE WIRING	-1.1
EXTERNAL INSULATION	-2.6
AT ENTRY	142.8
LESS: ABLATION MATERIAL	-42.0
END OF MISSION	100.8
C.G. & INERTIAS AT ENTRY	
X AXIS C.G.* (PERCENT)	0.35
I_X (ROLL) $CM^2/10,000$	11,262
I_Y (PITCH) $CM^2/10,000$	6,884
I_Z (YAW) $CM^2/10,000$	6,833

*EXPRESSED AS PERCENT OF DIAMETER AFT OF THE CONICAL FOREBODY AND THE SPHERICAL AFTERBODY.

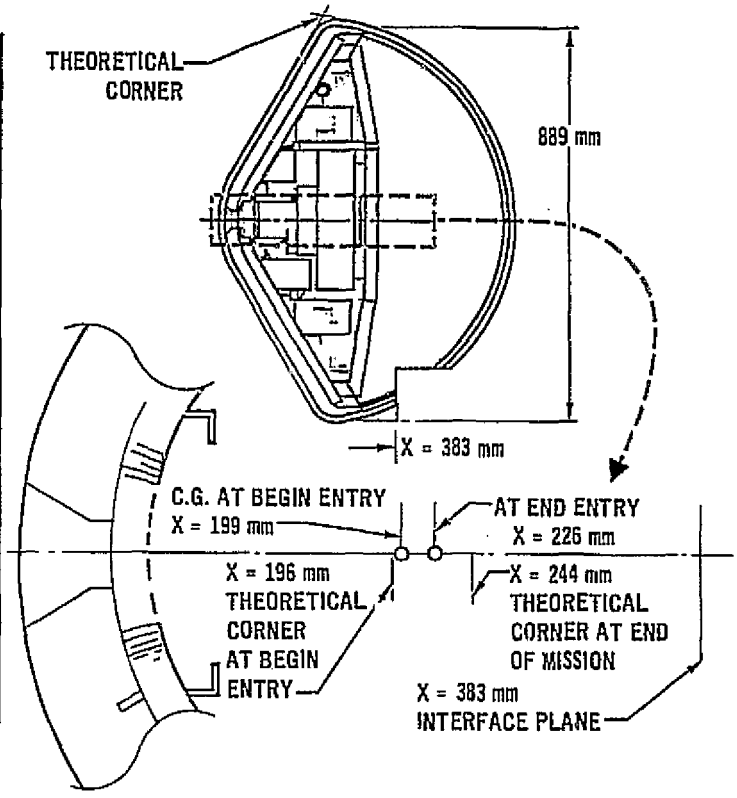

FIGURE 55

MASS PROPERTIES

PJF 79 FLYBY MISSION

SUBSYSTEM	WEIGHT LB
STRUCTURE	30.06
HEAT SHIELDS	151.18
HEATERS & INSULATION	15.32
COMMUNICATIONS & DATA HANDLING	21.09
ELECTRICAL POWER	20.43
PYROTECHNICS	8.24
SCIENCE PAYLOAD	32.88
INSTRUMENTATION	1.60
WEIGHT MARGIN (10%)	27.97
PROBE WEIGHT	308.77
LESS:	
INTERFACE WIRING	−2.35
EXTERNAL INSULATION	−5.86
AT ENTRY	300.56
LESS: ABLATION MATERIAL	−92.59
END OF MISSION	207.97
C.G. & INERTIAS AT ENTRY	
X AXIS C.G.* (PERCENT)	0.03
I_X (ROLL) – SLUG FT^2	7.074
I_Y (PITCH) – SLUG FT^2	4.923
I_Z (YAW) – SLUG FT^2	4.793

*EXPRESSED AS PERCENT OF DIAMETER AFT OF THE CONICAL FOREBODY AND THE SPHERICAL AFTERBODY.

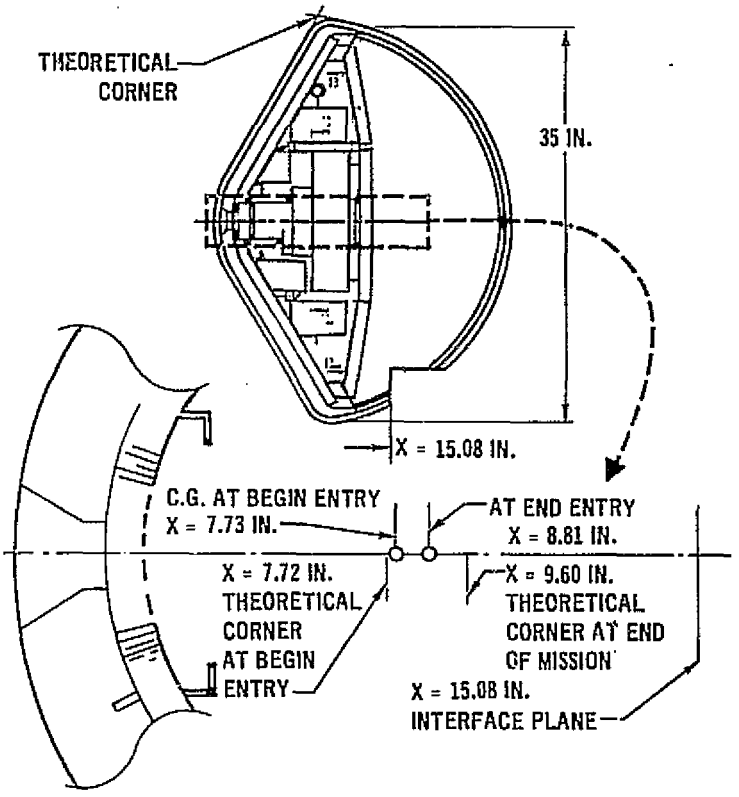

FIGURE 56

shown in Figure 57. A standard thickness for insulation is used for estimates based on analysis and extrapolation of current data available. The 125 kg/m^2 serves as an acceptable average for first order effects. Progressive refinements are underway in modeling this change.

An evaluation of ballistic coefficient as a function of time reveals that M/C_DA decreases as material is consumed during entry. Since mass loss exceeds base area decrease, the ballistic coefficient decreases as illustrated in a γ = -7.5 deg into a Nominal model. (Note: C_D variation with Mach number is also accounted for in this curve.) Thermochemical recession accounts for a nominal 3.3 cm and mechanical erosion 0.9 cm at the stagnation point for a probe having a typical value of 125 kg/m^2 constant coefficient as shown in Figure 57. The value changes during the mass loss more nearly as shown in Figure 58. A ramp change in M/C_DA will be incorporated into heat protection studies, and, then, when all first and most second order effects (such as surface roughening) are understood a curve of M/C_DA will be used to define mass loss which will use total heat or heating rates as the independent variable. These steps will steadily improve probe flight characterization, especially deceleration rate and mass loss rate.

The design of the heat shield was found to be ultra-conservative at the corners. A time history of predicted recession indicated that some thinning could be accomplished. The drive to do so is based on center of gravity location rather than weight reduction, per se. Figure 59 illustrates the progressive change in corner dimensions, assuming uniform ablation. Note that internal dimensions of the forebody structure are also affected. The reduction in weight does partially offset weight added in the science payload.

Equipment Arrangement

The probe internal equipment is packaged in toroidal segments that fit between the integrally machined rings. The equipment is attached to the rings by simple lug fasteners. The purpose of tailored equipment packaging

C-2

CARBON PHENOLIC RECESSION HISTORY

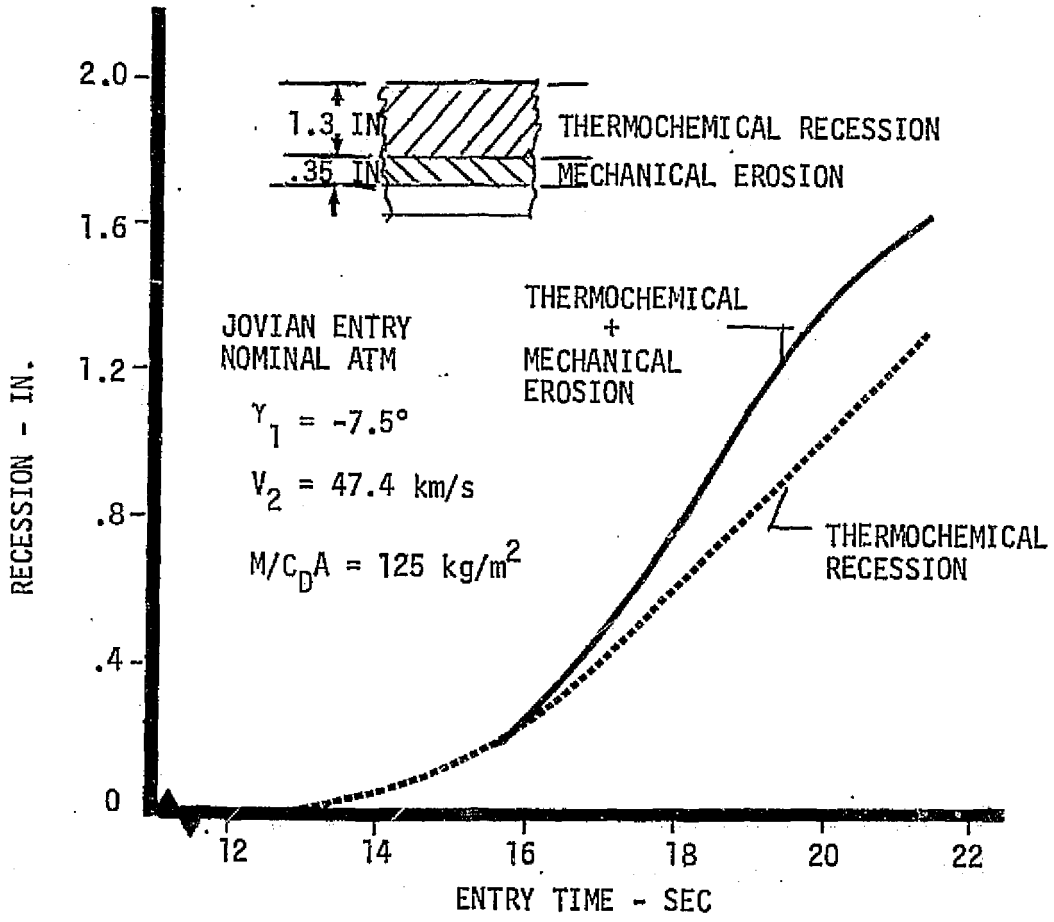

FIGURE 57

BALLISTIC COEFFICIENT VS ENTRY TIME

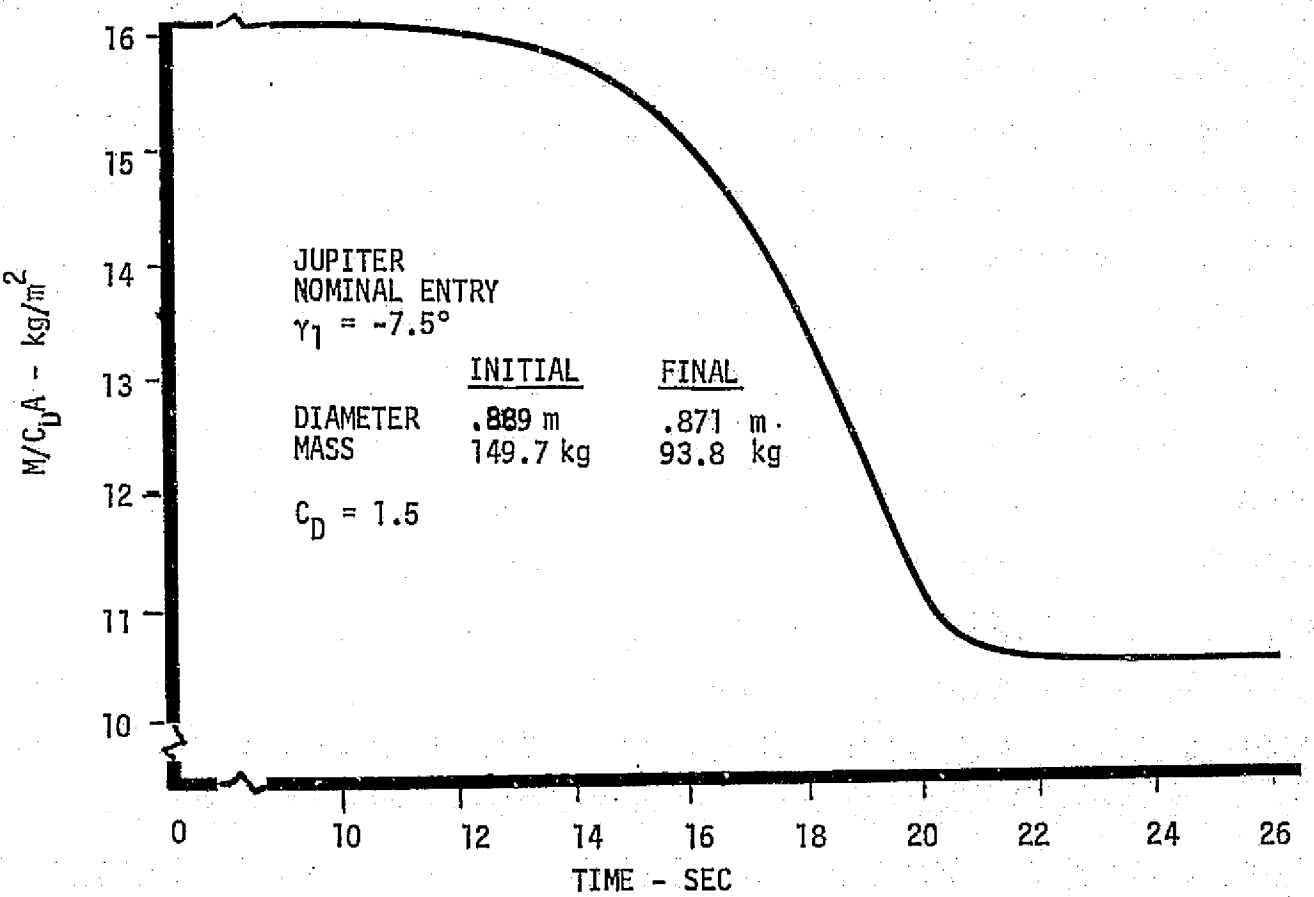

FIGURE 58

HEAT SHIELD CORNER RECESSION

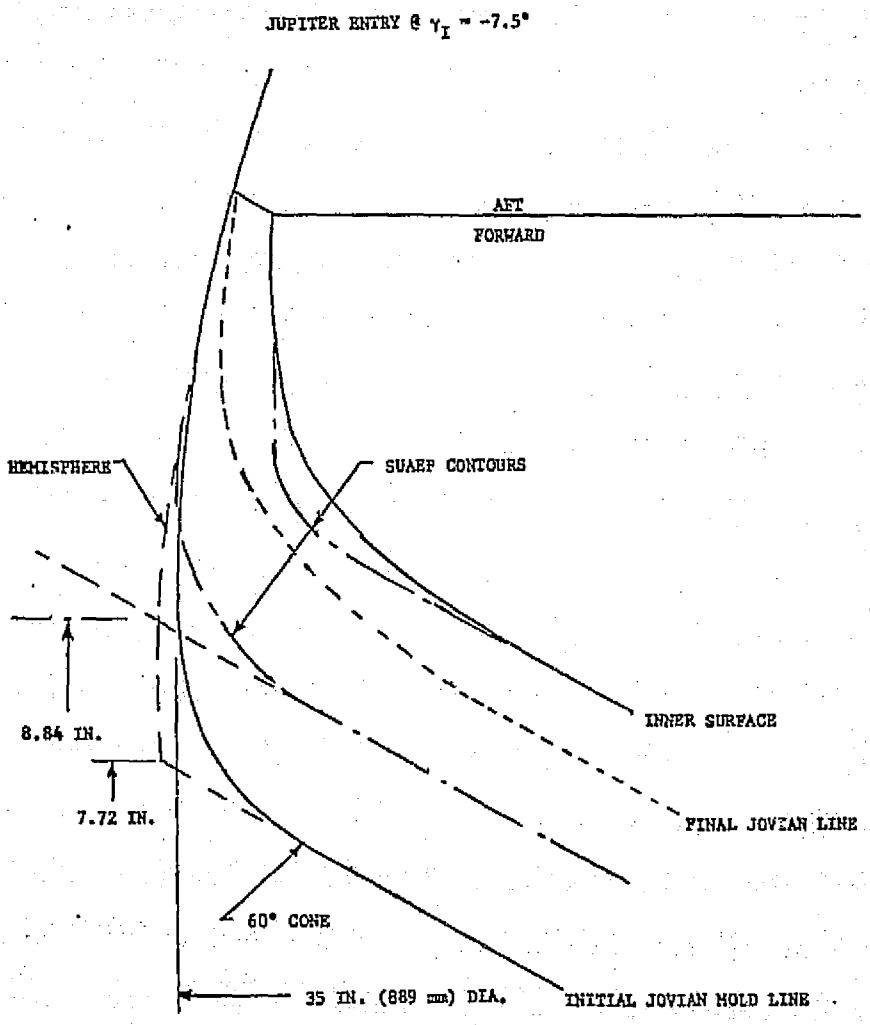

FIGURE 59

is to keep the probe center of gravity forward, to provide uniform load distribution, and to achieve a $I_{roll}/I_{\perp}$ ratio of 1.65. These factors increase aerodynamic static and dynamic stability and pre-entry spin-stability. They also assist in maintaining uniform internal temperature distributions. The toroidal arrangement includes circumferential wiring and peripheral connectors. The entire equipment section is enclosed by a foam-insulated cover that is attached to the outer structural box ring and supported in the center by 3 bipod fittings that bear on the inner rings. A disc-shaped (34.3 cm dia. x.32 cm thick) micro-strip antenna is supported on the equipment cover under the 2.54 cm foam insulation. The antenna has an unrestricted beam width of more than 90 degrees through the aft hemispherical heat shield.

The aft heat shield has an access door for arming the probe's pyrotechnic systems and one or two jettisonable ports for science instrument viewing and deployment, depending on mission instrument complement. The ports are jettisoned by compressed spring energy which are released by pyrotechnic bolt cutters. The aft heat shield has a small hole for passage of the probe-to-spacecraft umbilical. This umbilical is severed close to the surface of the probe by a spacecraft-adapter-mounted, pyrotechnic cutter just prior to probe release from the carrier bus.

The probe internal temperature control is a semi-passive system. While the probe is attached to the spacecraft, internal temperatures are maintained by thermal evolution of radioisotope heaters with some output to the three spacecraft adapter attach points. Temperature sensors, located on the spacecraft adapter, control the heaters on the adapter when temperature regulation is required. After separation the internal temperature is maintained between acceptable equipment limits by calculated heat balance between the internally generated heat from radio-isotope heater units (RHU's of 1 watt each) and conductive/radiative losses through the probe structure and an external multilayer insulation blanket. The main heat loss is via the same three attachment points. The external blanket is made of 25 layers of goldized mylar separated by insulative plastic-net separators. The blanket is nominally 1.27 cm (.50 in) thick. The insulation is tuned or adjusted in transmissibility before flight by removing partial patches that are built into the outer layers of the insulation.

The configuration for probe stowage on the Pioneer spacecraft is on the bus' shadowed side. Probe release from the spacecraft is by simultaneous gas activation of three ball-lock release devices. Separation is also accomplished by these three ball-lock release devices. Separation is accomplished by 3 matched springs mounted concentrically with these release fittings. The three springs impart a 0.5 m/sec relative separation velocity. Once released the probe functions fully autonomously; the spacecraft initiates the deflection maneuver after a timed interval that ensures adequate physical clearance of the probe. Premature firing of deflection thrust chambers could alter the probe's attitude even though it is rotating at five revolutions per minute. This spin-rate is the nominal spin-rate for the Pioneer spacecraft but is a satisfactory balance between high rates to get uniform ablation during entry and low rates to aid rapid tip-over in the atmosphere. The spinning during descent to the atmosphere also maintains the probe axis aligned to the release condition. In the case of an undeflected Pioneer this attitude is Earth-line oriented. For either a Mariner release or a deflected Pioneer release the attitude is a zero angle of attack at peak heating attitude as described under System Analysis.

Radiation Environment

The pre-entry environment of Jupiter is considered to be hazardous to an entry probe in that particles are trapped in the magnetosphere. The deleterious effects of the radiation emitted by the trapped electrons and protons can be minimized by synchronizing the approach to penetrate the wobbling magnetodisc at a favorable time. A typical trajectory for the probe was established to permit analysis of the radiation dose to be encountered by a probe. The dose rates as a function of radial distance for the trajectory are plotted in Figure 60 for three typical phasings. By parametrically choosing different phasing angles for passage through the particle belt various total doses can be obtained. The results of this analysis are illustrated in Figure 61. They show a distorted sine wave and a variation of up to four in total dose. It is apparent from the absolute values shown, that synchronizing the approach to alleviate the exposure is a mission constraint that should be imposed. Fortunately, the planet rotates rapidly, so imposition of a specific phasing does not overly restrict the

JUPITER DOSE RATE PROFILES FOR DIFFERENT PHASING ANGLES

o PJO_p '80 ORBITER-PROBE MISSION

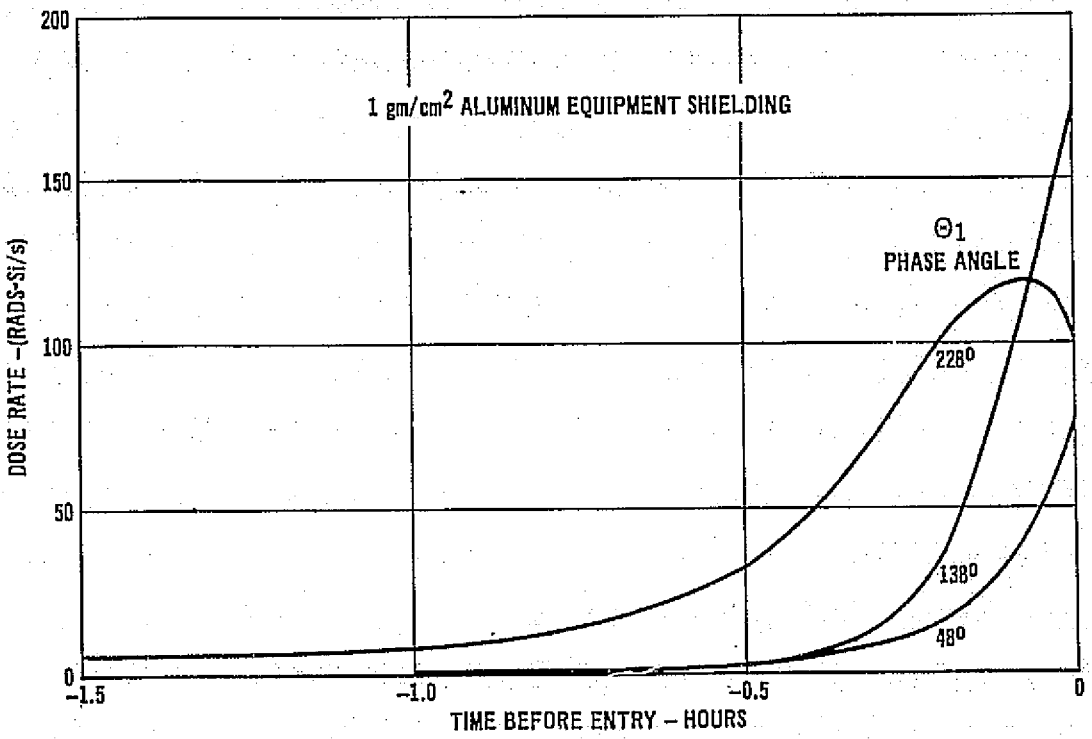

FIGURE 60

JUPITER ENTRY PROBE RADIATION EXPOSURE

- PIONEER 10 MODEL OF TRAPPED PARTICLES
- D_2 MODEL OF MAGNETOSPHERE
- 1 gm/cm^2 ALUMINUM EQUIVALENT SHIELDING

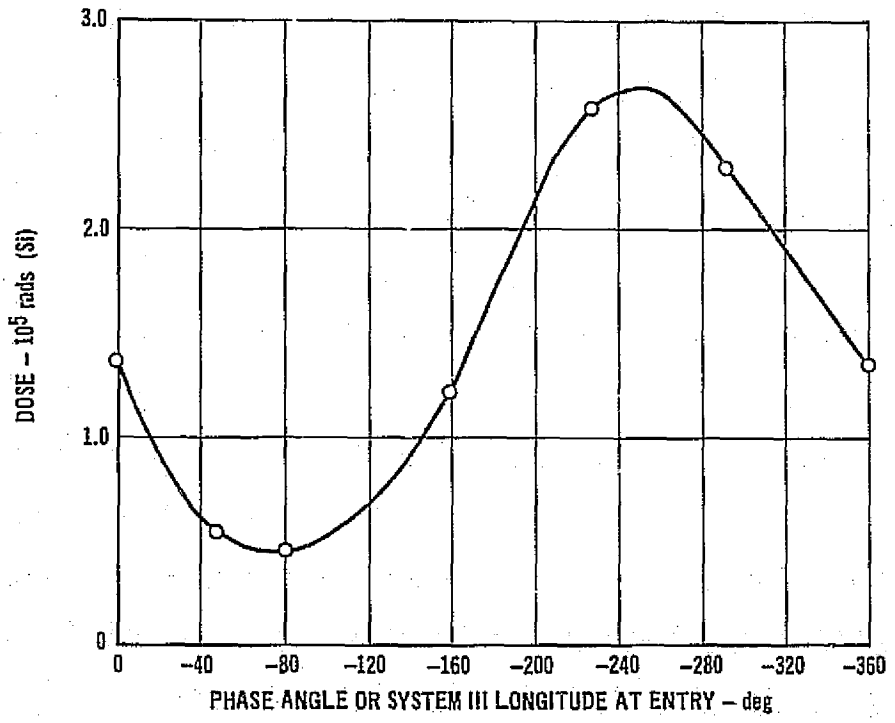

FIGURE 61

choice of entry windows. The synchronization requirements are added to the latitude, entry angle and entry velocity requirements.

The structure of the probe inherently contains some shielding for the electronics. The packages by and large are all within a thick carbonaceous and metallic cone that extends well back. The most vulnerable direction is aft where the materials provide very little mass shielding. The more energetic particle radiation will pass through the aft heat shield to the equipment section. A rigorous study is underway on the shielding provided by metal boxes and other materials, jointly by TRW and McDonnell Douglas Astronautics. The study will proceed to selection of internal components that are resistant to high energy radiation.

Instrument Installation

The science instruments are located in the probe as shown in Figure 47. In each case primary consideration was given to packaging for survival of high deceleration entry loads and c.g./balance constraints.

Of the five science instruments three viewing instruments (visible/IR flux meter, nephelometer and the energetic particle detector) are installed aft of the equipment cover. There instruments require thermal insulation wrap to maintain in-transit temperature (nonoperating) of -40°F to +20°F. The remaining instruments inside the equipment cover are maintained within their temperature limits.

The accelerometer package is attached to rigid structure in the hub section of the mass spectrometer analyzer section. This positions the longitudinal accelerometer axes along the center line of the probe with the proof mass as close as possible to the probe's center of gravity.

The pressure gage is located between the two outer rings of the probe at 13 in radius from the probe longitudinal center line. Pressure sampling is obtained from a tube with the inlet collocated with the mass spectrometer inlet probe.

The temperature gage consists of two components, the deployable sensor unit and the electronics package. Before deployment the sensor unit is positioned behind the forward heat shield in the vicinity of the probe maximum diameter.

Upon deployment the sensor unit is located in a region of high local dynamic pressure within the flow field. The sensor is extended approximately two centimeters beyond the probe boundary layer.

The temperature amplifier electronics package is mounted to the two outer rings at a 13 in.radius from the probe longitudinal centerline near the deployable sensor.

The neutral mass spectrometer and sampling system is a self-contained unit located symmetrically above the probe centerline. Attachment to the probe is accomplished by three fittings extending from the structural rings. The forward sampling section butts against the conical apex of the probe structure for deceleration and side head restraint. Their mounting arrangements provides for thermal expansion and high deceleration loads.

The gas chromatograph is packaged in a toroidal structural box, attached to adjacent probe structural rings and located next to the mass spectrometer to provide minimum length sampling tubes. The tube is tapped from the mass spectrometer inlet manifold.

The visible/IR flux meter is mounted to the aft equipment cover at the probe maximum diameter. A spring-loaded,four-bar mechanism extends the sensor outside the probe mold line in the free stream. A door in the aft heat shield is jettisoned to allow sensor deployment .

The nephelometer is located in the aft hemisphere of the probe near the maximum diameter and looks out perpendicularly to the spin axis of the probe. The instrument is recessed within the probe to prevent the accumulation of atmospheric condensation or dust particles on an exterior window. A viewing port is opened in the heat shield at -3 g_E just prior to the initiation of nephelometer measurements.

The energetic particle detector is housed in two packages. The detector aperture is mounted on the aft equipment cover at the probe maximum diameter. The electronics are packaged in the probe equipment section just forward and adjacent to the detector aperture package.

SUBSYSTEM DESIGN

The subsystems of the entry probe have all been reexamined to assure compatibility with the objectives and requirements of a Pioneer Jupiter Probe in 1979 and a Pioneer Jupiter Orbiter Probe flight in 1980. The subsystem most affected by these missions is the communications. Because the orbiter mission is more constrained by the exigencies of having to enter an orbit immediately after the receipt of probe-gathered data, this particular mission (PJO_P'80) is herein described. Both missions are difficult, but fewer options are open in the orbiter-probe mission. The attenuation of the signal and the geometry necessitate increasing power to a 60W level; and up to 90 W is not out of the question if adverse tolerances are worse than those assumed.

The heat protection subsystem is slightly changed from earlier entry studies. Refinements in analysis and the accumulation of data, (that the real atmosphere lies near Nominal and Warm models) leads to the conclusion that modest reductions in protection can be effected especially at the corner. The science and engineering instrument additions coupled with a transmitter power increase consumes more of the energy provided than that previously reported.

Thermal studies indicate that equipment temperatures rise at a faster rate entering Jupiter but, as yet, not critically in the short duration Jupiter descents. The pyrotechnics have changed because the continuous flow neutral mass spectrometer is accommodated. This report illustrates a continuous type, but a repackaging study is incomplete. The analysis and data rates are based, however, on the continuous form which is now the baseline instrument.

Entry Heat Protection

Entry into Jupiter will impose a severe entry heating environment that must be dissipated by an efficient and reliable heat protection system. To reduce the magnitude of heating, it is desirable to enter the planet at as shallow an angle (within the aiming uncertainties) as practicable, near the equator (to obtain the maximum benefit of the planet's rotation) and to utilize a blunt configuration with low ballistic parameter (in order to decelerate at high altitudes). Figure 62 illustrates the heating and

JUPITER SHALLOW ENTRY ENVIRONMENT

- NO BLOWING
- STAGNATION POINT

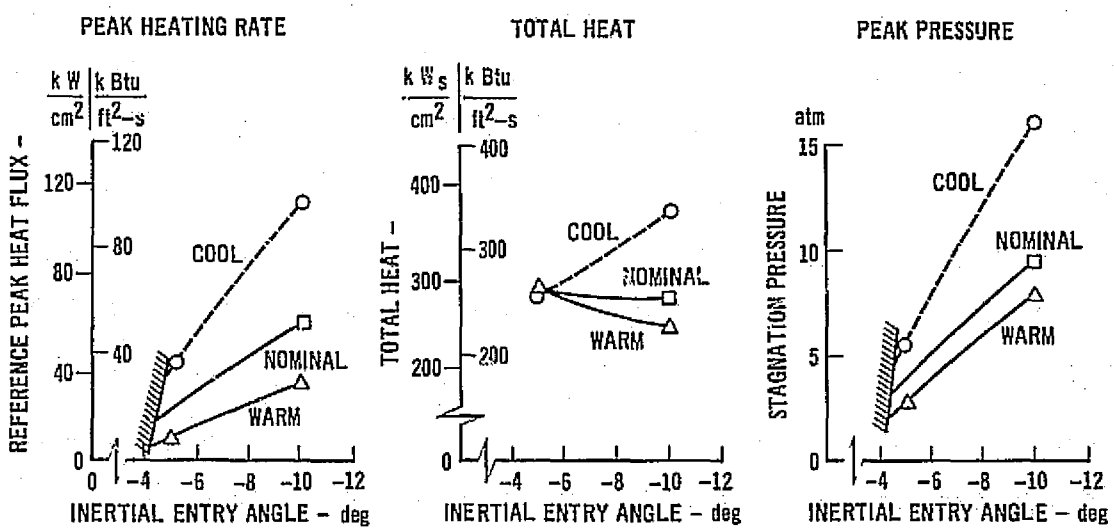

FIGURE 62

pressure environment associated with shallow entries for the three monograph models (Reference 5 defined atmospheres). Preliminary analyses of the Pioneer 10 atmospheric structure experiments indicate an atmosphere model, at least in the high altitudes where heating actually occurs, that is very similar to the monograph defined Nominal Jupiter model. The probability of entering at shallow angles into an atmosphere,that produces less severe heating than the Cool or the Nominal model,can greatly alleviate the heating problem and make the Jupiter mission within the realm of feasibility of state-of-the-art heat protection designs.

Figure 63 shows a comparison of the net heating and pressure histories expected for Jupiter probe entry with the environment encountered by a missile control surface (flap) protected with a carbon phenolic heat shield. The comparison is in terms of net heating reaching the surface, that is, the reduction in heating due to blowing has been accounted for. The main difference in the two environments is that the (net) heat flux reaching the surface of an outer planet probe is primarily radiative and the shock layer gas is a mixture of hydrogen/helium, whereas, in missile flights the heating is convective and the shock layer gas is oxygen-rich air. The difference in gas composition should have very little effect on material performance because the surface is in the sublimation regime during the high heating regime. This conclusion has been verified in available ground test facilities. The difference in material performance between a convective versus a radiative environment should be small since carbonaceous materials are opaque to radiation and absorb the incident radiative energy at the surface just as in the instance of convective heating. In other words, both forms of energy are absorbed on the surface and this energy is primarily dissipated by sublimation of the carbonaceous char. The rate of sublimation and the recession rate are dependent on the incident energy flux whether radiant or convective(or both)to the surface. Therefore, the probe heat shield that receives the higher energy flux, as shown in Figure 63, will recede at a faster rate. On the other hand, the heat shield in both entry cases will attain similar surface sublimation temperatures. Note that entry surface pressures are similar. In both cases, the heat shield will have thin but similar char layer thickness due to the high recession rates. Therefore, both will experience steep, though similar,

APPLICABLE ENTRY HEATING FLIGHT EXPERIENCE

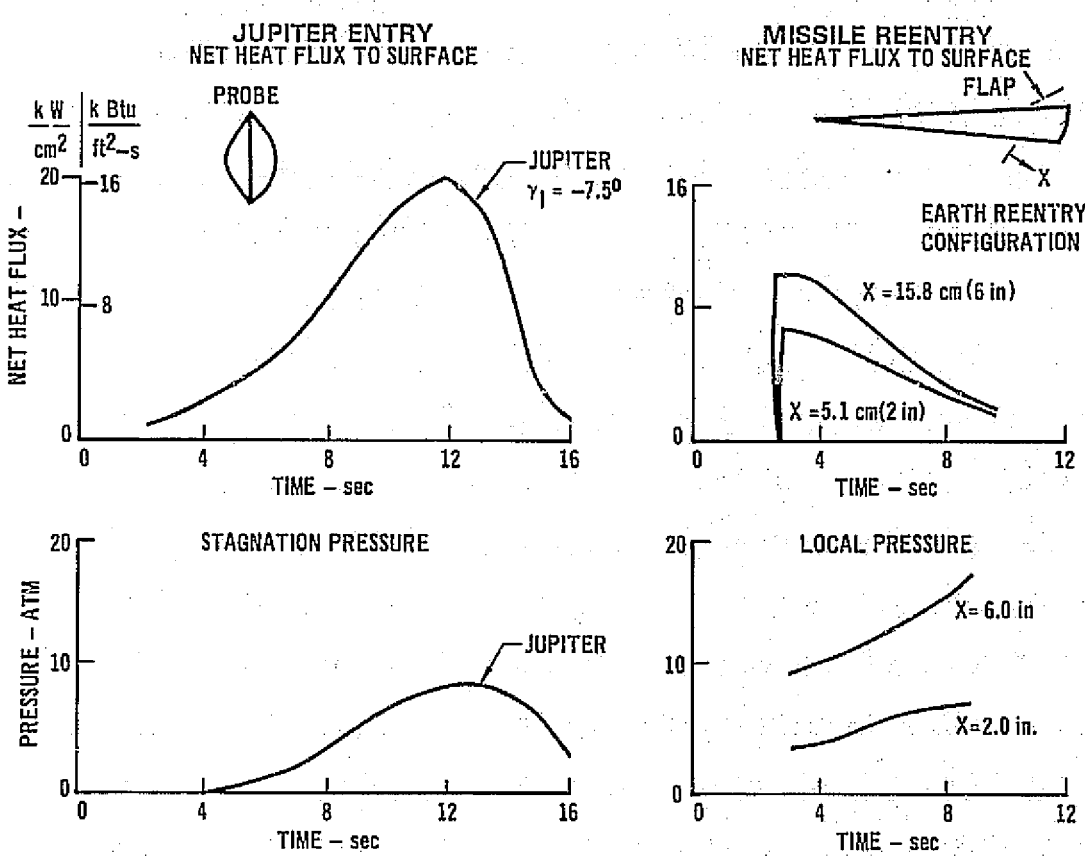

FIGURE 63

temperature gradients in the char which means similar char thicknesses and temperatures on both sides of the char layer. This similarity permits direct application of the missile flap technology data to validate the probe heat shield design at this stage of probe development.

Figure 64 presents the carbon phenolic heat shield thicknesses and weights needed to limit the fiberglass substructure face to 700°K (800°F) maximum for the design value of entry angle (γ = -7.5 degrees). Because of the intense heating environment, a large portion of the initial thickness is consumed by sublimation (herein labeled thermochemical recession) and by mechanical erosion as estimated from missile flight data correlations. For the shallow entry envelope shown, about 35 to 45% of the probe weight must be allotted to heat protection.

CARBON PHENOLIC HEAT SHIELD REQUIREMENTS

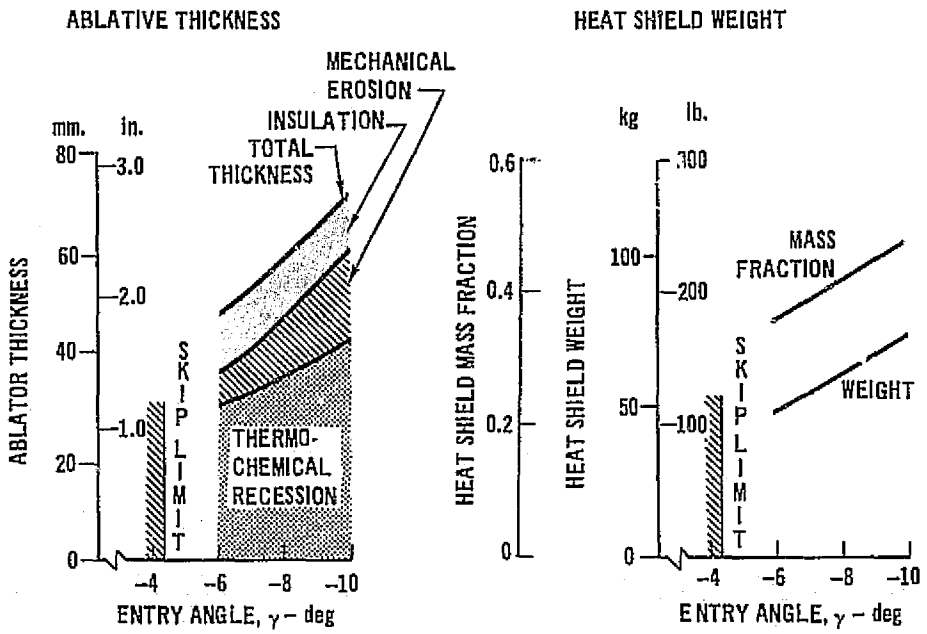

FIGURE 64

New advances in heat shield technology have been aimed at developing materials that reflect the incident shock layer radiation rather than absorbing it as do carbonaceous materials. A high density, high purity all-silica material appears to be the most promising reflective heat shield material and is currently being developed at MDAC-E. A characteristic of the reflective concept is that heat shield weights decrease with steeper entries, since a greater portion of the incident heating is radiative, thus the shallow entry constraint

($\alpha < -15°$) required for the carbon-phenolic heat shield may be modified if the reflective material achieves the good performance indicated by preliminary work. This achievement is sought because communications are enhanced by steep entries ($\gamma > -7.5$ degrees), whereas, heat protection thicknesses are decreased by shallow entries (-7.5 degrees > γ > skip-out boundary of -4 degrees).

The design of the structure is essentially unchanged from the description given in Reference 1. There are differences in the precise shape of the outer ring and in hole patterns on the attachment rings, but these are superficial. Hence, repetition is unnecessary.

Telecommunications

The telecommunications subsystem design is based on the Ames Research Center trajectories and the recommended Outer Planets Probe Science Advisor Group science payload in Figure 46. Details of the analysis of this design are contained in Reference (13). The design proceeds in three steps: first, the missions (trajectories), antenna patterns and carrier frequency are parametrically investigated to determine the optimum mission/radio characteristics. Second, the science payload requirements together with the engineering (housekeeping) requirements are formulated into detailed data handling systems. Finally, the combinations of the radio and data systems are evaluated to define an optimal telecommunications system.

The starting point for the communications subsystem design is the relative trajectories of the spacecraft and the probe, from entry at $\gamma = -7.5$ degrees to 30 minutes after entry where the probe is at either the 30 atm level (for the Nominal atmospheric model) or at the 22 atm level (for the Warm atmospheric model). The end points of the three trajectories investigated are tabulated on the next page. In addition to these trajectories (Options A,B, and C), a fourth trajectory was supplied (Option D) which was received too late in the study to be analyzed in detail.

The Options B and C are baselines that direct the spacecraft to a nearly equatorial Jovian plane. Option A is for the spacecraft in the plane of probe entry. After Option A had been selected for study, Ames Research Center formulated another equatorial spacecraft plane trajectory with similar communications geometry. This is Option D. Figure 65 illustrates the relative geometry of the Option A mission but it is representative of Option D, also.

TABLE OF AMES RESEARCH CENTER RELATIVE TRAJECTORY DATA

MISSION OPTION	PROBE ASPECT ANGLE (DEG)	SPACECRAFT ASPECT ANGLE (DEG)	COMMUNICATION RANGE (KM)	CONDITION
A	40.8	49.5	76,674	ENTRY(1)
	11.7	96.7	58,541	EOM(2)
B	41.5	48.2	81,375	ENTRY
	17.5	92.6	63,143	EOM
C	43.0	46.8	77,644	ENTRY
	15.9	95.1	58,671	EOM
D	40.4	49.4	75,200	ENTRY
	13.0	99.4	58,400	EOM

(1) ENTRY: t = 0 @ probe altitude = 450 km

(2) END OF MISSION (EOM): taken as t = 30 min (the design goal for transmission)

RELATIVE POST ENTRY GEOMETRY* (OPTION A)

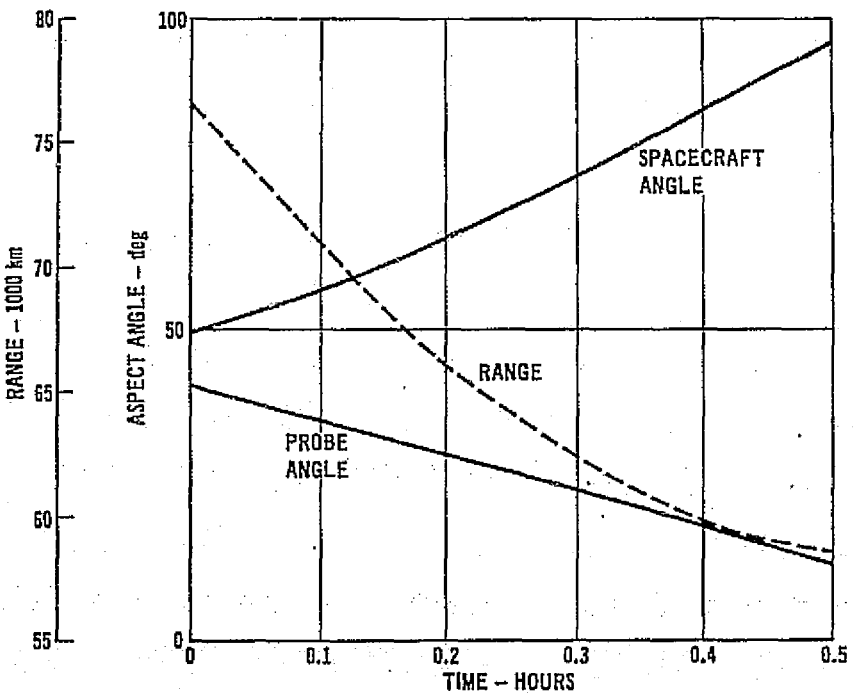

SEE FIGURE 6 FOR DEFINITION OF GEOMETRY

FIGURE 65

The first step in the design study is an investigation of the effects of carrier frequency. From Reference 5, which defines the environment of Jupiter, it is readily seen that planet noise and synchrotron noise as well as atmospheric absorption favor high frequencies. On the other hand ionospheric loss, antenna size, and free space loss favor lower frequencies. A parametric study from 400 to 1000 megahertz (MHz) indicated a fairly broad null about 400 megahertz with probe beamwidths between 66 and 114 degrees. Given the carrier frequency, a three-dimensional parametric analysis of probe beamwidth, spacecraft beamwidth and spacecraft beamcenter was conducted. Figure 66 is illustrative of these analyses. For a given probe beamwidth and spacecraft beamwidth-beamcenter the optimal (minimum) transmitter power required is a condition where the power at the initial portion of the mission exactly equals the power at the end of the mission (on the skirts of the beams in either case). For the three missions investigated, considering probe beamwidths from 66 degrees (aperture limit) to 114 degrees, spacecraft beamwidths from 40 degrees (physical size limitation) to 70 degrees and spacecraft beamcenters from 35 to 70 degrees, the optimal combination for minimum power per bit is 64/44 watts/bit for a communication link having a 66 degree probe beamwidth and a 50 degree spacecraft beamwidth centered at 56 degrees from the outbound axis of the spacecraft. The frequency remains at 400 MHz but continuing studies may result in a higher frequency. Communications is still a marginal link in the probe design, especially in a Jovian environment. (see the parametric analysis in Mission Analysis).

The scientific data requirements are summarized in Figure 46. From the data handling system viewpoint the requirements can be broken into two portions. First, the preentry portion provides radiation measurements and high rate deceleration values at a time when transmission is not available due to unfavorable aspect angles and entry plasma blackout. High rate engineering heat shield information is also desirable in this portion of the mission; provisions for heat shield data are more complete than in the SUAEP design. Second, the post-entry science data gathering portion which is during which the preentry information must also be transmitted (interleaved).

The preentry (actually pretransmission period) data can be accommodated by a 2000 bit radiation store, a 14,736 bit deceleration store and a 6092 bit heat shield store. Three alternatives were investigated for the post entry data.

EXAMPLE OF POWER PARAMETRIC ANALYSIS

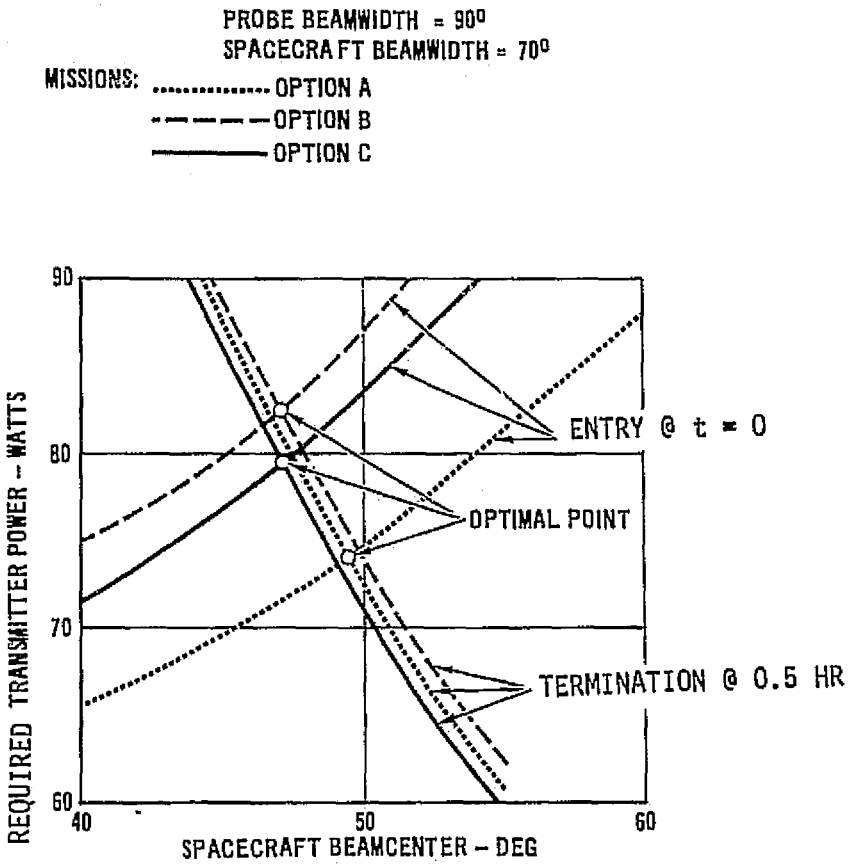

FIGURE 66

POST ENTRY FORMATS

Instrument	Format 1	Format 2	Format 3
Neutral Mass Spectrometer	12 bps	12 bps	2 bps
Gas Chromatograph	.5 bps	.5 bps	.4 bps
Visible-IR Flux Radiometer	3 bps	2 bps	2 bps
Nephelometer	1.5 bps	2 bps	2 bps
Other Science (p, T, g)	.5 bps	.5 bps	.2 bps
Engineering Rate	2 bps	2 bps	2 bps
Total Post-Entry Rate	23 bps	22 bps	10 bps

The essential differences between the designs are that Formats 1 and 2 have a continuously sampled neutral mass spectrometer (12 bps) vs Format 3 which only transmits the spectrometer peaks (2 bps), and that the other science (pressure, temperature and accelerations) are varied one from another to emphasize different species of data.

At this point a radio system evolved (64 watts/44 bps) which has a preentry store sized for 22,828 bits and three post-entry, real-time rates conceived (10, 22 and 23 bps). The remaining task is to marry the designs. Essentially, this means reading out the preentry store together with the post-entry, real-time data and in sizing the transmitter. Figure 67 illustrates the trade. It is seen that the combinations of readout rates and real-time rates are bounded on one side by transmitter size in the current state of the art and on the other by the inability of the system to dump totally the preentry store. Considering that the 60 watt, 400 megahertz, state-of-the-art bound is "soft", i.e., a slight link penalty may be acceptable, whereas, a minimum readout of the preentry store is a "hard" limit, acceptable systems range from the 24 bps design (24/23 sps) at a 4:3 (real: playback) interleave ratio to a 10 bps design with 2:3 to 1:3 interleave. Because a 12 bps neutral mass spectrometer (24 or 22 bps design) provides more constituency data, the 2 bps spectrometer (10 bps design) was not considered further. A reasonable choice, with simple interleaving is the 22 bps real-time 1:1 interleave. For a 60 watt transmitter this imposes only a -0.28 dB link penalty at the entry condition.

The data handling functional block diagram is shown in Figure 68 with the readout of the stores in Figure 69. Prior to entry an onboard clock initiates the data system ON. From this point, nominally at 2 Jovian radii, an energetic particle sensor begins filling its 2000 bit store, and the acceleration processor monitors the increasing longitudinal accelerometer output for -0.01 g_E+

(backed up by a g-switch) the accelerometer data between -0.0004 $g_{E}\uparrow$ and -0.01 $g_{E}\uparrow$ is trapped in this line and high sampling rate deceleration data is then stored. On sensing -3 $g_{E}\downarrow$ on the down-side of the peak, the preentry processors are terminated. Next, the post-entry processors and radio transmissions are initiated. As the receiver on the spacecraft must search in frequency for the probe signal (Doppler effects), a 2 minute delay line, real-time acquisition store assures the first real-time data is then interleaved with the real-time data. The margin history for the link is given in Figure 70.

DATA HANDLING SYSTEM SELECTION

REAL TIME SYSTEM	PARAMETER	REAL TIME: STORE INTERLEAVING 4:3	1:1	2:3	1:2	2:5	1:3
24 PBS (23 BPS DESIGN X24/23 SPS)	1	18.0	24.0	36			
	2	42.0	48.0	60			
	3	1.23	1.64	2.46			
	4	61.09(S)	69.82(S)	87.27(S)			
	5	- 0.08	-0.66	-1.63			
22 BPS	1	16.5	22.0	33.0	44.0	55.0	
	2	38.5	44.0	55.0	66.0	77.0	
	3	1.13	1.50	2.26	3.01	3.76	
	4	56.0	64.0 (S)	80.0 (S)	96.0 (S)	112.0 (S)	
	5	+0.30	-0.28	-1.25	-2.04	-2.71	
10 BPS	1	7.5	10.0	15.0	20.0	25.0	30.0
	2	17.5	20.0	25.0	30.0	35.0	40.0
	3	0.51 (U)	0.68 (U)	1.03	1.37	1.71	2.05
	4	25.45	29.09	36.36	43.64	50.91	58.18
	5	+3.72	+3.14	+2.18	+1.38	+0.71	+0.13

PARAMETER
1 PREENTRY PLAYBACK RATE, BPS
2 TRANSMITTED DATA RATE, BPS
3 NUMBER OF DUMPS IN 26 MIN = RATE X26X60/22828
4 TRANSMITTER POWER, WATTS, = RATE X64/44
5 60 WATT TRANSMITTER PENALTY/ADVANTAGE, dB

NOTES:
(S) BEYOND THE STATE OF THE ART
(U) UNACCEPTABLE

FIGURE 67

DATA HANDLING SYSTEM

PJO$_p$'80 ORBITER PROBE MISSION

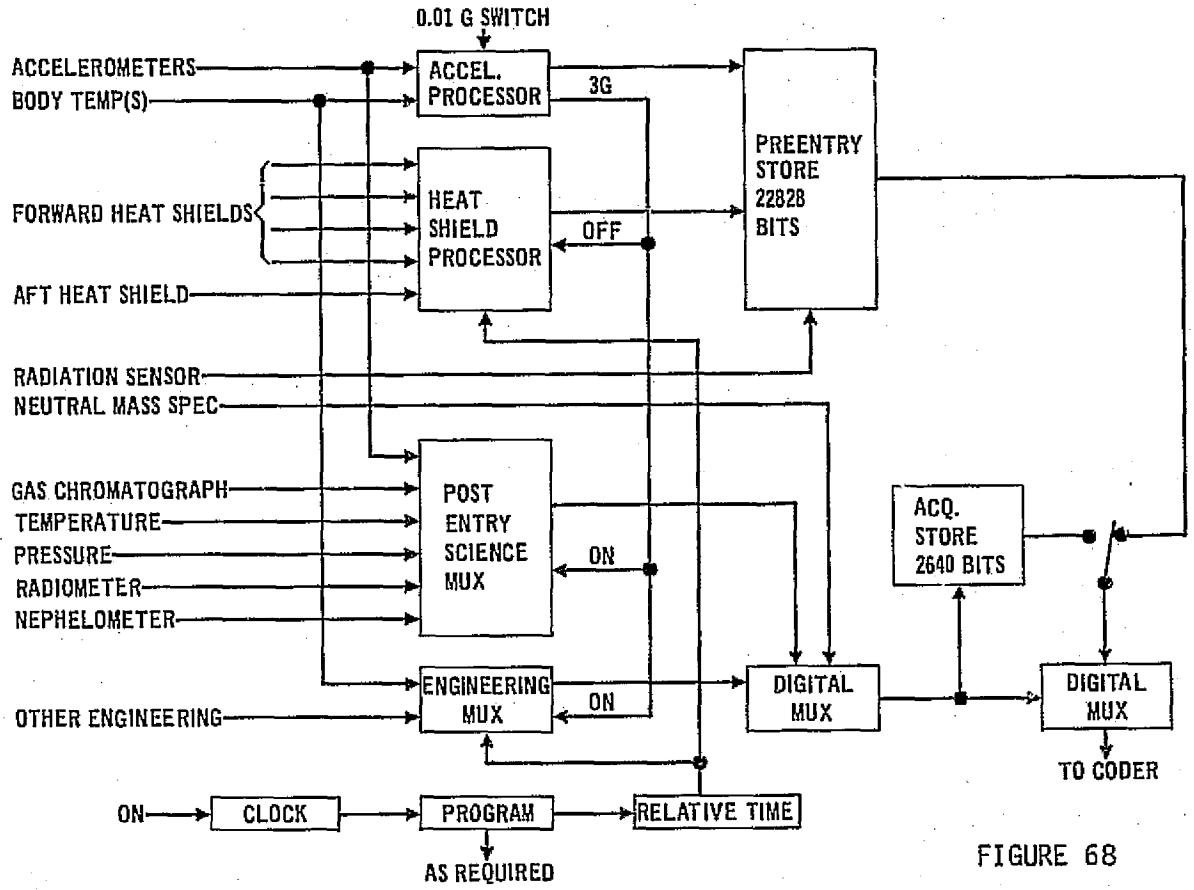

FIGURE 68

DATA STORAGE AND TRANSMISSION

STORAGE CAPABILITY

o PJO$_p$'80 ORBITER-PROBE MISSION

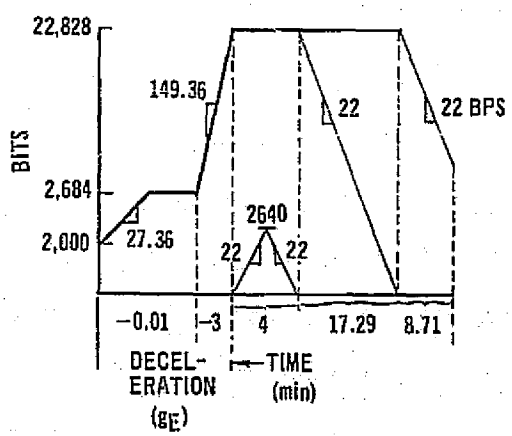

FIGURE 69

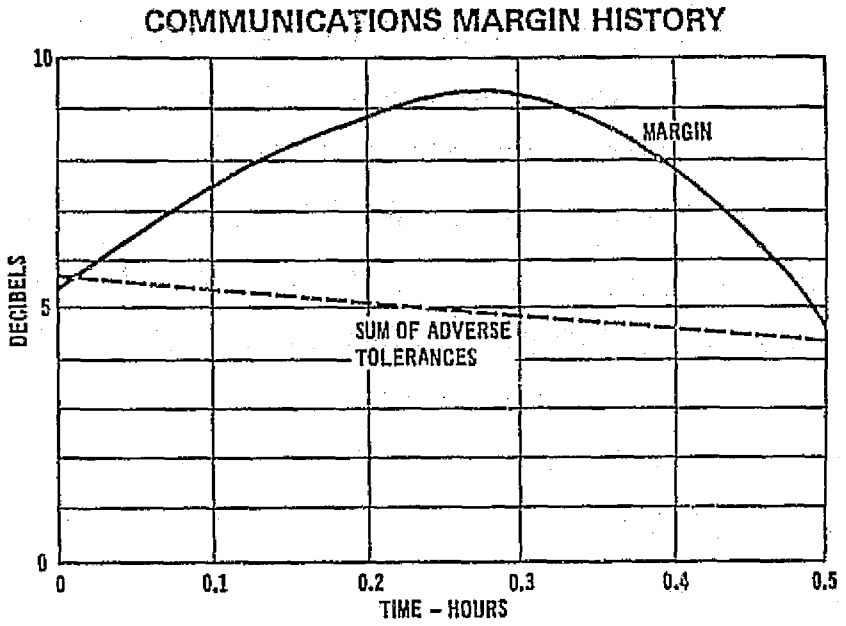

FIGURE 70

The post-entry science data formats are revised to accommodate the addition of the gas chromatograph and the visible-infrared flux meter. Two formats designs are shown in Figure 71, one of which includes rates recommended by Ames Research Center and an alternate which simplifies data handling, particularly the complete or partially redundant dumping of the preentry store. Both systems work well but in Design B only the average of every ten scans of the neutral mass spectrometer are transmitted.

The probe design now accommodates 20.4 kg of scientific instruments, and an increased engineering instrument complement as listed in Figure 72. Direct measurement of heat shield response to atmospheric heating in four forward heat shield and one aft heat shield locations are included with previously required calibration and housekeeping information. All of the engineering sensors are sampled during preentry data storage and post-entry, real-time transmission. These provisions will aid in data interpretation and, if needed, fault determination enroute or during post-mission data reduction.

The engineering sensors could be cycled during interplanetary transit to check on probe status. The probe accelerometer can be used in all spacecraft maneuvers for comparison with spacecraft propulsion performance checks. However, merit is also seen by MDAC-E in leaving the probe completely dormant during all post-launch activities (except Ni-Cd battery discharge-recharge cycling) to avoid use degradation.

POST ENTRY SCIENCE DATA HANDLING*

INSTRUMENT	BIT RATE		
	DESIGN A1	DESIGN A2	DESIGN B
NEUTRAL MASS SPECTROMETER (NMS)	12.0	12.0	2.0
GAS CHROMATOGRAPH (GC)	0.5	0.5	0.4
PRESSURE (P)	0.5	0.5	0.2
TEMPERATURE (T)	0.5	0.5	0.2
ACCELERATION ($\ddot{X}$)	0.5	0.5	0.2
($\ddot{Y}$)	0.5	0.5	0.2
($\ddot{Z}$)	0.5	0.5	0.2
RADIOMETER (R)	3.0	2.0	2.0
NEPHELOMETER (N)	1.5	2.0	2.0

FORMAT DIAGRAMS

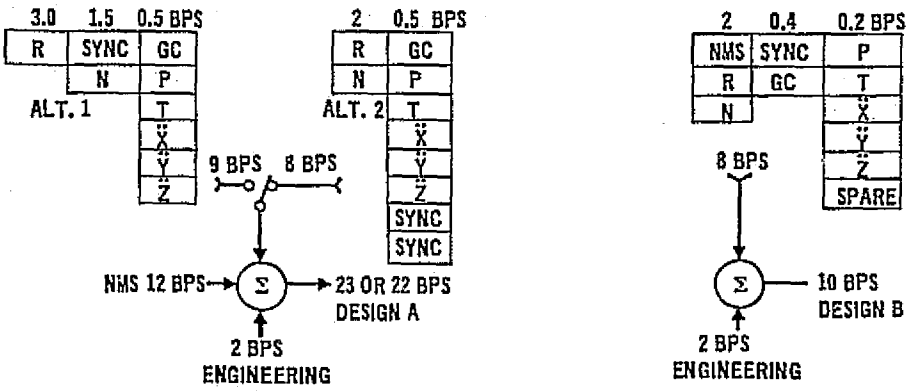

*SEE FIGURE 20 FOR DATA HANDLING SYSTEM WITH PREENTRY DUMP

FIGURE 71

ENGINEERING MEASUREMENT LIST

PARAMETER	INPUT VOLTAGE RANGE (VDC)	TYPE	QUANTIZATION (BITS/WORD)	SAMPLE RATE (SPS)
FORWARD HEATSHIELD SENSOR 1	0–40mV	DELL[1]	6	5 & 1
FORWARD HEATSHIELD SENSOR 2	0–40mV	DELL	6	5 & 1
FORWARD HEATSHIELD SENSOR 3	0–40mV	DELL	6	5 & 1
FORWARD HEATSHIELD SENSOR 4	0–40mV	DELL	6	5 & 1
AFT HEATSHIELD SENSOR	0–40mV	DELL	6	5 & 1
HEATSHIELD TEMPERATURE NO. 1	0–5	SEHL[2]	6	5/6 & 1/336
HEATSHIELD TEMPERATURE NO. 2	0–5	SEHL	6	5/6 & 1/336
HEATSHIELD TEMPERATURE NO. 3	0–5	SEHL	6	5/6 & 1/336
AFT SHIELD TEMPERATURE NO. 1	0–5	SEHL	6	5/6 & 1/336
AFT SHIELD TEMPERATURE NO. 2	0–5	SEHL	6	5/6 & 1/336
ACCELEROMETER TEMPERATURE	0–5	SEHL	6	5/6 & 1/42
PRESSURE GAGE TEMPERATURE	0–5	SEHL	6	1/42
TRANSMITTER CRYSTAL TEMPERATURE	0–5	SEHL	6	1/336
BATTERY TEMPERATURE	0–5	SEHL	6	1/42
DHS TEMPERATURE	0–5	SEHL	6	1/336
BATTERY VOLTAGE	0–5	SEHL	6	1/42
VOLTAGE STANDING WAVE RATIO (VSWR)	0–5	SEHL	6	1/42
TRANSMITTER POWER	0–5	SEHL	6	1/42
RELATIVE TIME (INTERNALLY GENERATED)			12 BIT WORD	1/42
ACCELEROMETER RANGE – CHANGE NO. 1	0–5	BL[3]	ONE 6 BIT WORD	ON OCCURRENCE
ACCELEROMETER RANGE – CHANGE NO. 7	0–5	BL	ONE 6 BIT WORD	ON OCCURRENCE
G-SWITCH ACTUATION	0–5	BL	ONE 6 BIT WORD	ON OCCURRENCE
PYRO RELAY STATE	0–5	BL	ONE 6 BIT WORD	ON OCCURRENCE

1 DELL-DOUBLE ENDED LOW LEVEL
2 SEHL – SINGLE ENDED HIGH LEVEL
3 BL – BILEVEL
IN ADDITION, INTERNAL INSTRUMENT CONDITION DATA ARE CONTAINED IN ITS DATA STREAM.

FIGURE 72

The telecommunications design is summarized in Figure 73. Included in the figure are two design alternatives which have not been fully explored. In the radio design an attractive alternative would be to use the two spacecraft receiving antenna patterns which is actually one physical antenna with an electronic beam-center switch. This probably would decrease the transmitter power by one-half; thereby, reducing cost and development risk. Such an antenna would be larger than one with a single beamcenter, and, hence, would physically benefit from higher frequencies. The Jovian noise environment is better known at high frequencies. If peak neutral mass spectrometer data only is adequate (rather than continuous samples), then the 10 bps real-time rate will definitely decrease the transmitter power required. This alternative to data collection deserves further study to ascertain the ability to reconstruct the atmosphere.

SUMMARY AND ALTERNATIVES

o PJO_P'80 ORBITER - PROBE MISSION

DESIGN SUMMARY

COMMUNICATIONS

- 400 MHz
- 44 BPS
- 60 WATT
- NONCOHENT TRANSMISSION
- CONVOLUTIONALLY CODED
- HARD DECISION DECODED
- 66° TRANSMIT ANTENNA
- 50° RECEIVE ANTENNA AT A 56° CONE ANGLE

DATA HANDLING

NEUTRAL MASS SPEC	= 12 BPS
POSTENTRY SCIENCE	= 8 BPS
ENGINEERING	= 2 BPS
PREENTRY PLAYBACK	= 22 BPS
TOTAL	= 44 BPS

STORAGE

RADIATION	= 2000 BITS
ACCELERATION	=14,736 BITS
HEAT SHIELD	= 6092 BITS
ACQUISITION	= 2640 BITS
TOTAL	=25468 BITS

DESIGN ALTERNATIVES

COMMUNICATIONS

INCREASE TOTAL RECEIVED POWER BY SWITCHING INFLIGHT BETWEEN TWO SPACECRAFT ANTENNA PATTERNS. PROBABLY INCREASE CARRIER FREQUENCY TO 500 — 600 MHz TO REDUCE ANTENNA SIZE. RESULT IN APPROXIMATELY 1/2 TRANSMITTER POWER.

DATA HANDLING

REDUCE NMS RATE TO 2 BPS BY TRANSMITTING ONLY PEAK VALUES RATHER THAN CONTINUOUS ANALOG SAMPLES.

- BIT RATE = 30 BPS
- OUTPUT INTERLEAVE = 1:2
- TRANSMITTER = 44 WATTS

FIGURE 73

Electrical Power

The electrical power/energy requirements for the Jupiter Oribter Probe mission in 1980 are tabulated in Figure 74. The tabulation identifies all of electrical users and durations of use. The cummulative requirements are less than that required for a typical Saturn/Uranus entry so a modest weight reduction is available if the battery is sized for Jupiter. In the interest of commonality and growth potential this was not done.

EQUIPMENT POWER/ENERGY REQUIREMENTS

o PJO_p'80 ORBITER - PROBE MISSION

EQUIPMENT	UNIT POWER (WATTS)	TIME (MIN)	ENERGY (W-H)
ENTRY DETECTION:			
X-DAY CLOCK (2)	140×10^{-6}	72,000	0.34
G-SWITCH	0.2	47	0.15
DATA HANDLING SUBSYSTEM	10.0	77	12.83
TRANSMITTER-OSE/MOD	1.0	77	1.28
POWER AMPLIFIER	135	30	67.00
SCIENCE:			
MASS SPECTROMETER	11.0	40	7.33
GETTER PUMP HEATER	30.0	10	5.00
ORDNANCE RELAYS	3.0	0.001	0.05
GAS CHROMATOGRAPH	9.7	30	4.85
ACCELEROMETER	1.5	77	1.92
PRESSURE GAGE	1.2	30	0.60
TEMPERATURE GAGE	1.0	30	0.50
NEPHELOMETER	1.0	30	0.50
ENERGETIC PARTICLE DETECTOR	0.5	47	0.39
IR FLUX METER	3.0	30	1.50
ORDNANCE RELAYS	3.0	0.001	0.04
BATTERY HEATER	30.0	30	15.00
EQUIPMENT ENERGY			119.28
DISTRIBUTION LOSSES (5%)			5.96
TOTAL ENERGY REQUIRED			125.24

* ENERGY REQUIRED, PJ_p'79 MISSION = 98 W-hr

FIGURE 74

Heat Protection

New advances in heat shield technology have been aimed at developing materials that reflect the incident shock layer radiation rather than absorbing it as do carbonaceous materials. A high density, high purity all-silica

material appears to be the most promising reflective heat shield material and is currently being developed at MDAC-E. A characteristic of the reflective concept is that heat shield weights decrease with steeper entries, since a greater portion of the incident heating is radiative, thus the shallow entry constraint ($\alpha < -15°$) required for the carbon-phenolic heat shield may be modified if the reflective material achieves the good performance indicated by preliminary work. This achievement is sought because communications are enhanced by steep entries ($\gamma > -7.5$ degrees), whereas, heat protection thicknesses are decreased by shallow entries (-7.5 degrees > γ > skip-out boundary (-4 degrees)).

The design of the structure is essentially unchanged from the description given in Reference 1. There are differences in the precise shape of the outer ring and in hole patterns on the attachment rings, but these are superficial. Hence, repetition is unnecessary.

Thermal Control

The thermal control analysis is based on modeling sources of heat generation and transport and computing temperature histories. Figure 75 shows the major elements of the thermal control subsystem schematically. The multilayer insulation (MLI) blanket and radioisotope heater units (RHU's) provide passive thermal control during the long interplanetary journey and after separation. While still attached, the spacecraft augments the probe thermal control subsystem by controlling heat flow at the probe-adapter attachment points with an electrical heater and radiation surfaces on the adapter section. The entry heat protection system dissipates the high heating rates encountered during planetary entry as it descends into the atmosphere because the atmosphere has high heat capacity.

Little of the stored heat actually reaches the interior equipment section. A polyurethane foam cover forms the aft closure on the equipment bay and supports the microstrip antenna, however, controlled venting is permitted during Earth ascent and Jovian descent so pressure differentials remain small.

The heat shield temperature distributions, subsequent to aerodynamic heating, form the initial boundary conditions for the atmospheric descent portion of the thermal analysis. As the probe descends into the dense, relatively cold atmosphere, the heatshield surface cools very rapidly and approaches the temper-

ature of the ambient environment. The presence of a hydrogen-helium gas mixture and a steadily increasing atmospheric density result in high surface cooling rates that are 20 to 40 times greater than for Earth atmospheric descents. Thus, the major portion of the heat content of the heatshield flows back to the outer surface with only a small fraction being leaked to the interior by conduction, radiation, and internally by convection. Operation of the electronic equipment yields about 175 watts of electrical waste heat with the transmitter providing most of this heat (135 W). Ambient planetary gas is permitted to vent into the probe cavity during descent and provides a form of convective gas flow internally which prevents hot spots but at about 10 atm it becomes a heat source also. These heat transfer mechanisms are accounted for in the analysis.

THERMAL CONTROL SYSTEM

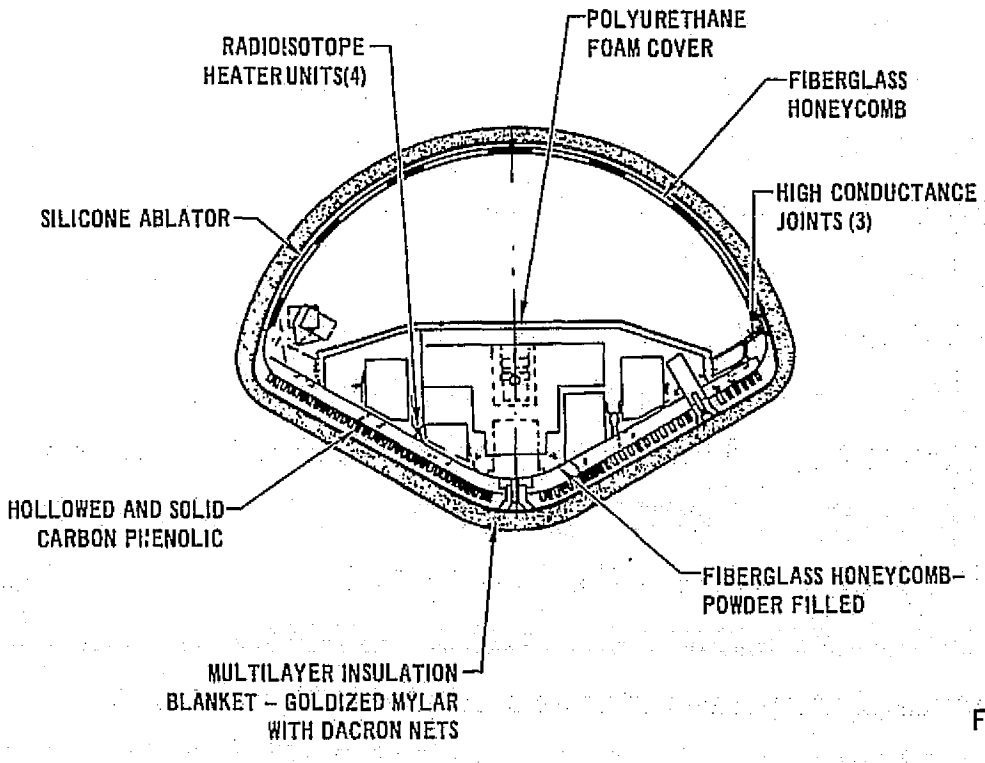

FIGURE 75

This tendency for temperature on the heat shield surface to decrease rapidly from the peak condition, bottom out and then rise again as the 10 atm condition is passed is illustrated in Figures 76 through 79. These histories show the effect of surrounding air on the external surface of the heatshield,

on the bondline temperature, and on the aluminum structure that is bonded to the honeycomb. The temperature of the aluminum does increase about 50°F in all cases. The differing temperatures are plotted in Figure 80 as a function of entry angle, γ. No appreciable dependency on atmosphere model is indicated. Thus, the remaining heatshield material and the insulation provided in the form of mixed silica and carbon materials effectively inhibits heat input variations. This insulation capability is being tested currently under a separate program. The data will extend the heat transport analysis over the full heatshield and probe equipment local transients.

FOREBODY HEATSHIELD TEMPERATURE
JUPITER ENTRY: NOMINAL ATMOSPHERE
ENTRY GAMMA = -7.5 DEGREES

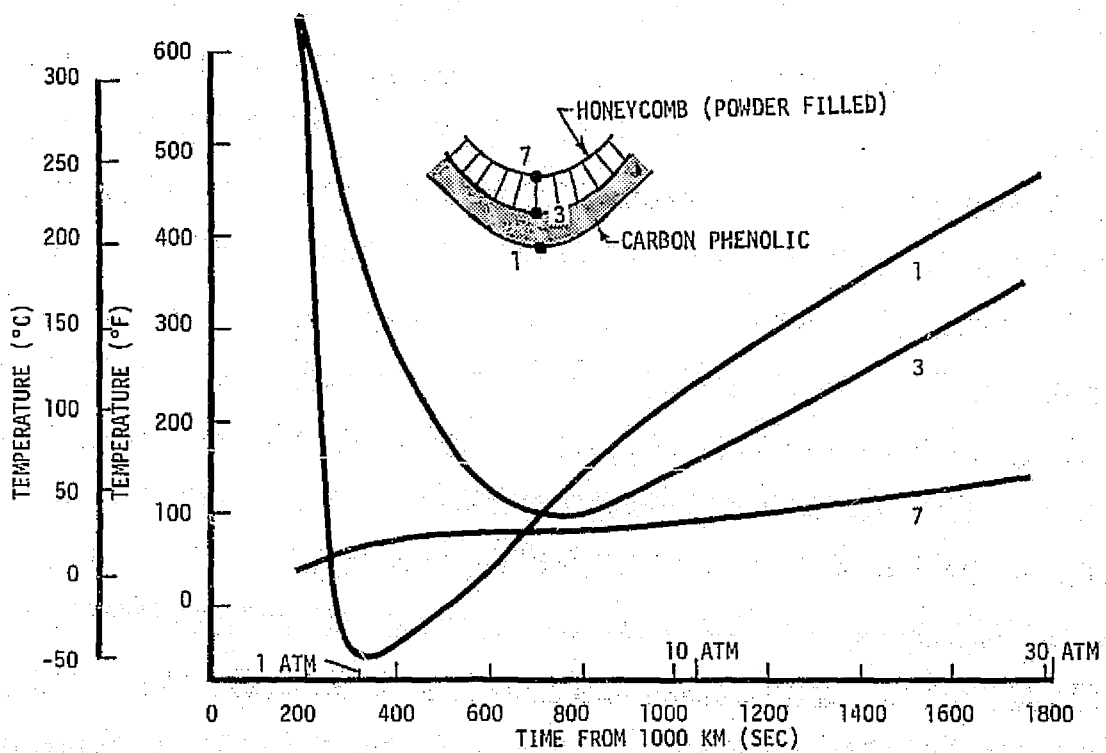

FIGURE 76

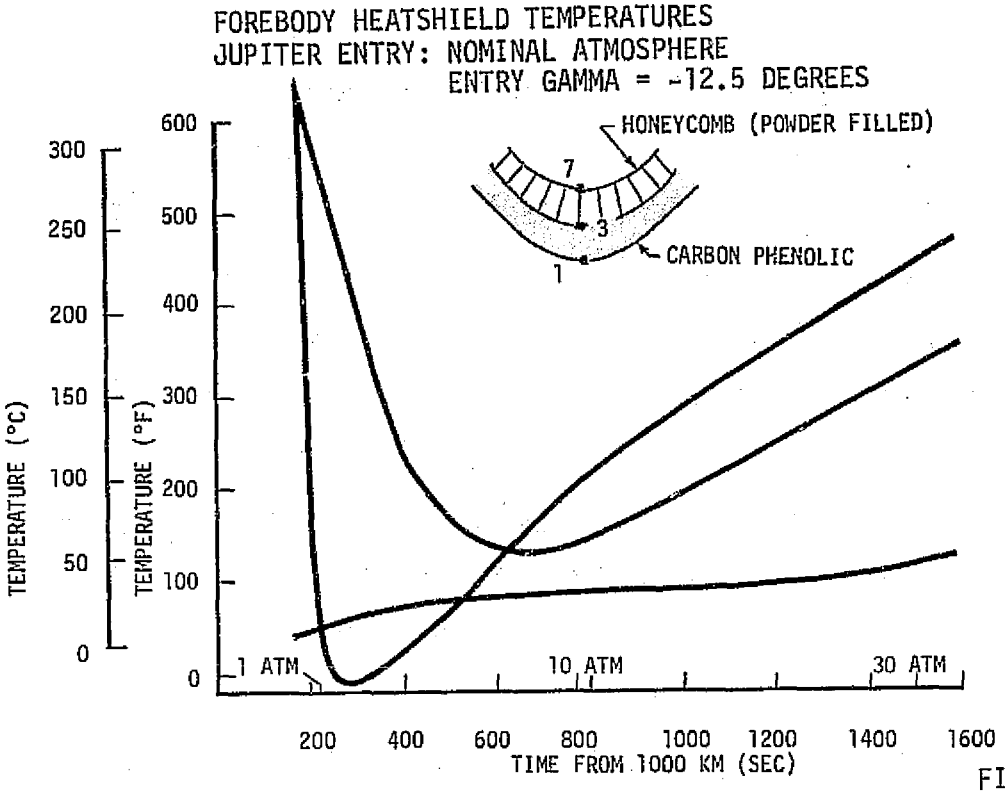

FIGURE 77

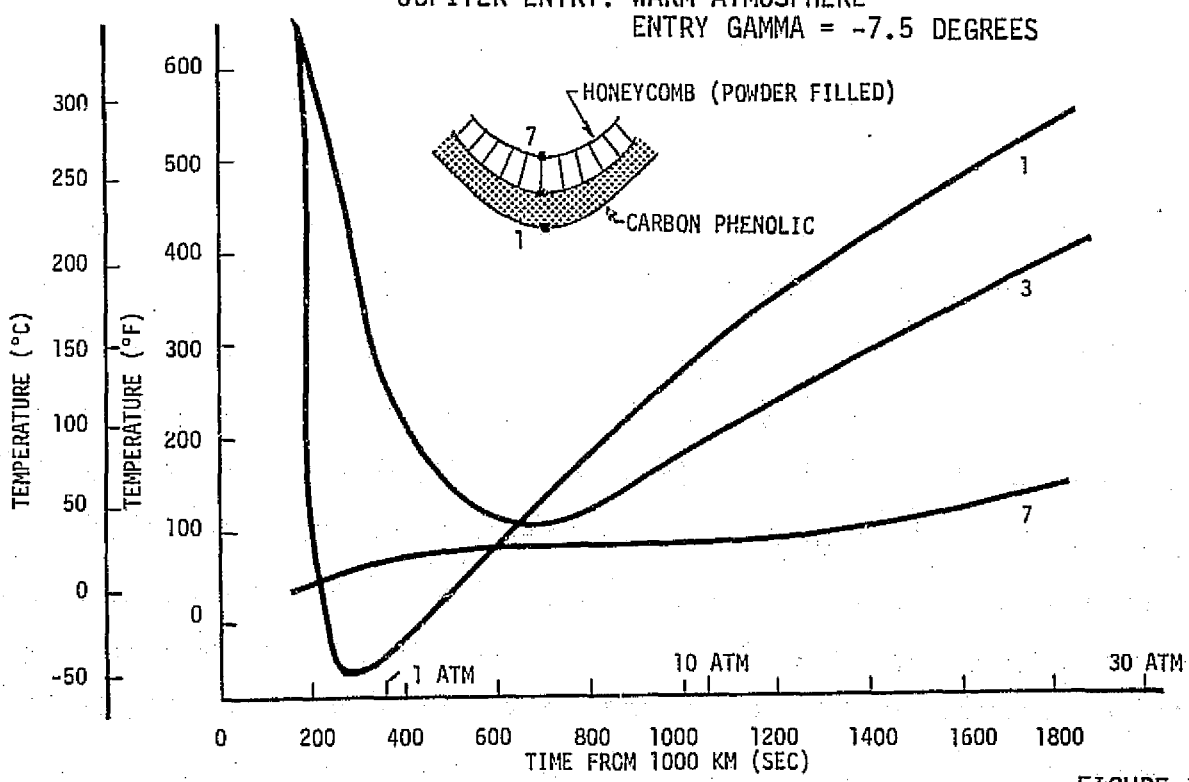

FIGURE 78

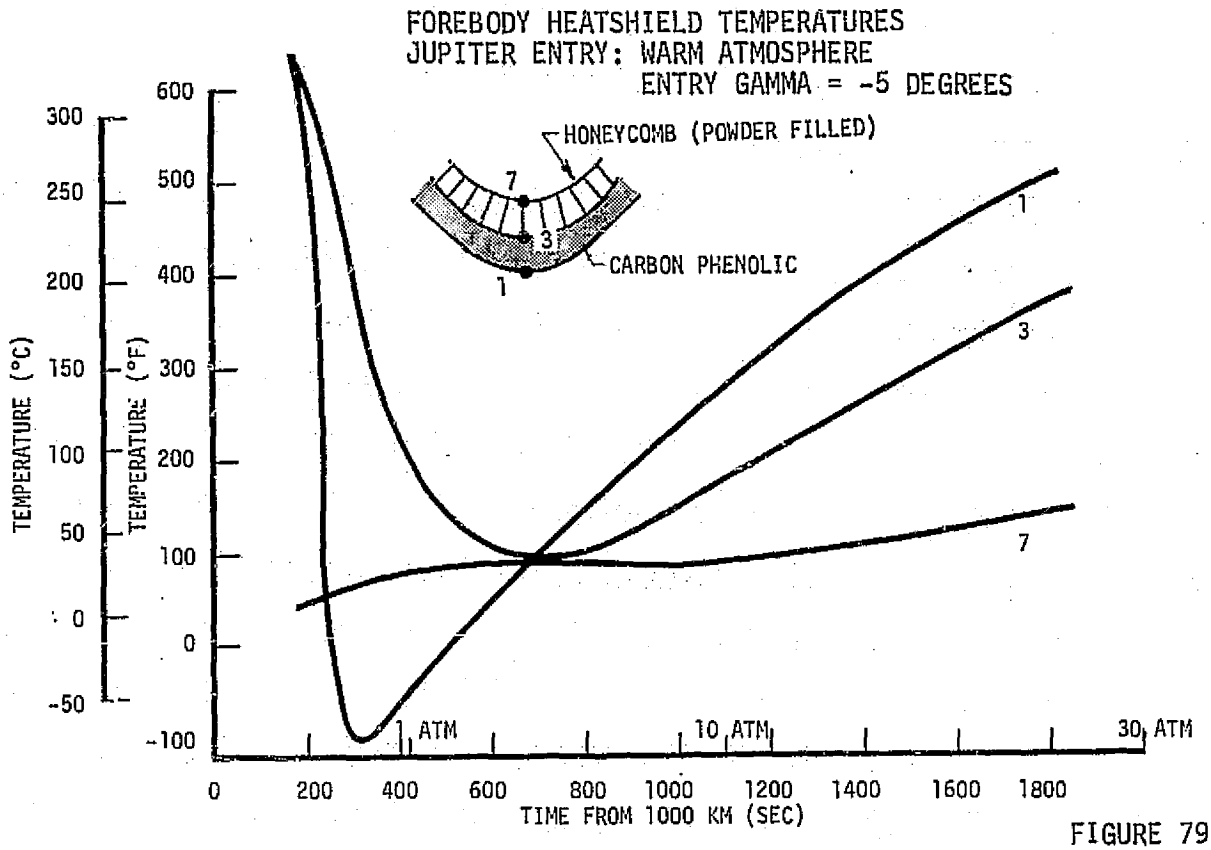

FIGURE 79

This analysis also included a check on equipment temperatures. Because the electronic components are limited to +160°F operating environments these heat producing elements must be designed to have adequate heat capacity and must be partially isolated from the two major heat sources: heat flow through the heatshield and via venting during entry. A temperature rise of 120°F can be expected in the transmitter in a 30 minute descent. This is precisely the design temperature difference from entry to end of descent without any margin remaining. Some improvement is therefore necessary. The solution to be studied first is increasing box wall thickness to provide greater heat capacity. The histories for each of the same conditions covered in the forebody nose temperature analysis is shown in Figures 81 through 84 with a summary of 30 atm (peak) values in Figure 85. In this case and in the forebody case the $\gamma = -12.5$ degree case was made to establish an upper limit. Although -10 degrees is probably the steepest angle to be used for an early probe, the parametric study is improved by interpolation from points beyond the most probable limit condition.

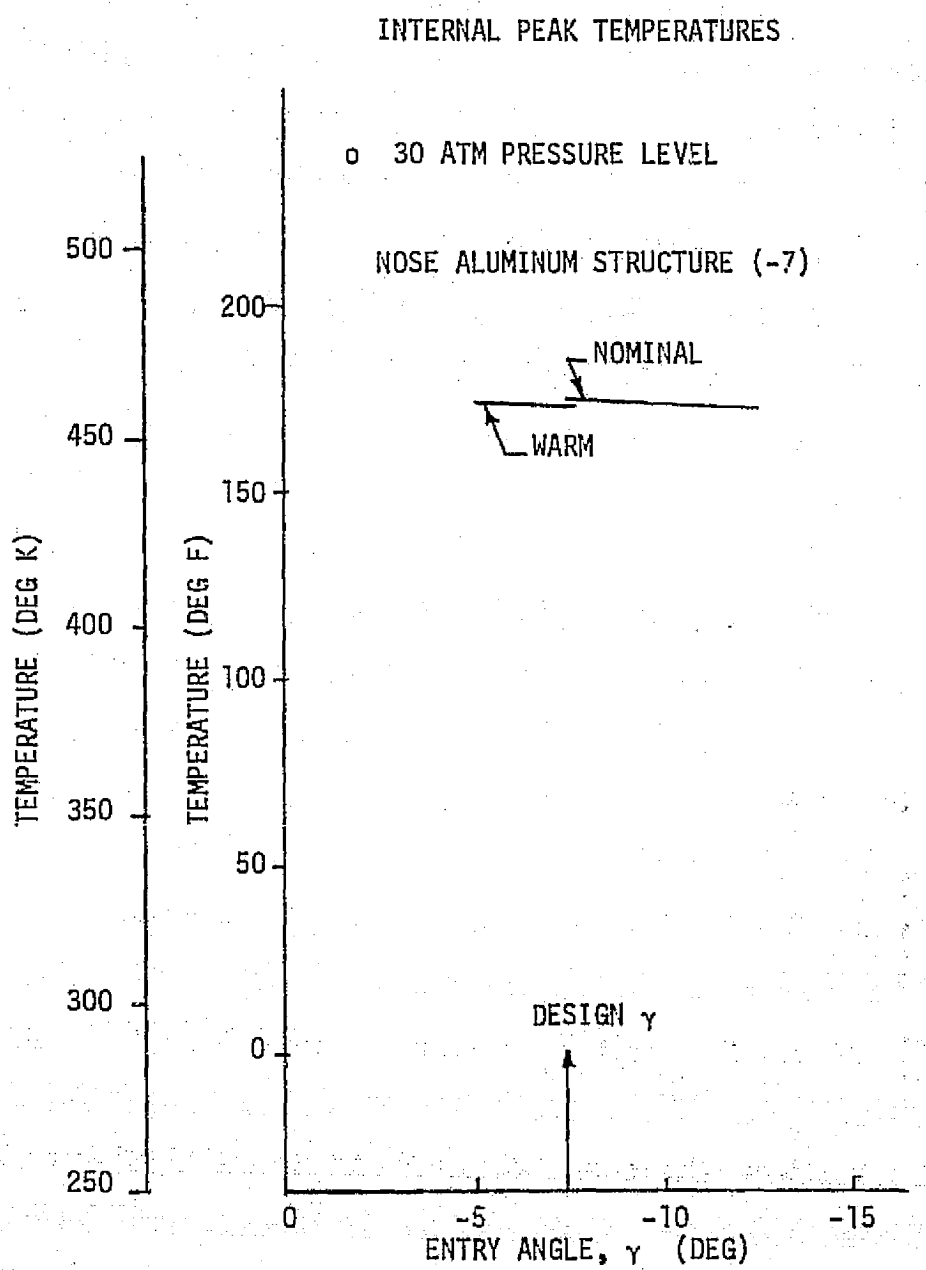
INTERNAL PEAK TEMPERATURES
o 30 ATM PRESSURE LEVEL
NOSE ALUMINUM STRUCTURE (-7)
NOMINAL
WARM
TEMPERATURE (DEG K)
500
450
400
350
300
250
TEMPERATURE (DEG F)
200
150
100
50
0
DESIGN γ
0
-5
-10
-15
ENTRY ANGLE, γ (DEG)

FIGURE 80

COMPONENT TEMPERATURES
JUPITER ENTRY: NOMINAL ATMOSPHERE
ENTRY GAMMA = -7.5 DEGREES

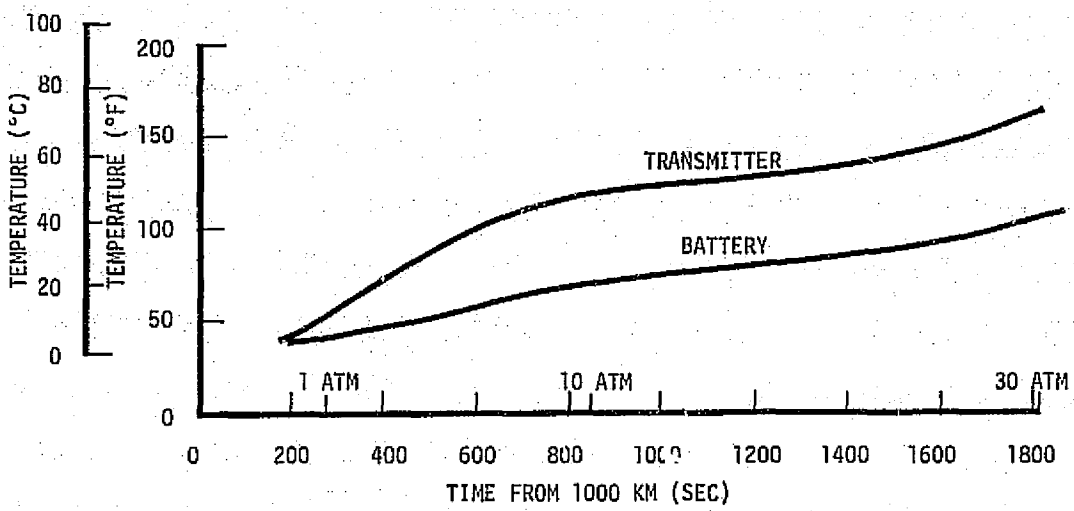

FIGURE 81

COMPONENT TEMPERATURES
JUPITER ENTRY: NOMINAL ATMOSPHERE
ENTRY GAMMA = -12.5 DEGREES

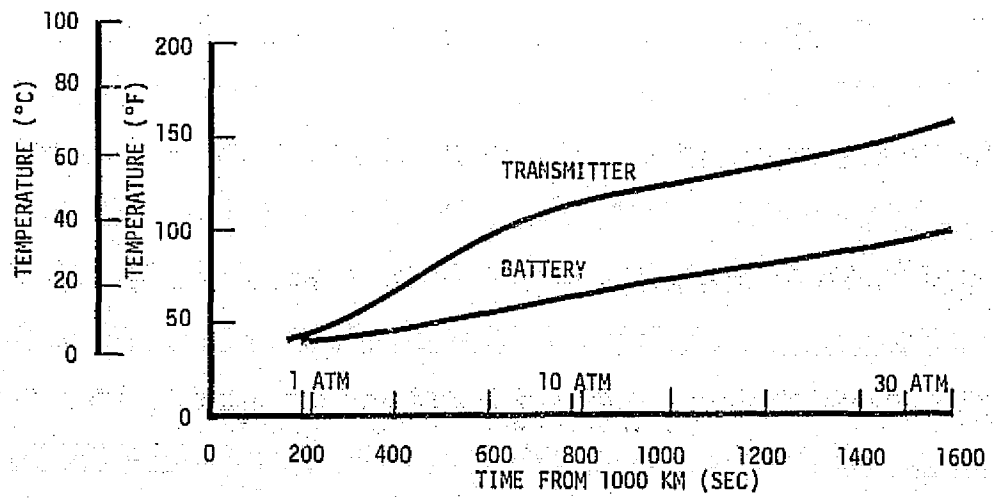

FIGURE 82

COMPONENT TEMPERATURES
JUPITER ENTRY: WARM ATMOSPHERE
ENTRY GAMMA = -7.5 DEGREES

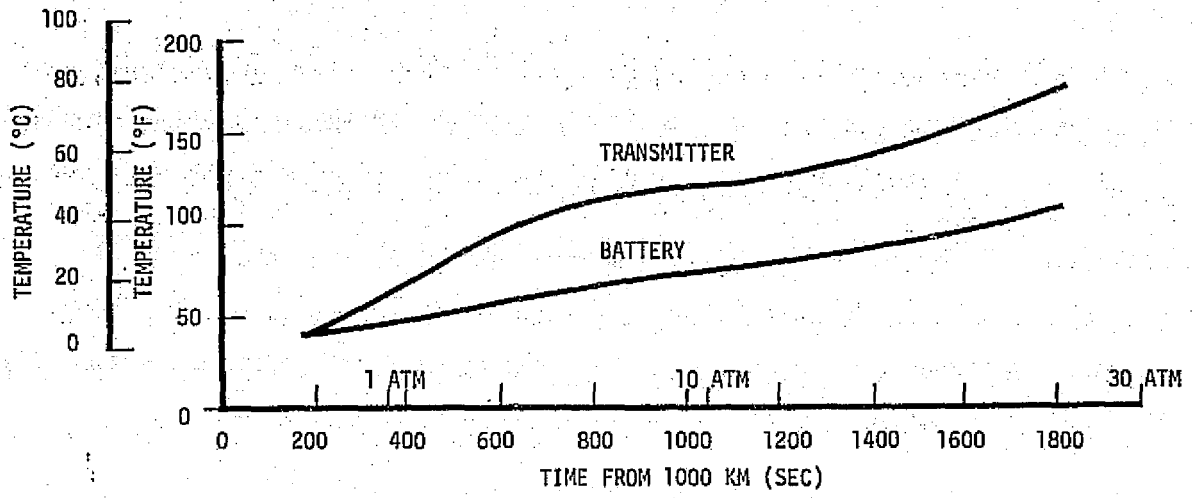

FIGURE 83

COMPONENT TEMPERATURES
JUPITER ENTRY: WARM ATMOSPHERE
ENTRY GAMMA = -5 DEGREES

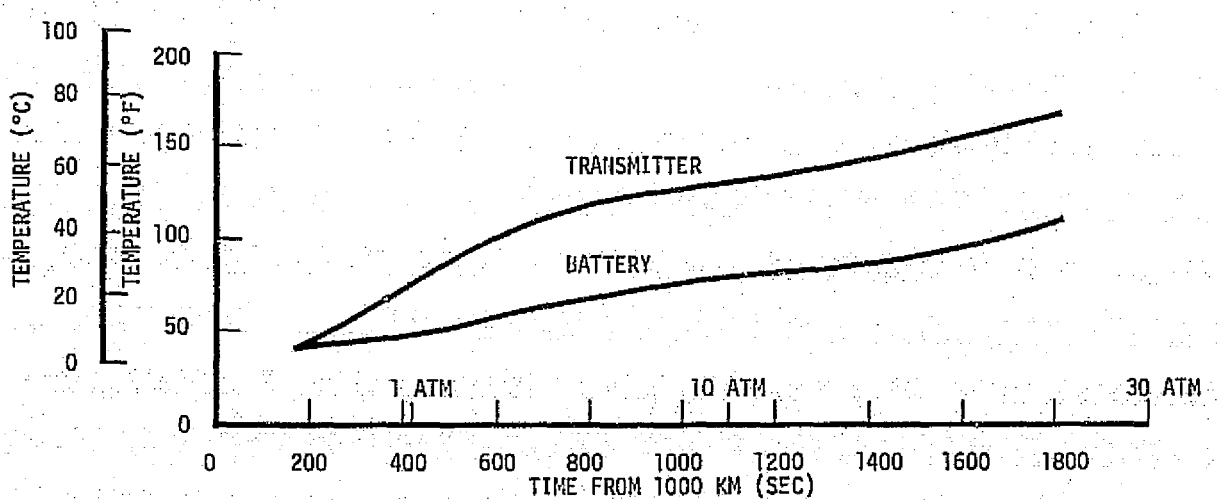

FIGURE 84

The thermal control subsystem is a simple, semipassive concept that maintains uniform temperatures inside during extremely-cold and extremely-hot phases of the mission. Validation of heat transport rates is underway: (1) the fiber-filled honeycomb rates are to be determined in laboratory tests, (2) a full scale engineering model is unde construction with built-in heat simulators; and (3) heat protection ablators are being tested for physical properties as well as for recession and erosion tendencies. RHU's have been used exter vely on prior programs as have polyurethane foams. Their capabilities are well understood. A program of evaluating multilayer insulation heat retention capability has been formulated (but not started). Again, use of the MLI material in similar applications permits confident designing with only validation testing required in the Probe Development Phase.

EQUIPMENT PEAK TEMPERATURES

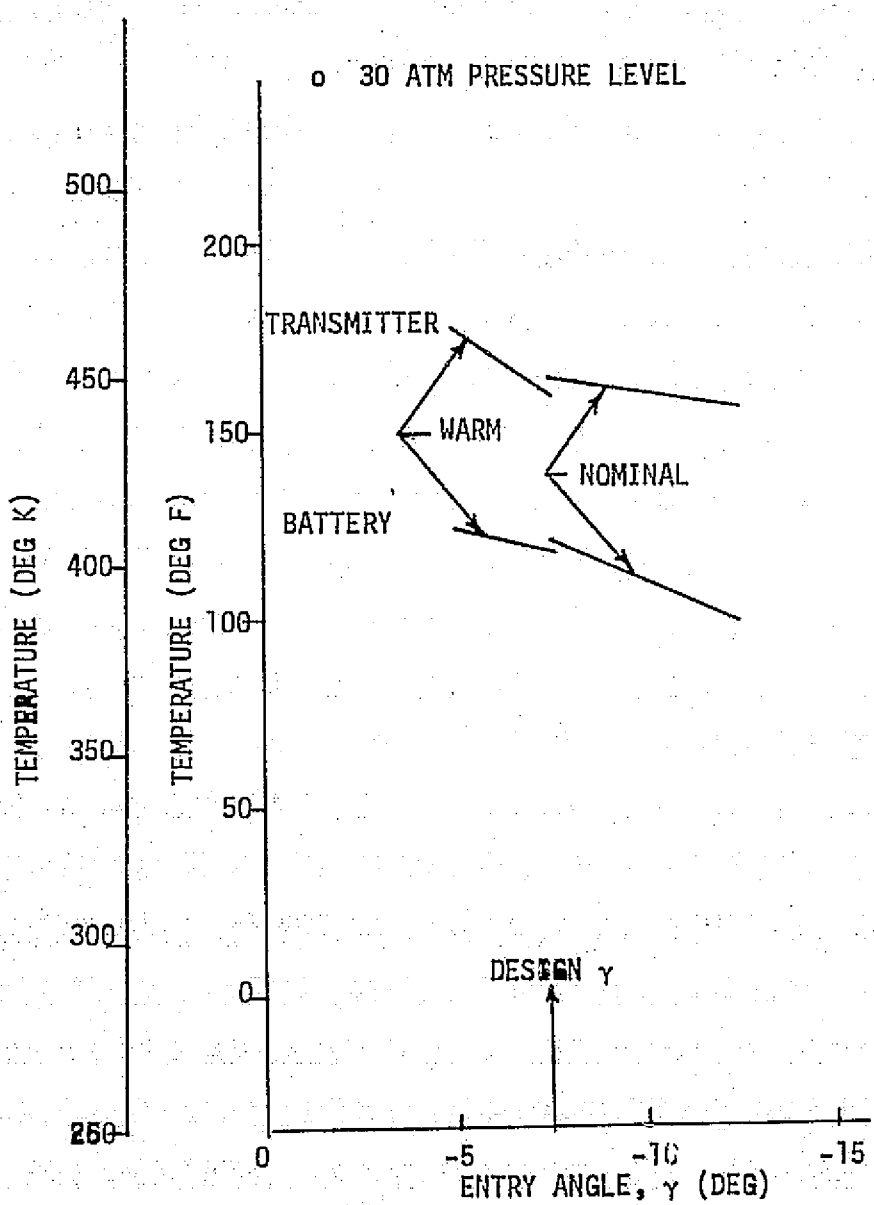

FIGURE 85

REFERENCES

1. MDC E0870, "Saturn/Uranus Atmospheric Entry Probe", Final Report, McDonnell Douglas Astronautics Co.-East, 18 July 1973

2. "Atmospheric Entry Probes for Outer Planet Exploration", A Technical Review and Summary, National Aeronautics and Space Administration, Ames Research Center, August, 1974

3. NASA TMX-2338, "Preliminary Analysis of an Atmosphere Entry Probe Mission to Jupiter", Byron L. Swenson, Larry E. Edsinger, Larry A. Manning, Susan M. Norma, Kenneth F. Sinclair, Alan J. Stratton and Edward L. Tindle, September 1971

4. Request for Proposal 2-24949 (MR-13), "Feasibility Study of Low Angle Planetary Entry", April 3, 1974

5. NASA SP-8-68, "NASA Space Vehicle Design Criteria (Environment), The Planet Jupiter (1970)", December, 1971.

6. Journal of the Atmospheric Sciences, No. 30, 718, 1973

7. Journal of the Atmospheric Sciences, No. 26, 826, 1969

8. Ap. J. (Astrophysics Journal), C. C. Kies, C. H. Corliss, H. K. Kiess, 132 221, 1960

9. Icarus, T. Owen, 10 355 (1969)

10. Science, D. L. Judge and R. W. Carlson, 183 317 (1974)

11. NASA SP-300,"Physics of the Solar System", Ch. 4., Washington, D. C. (1972)

12. "PAET, An Entry Probe Experiment in the Earth's Atmosphere", A. Seiff, D. E. Reese, S. Sommer, D. B. Kirk, E. E. Whiting and H. B. Nieman, Icarus 18 525-563 (1973)

13. OPP-25, "Preliminary ESRO PJOP'80 Telecommunications Design", C. A. Hinrichs, McDonnell Douglas Astronautics Co.-East, 7 November 1974.

14. CR-137591, "PIoneer Jupiter Orbiter Probe Mission - 1980 - Probe Description", R. E. DeFrees, McDonnell Douglas Astronautics Company, 11 November 1974.

APPENDIX I
HISTORY DATA FOR RADIATION PASSAGE STUDY FOR JUPITER PROBE MISSION

Time histories for probe and spacecraft zeocentric radius, latitude, and longitude and a cross-plot of zeocentric radius versus latitude are presented for the Jupiter 1979 flyby missions with varying entry latitudes.

The reference coordinate system, Figure I-1, is Jupiter-centered with the radius measured from planet center, latitude north (+) and south (-) of the planet equator, and longitude east (+) and west (-) of the meridian passing through the sub-Earth point. The Jupiter mission nominal consists of a probe entry flight path angle ($\gamma_I = -7.5°$) and entry latitude of 4.8° and spacecraft periapsis of 1.8 planet radii and phasing time of 0.4 hours. Off-nominal cases presented are for entry latitudes of +10°, 0°, -5°, -10°. Continuing study has revealed that $r_p = 1.7\ R_J$ appears to be superior to 1.8 for communication link duration. These data are used in determining fluences and dose rates encountered during passage through Jupiter's magnetosphere. Three charts are given for each entry angle.

REFERENCE COORDINATE SYSTEM

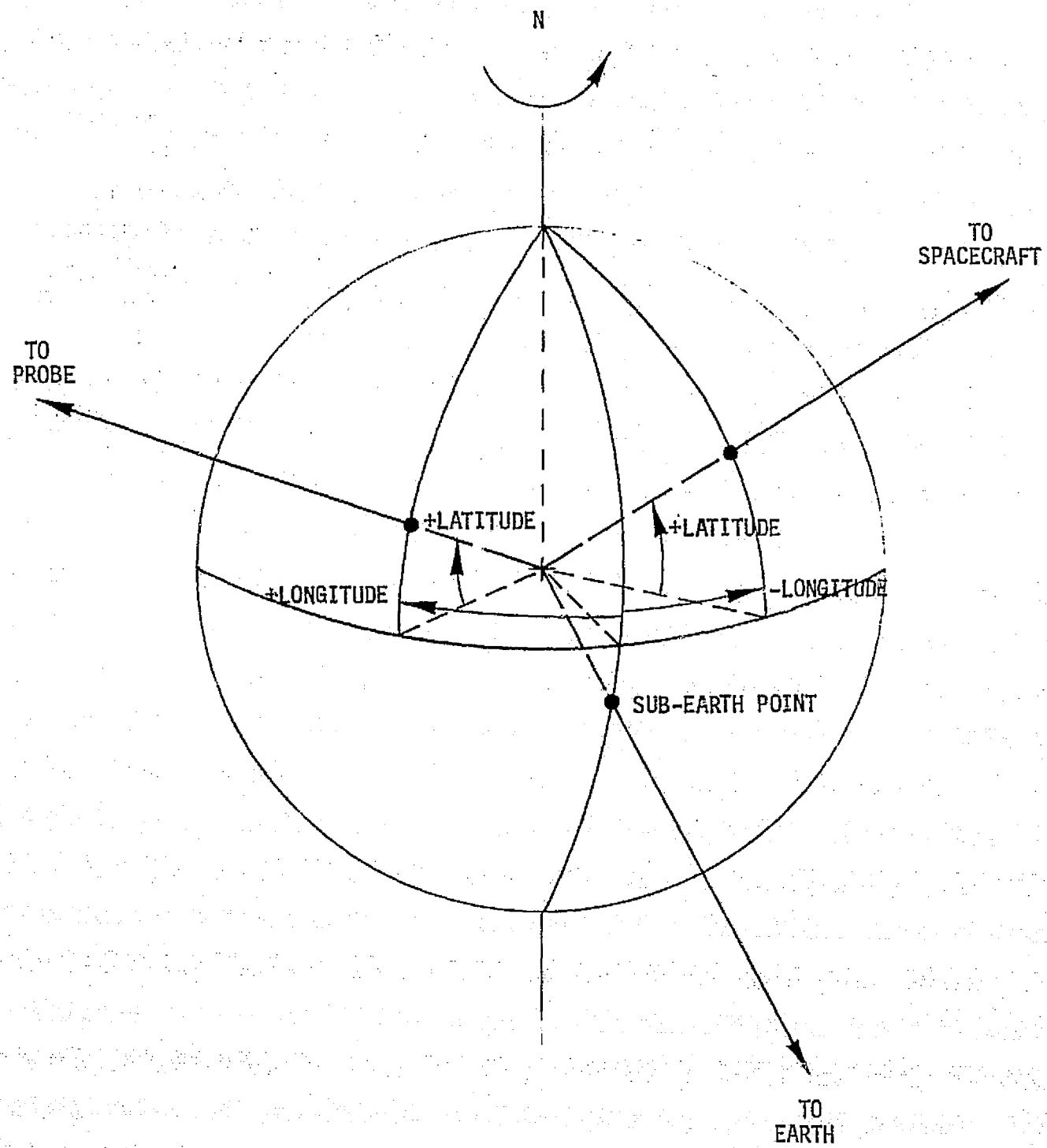

FIGURE I-1

ENTRY LATITUDE = +10°

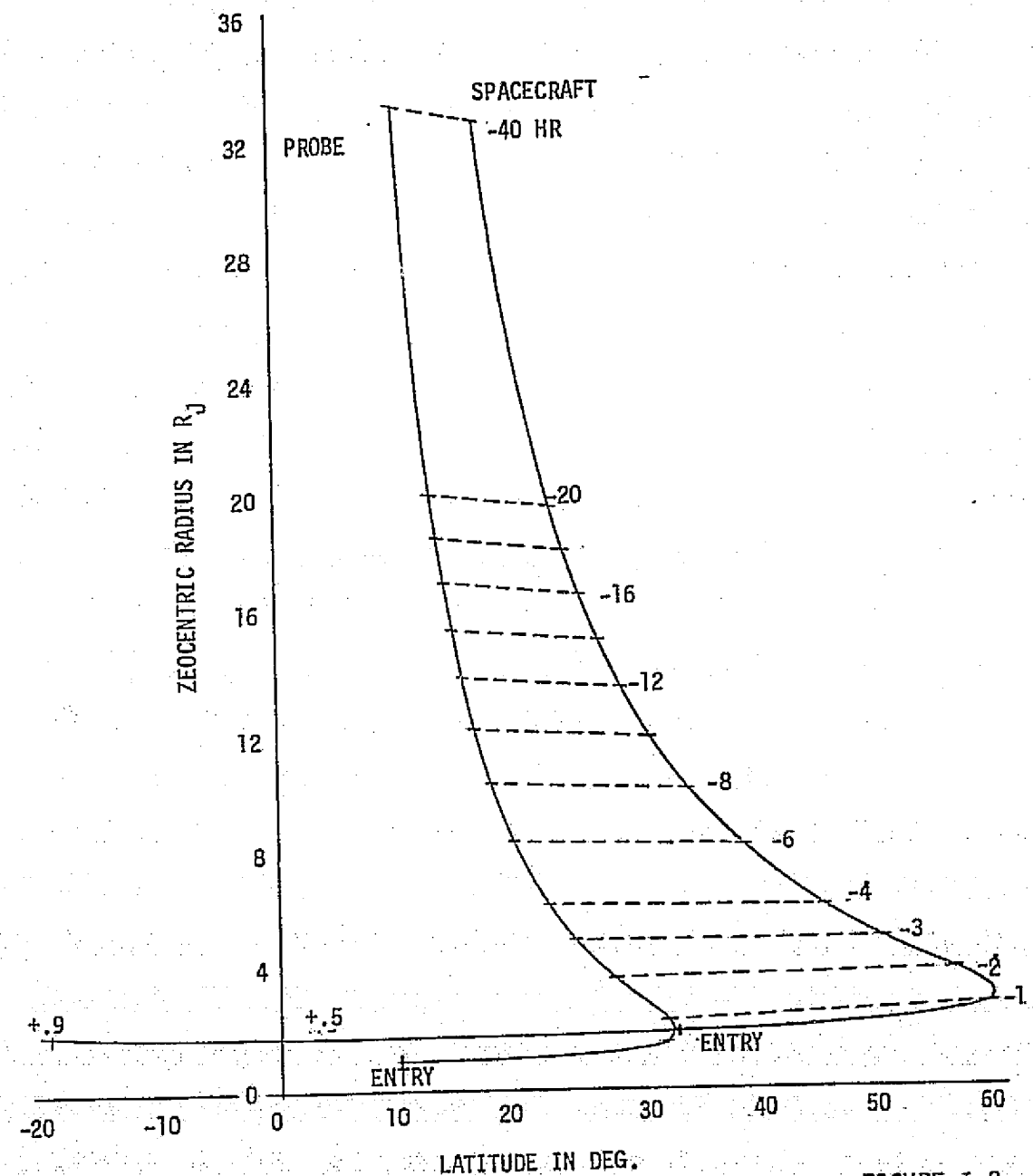

FIGURE I-2

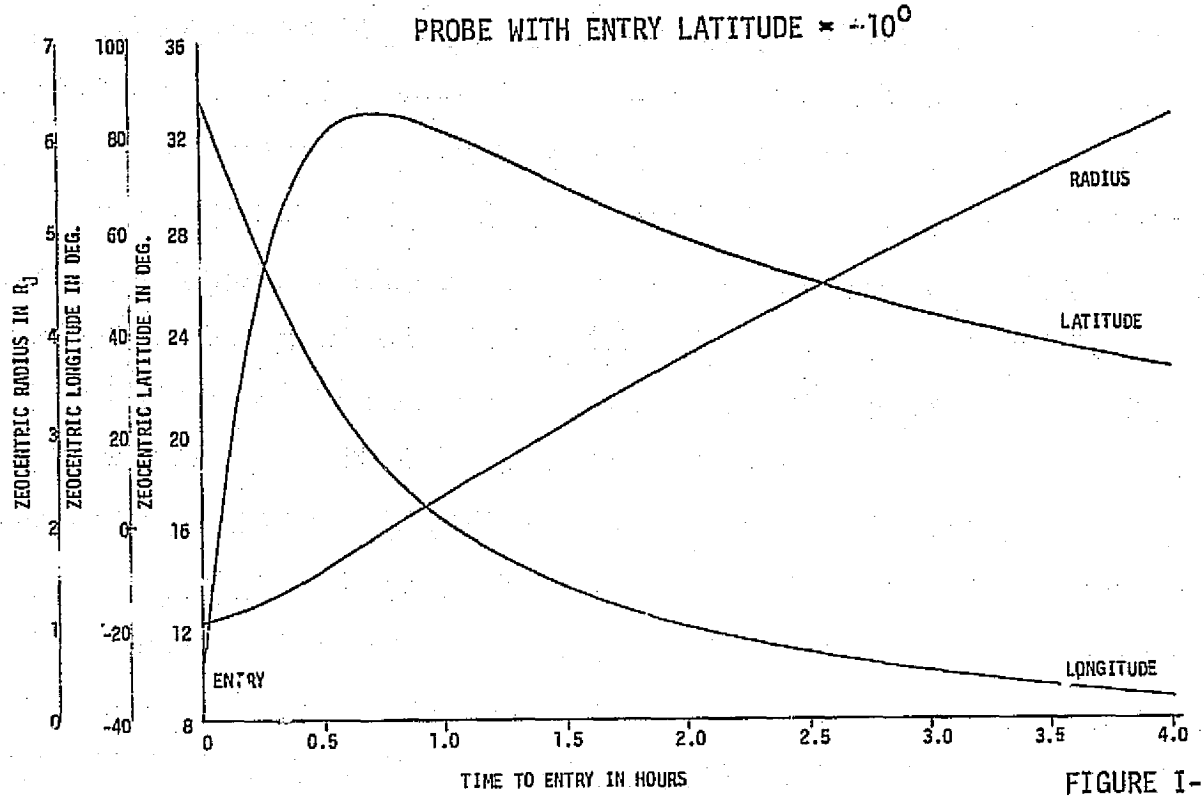

FIGURE I-3

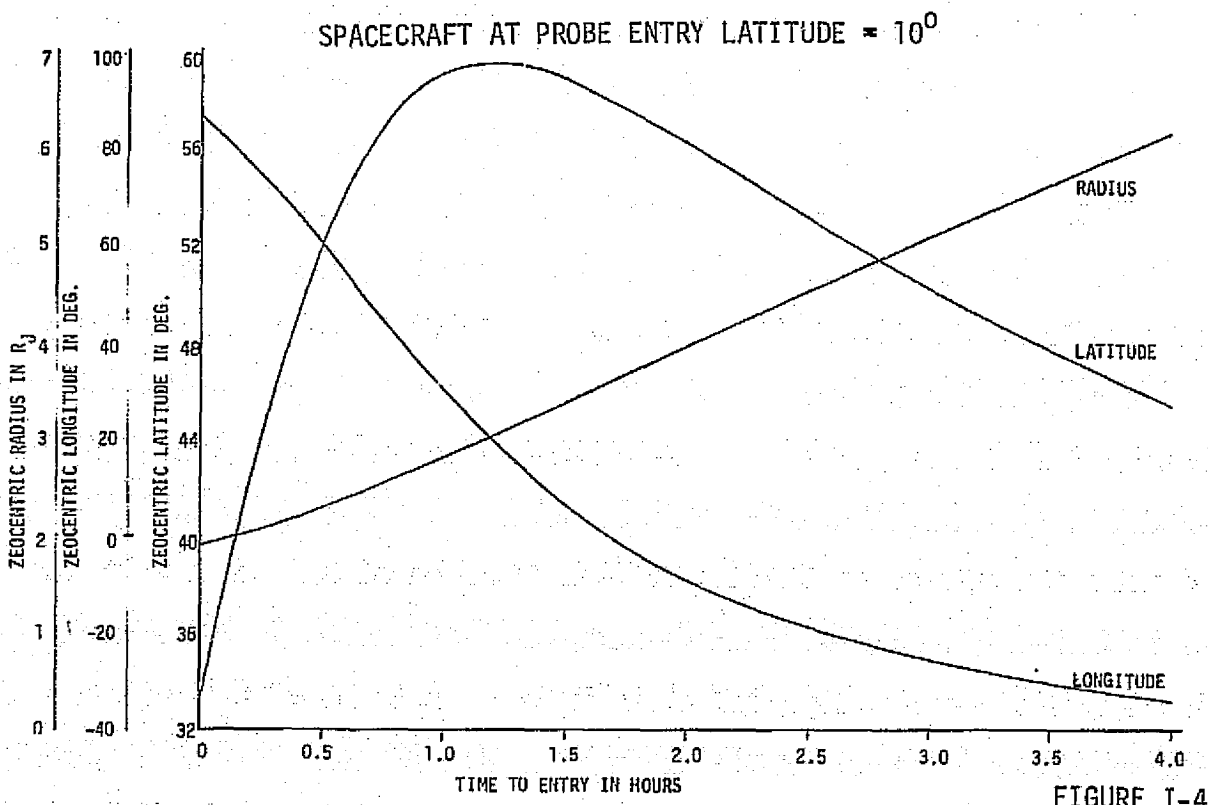

FIGURE I-4

ENTRY LATITUDE = +4.8°

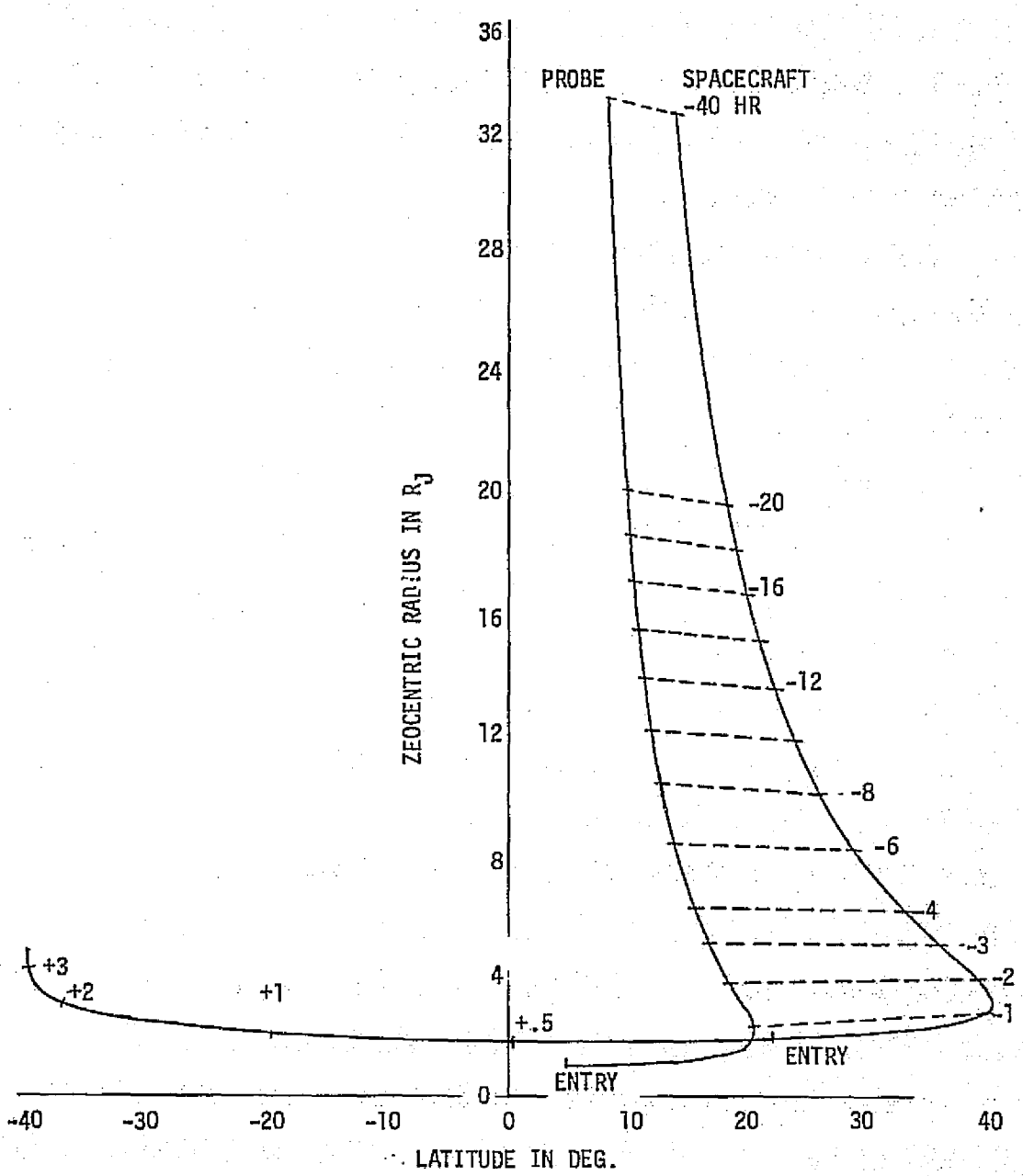

FIGURE I-5

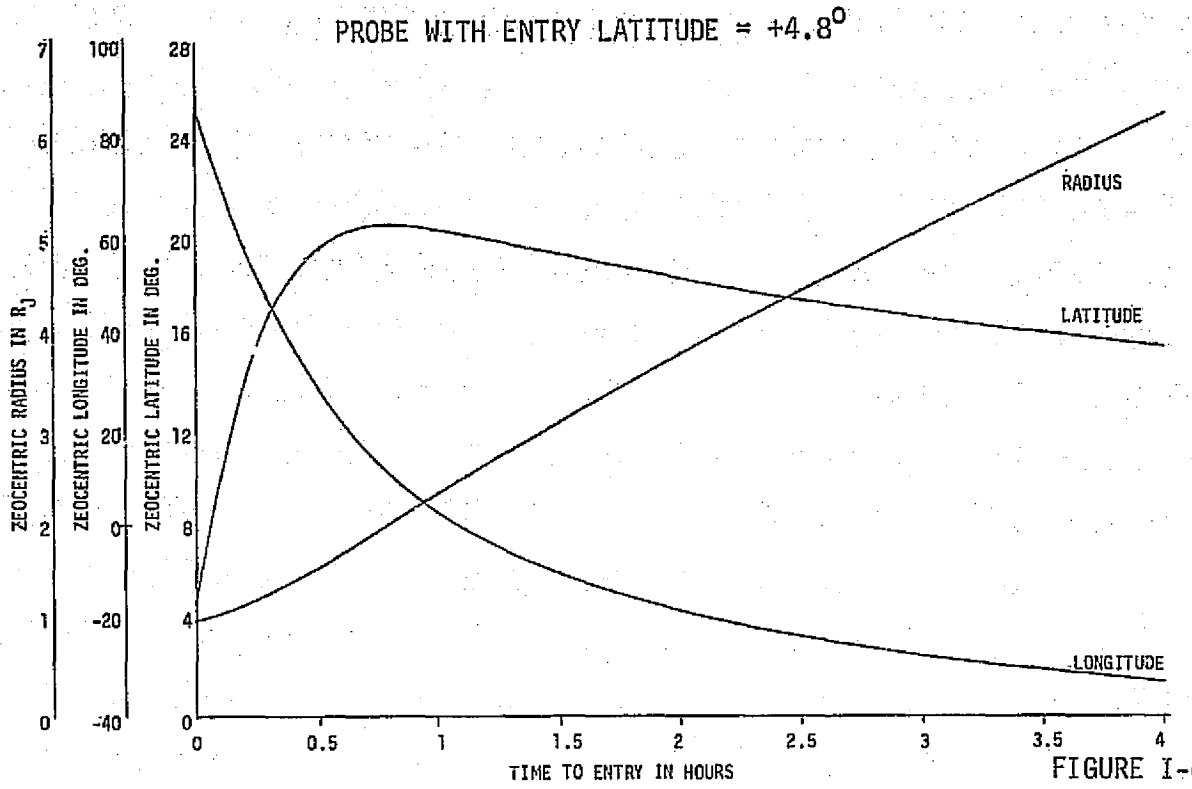

FIGURE I-6

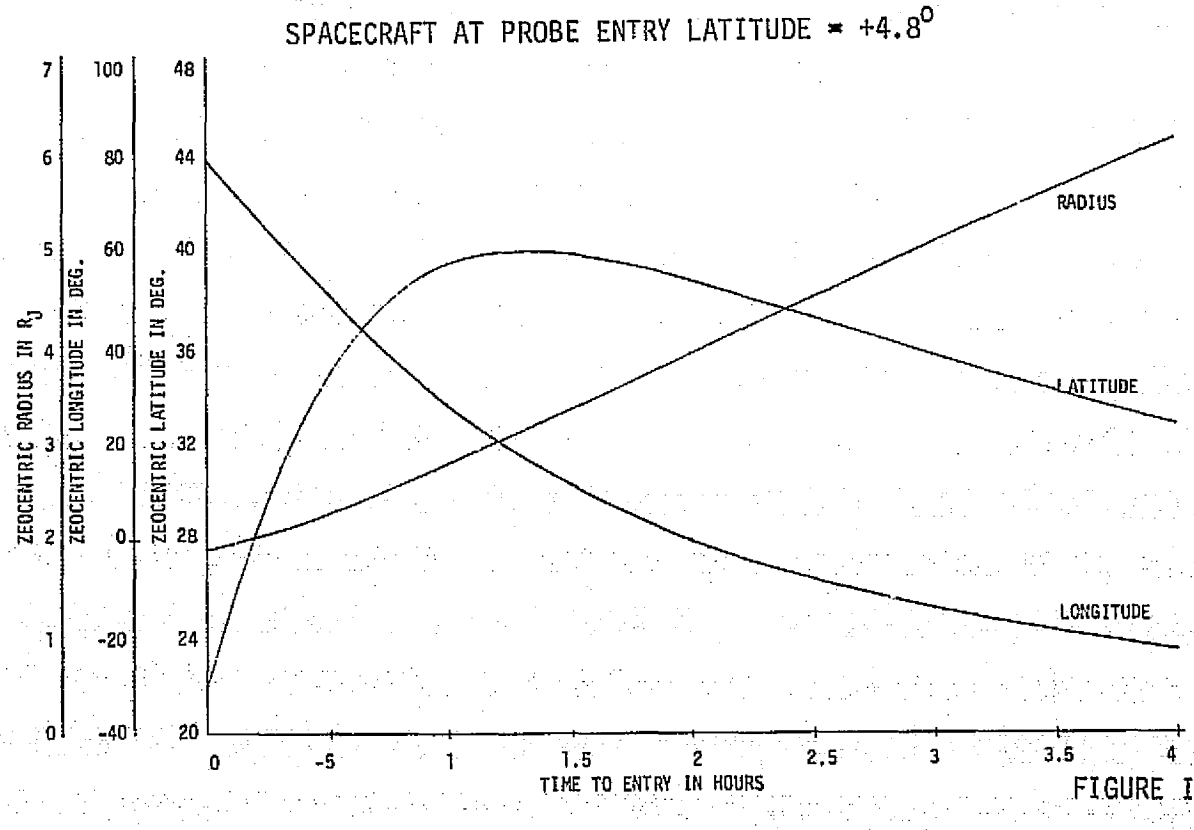

FIGURE I-7

ENTRY LATITUDE = 0°

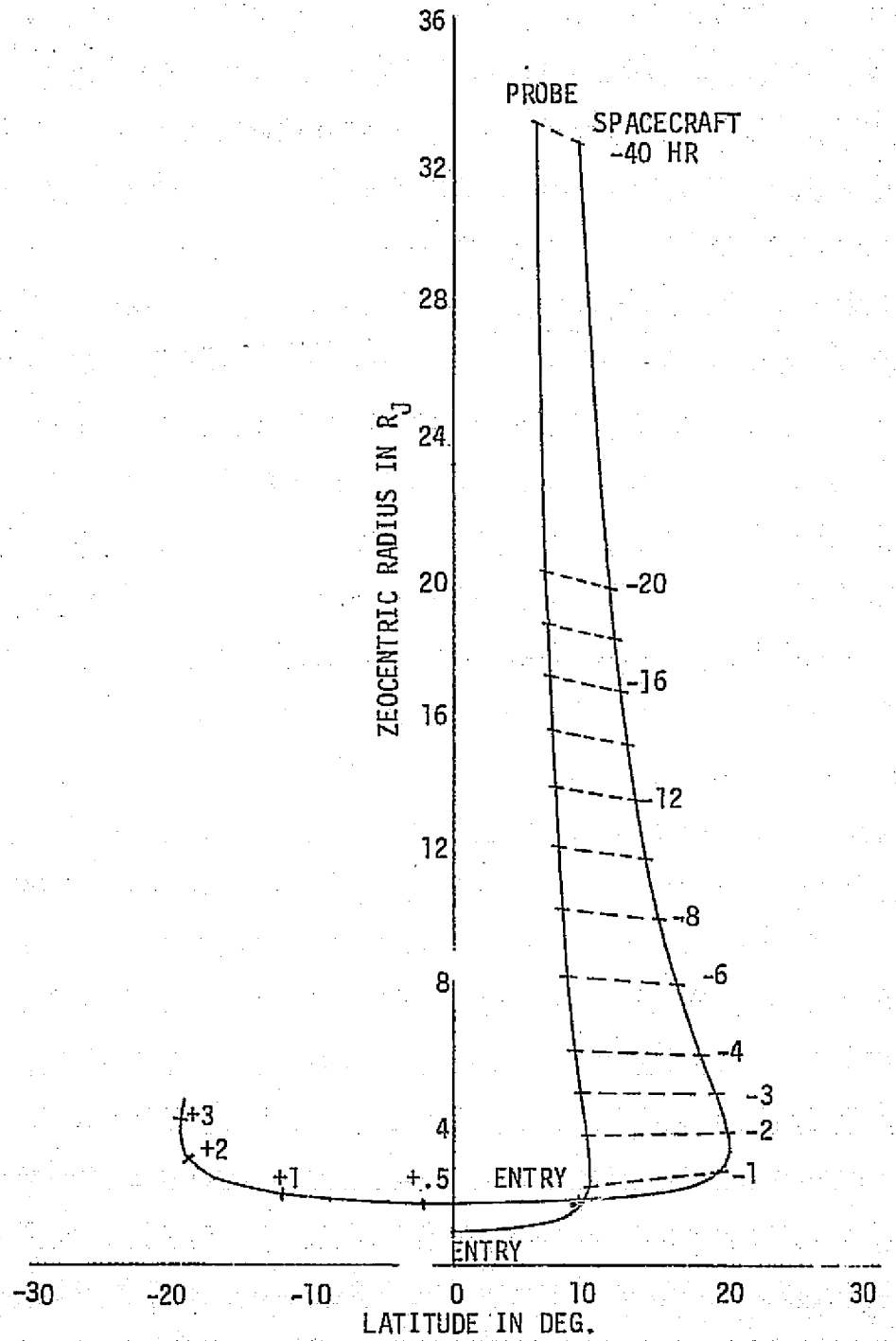

FIGURE I-8

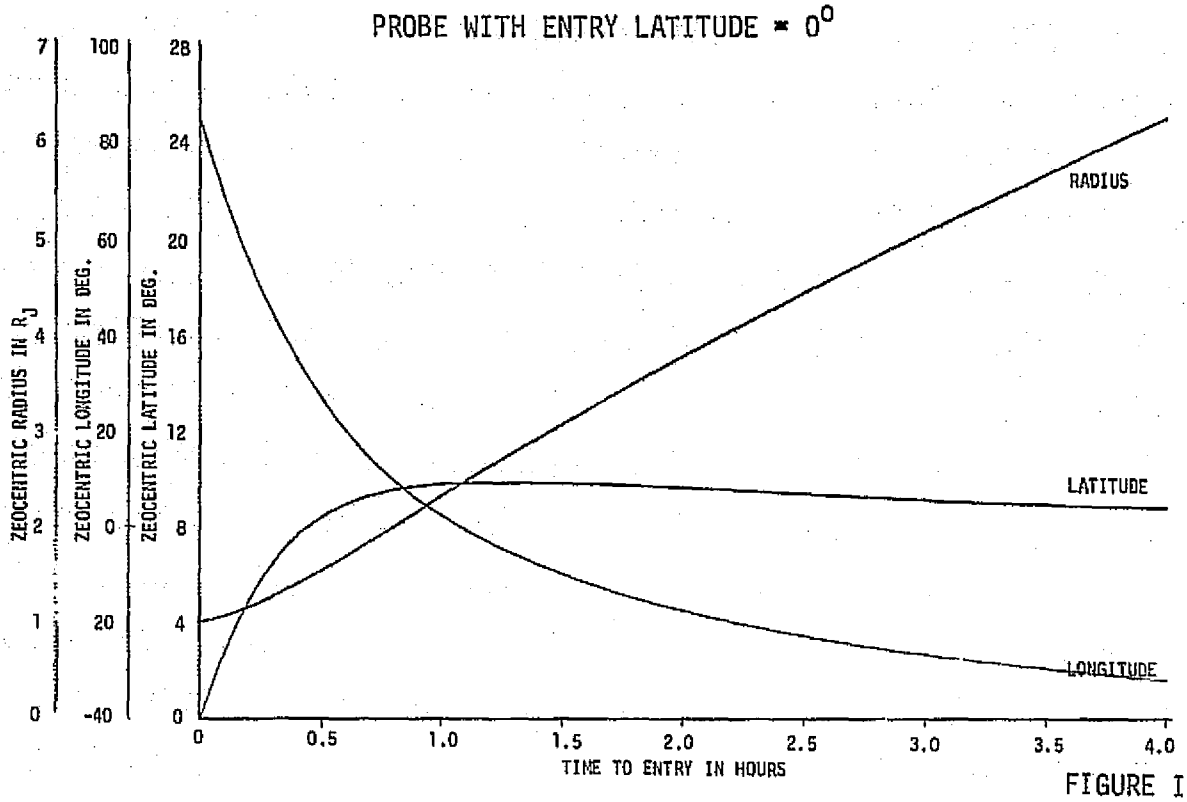

FIGURE I-9

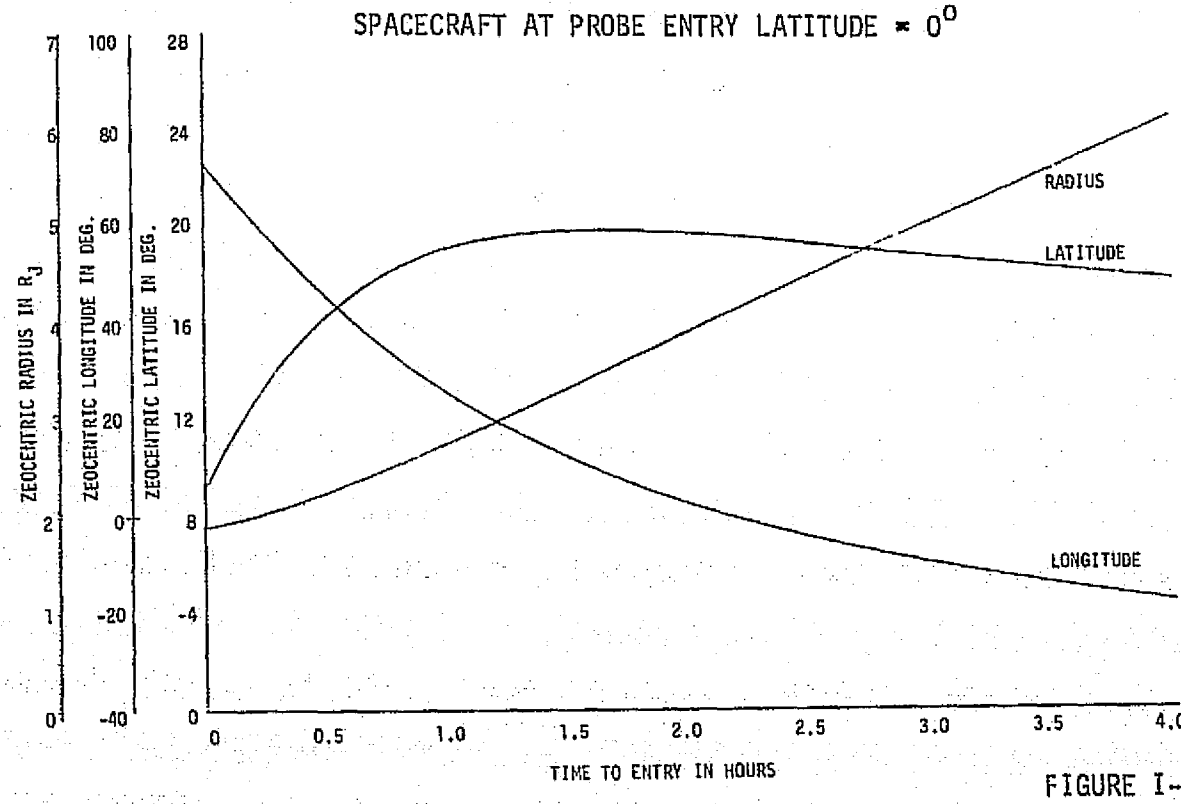

FIGURE I-10

ENTRY LATITUDE = -5°

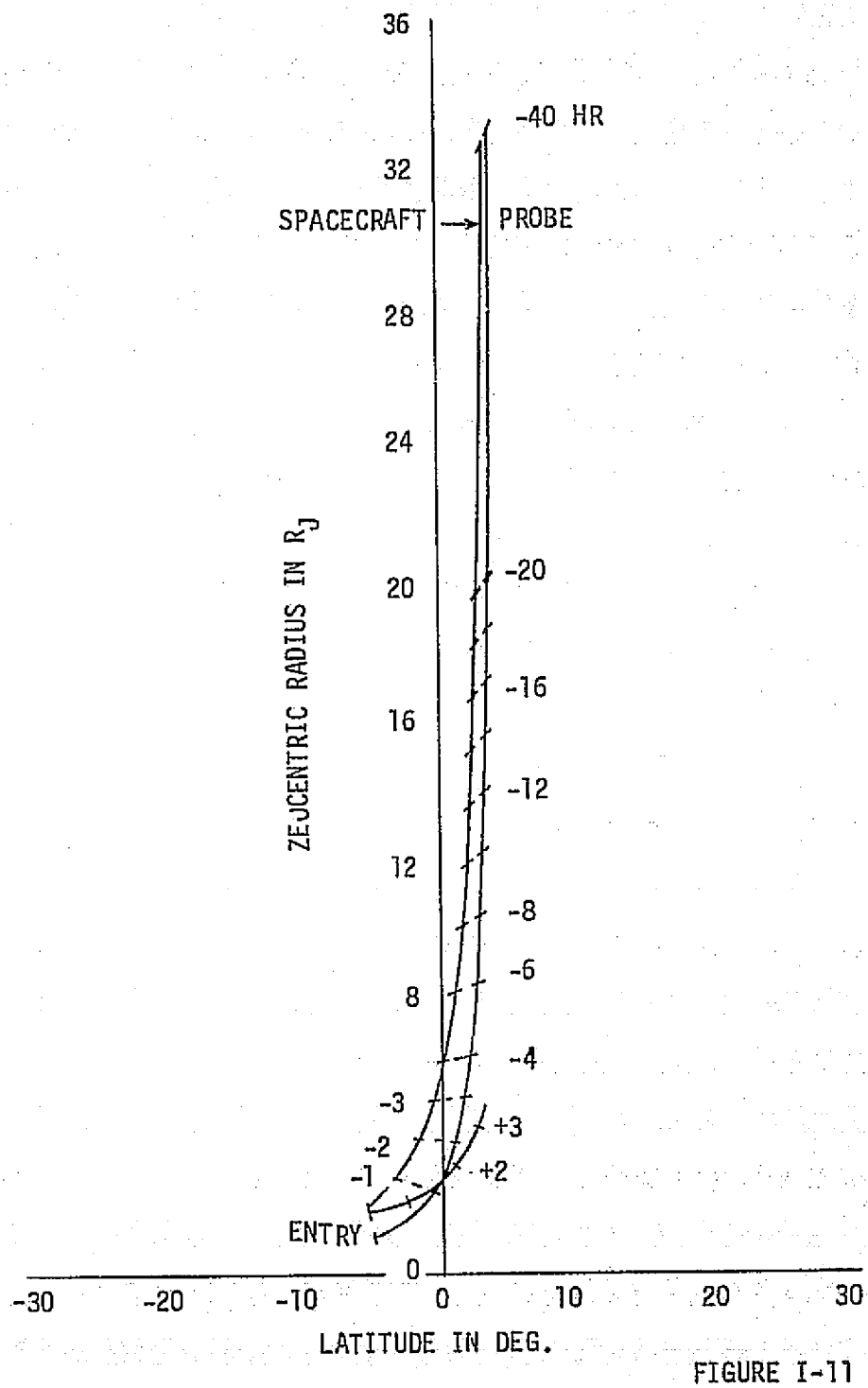

FIGURE I-11

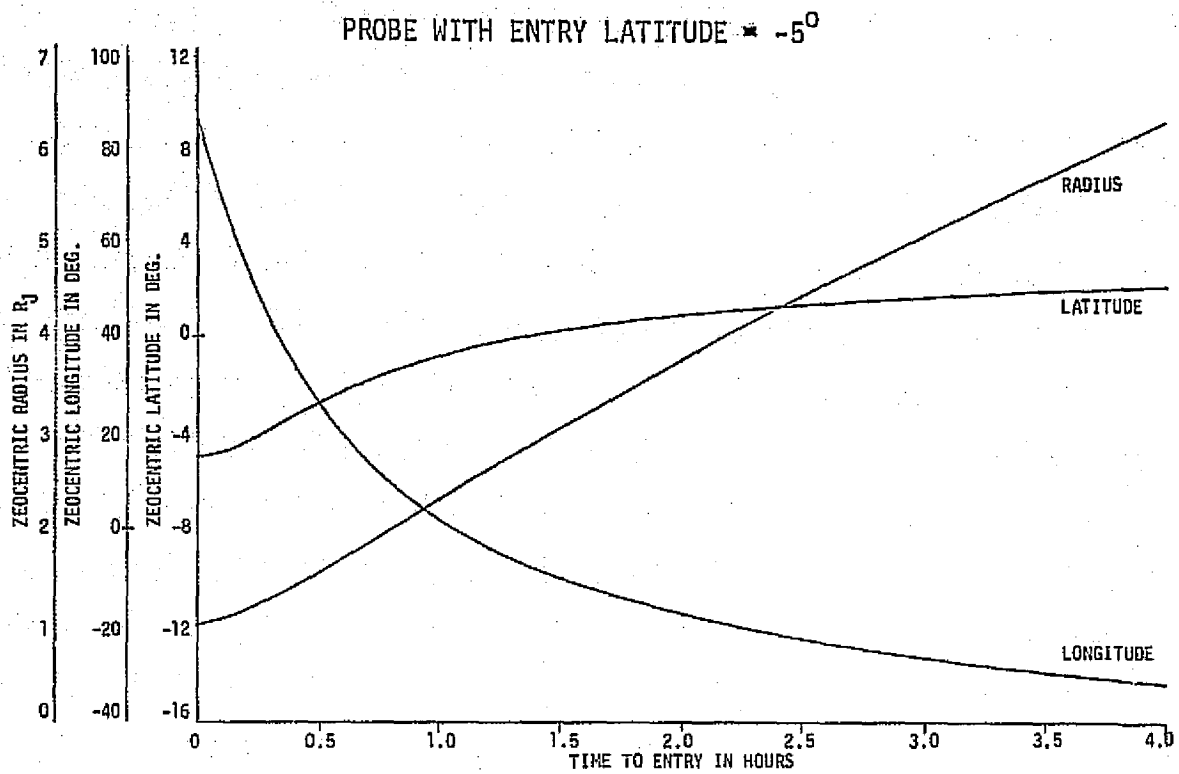

FIGURE I-12

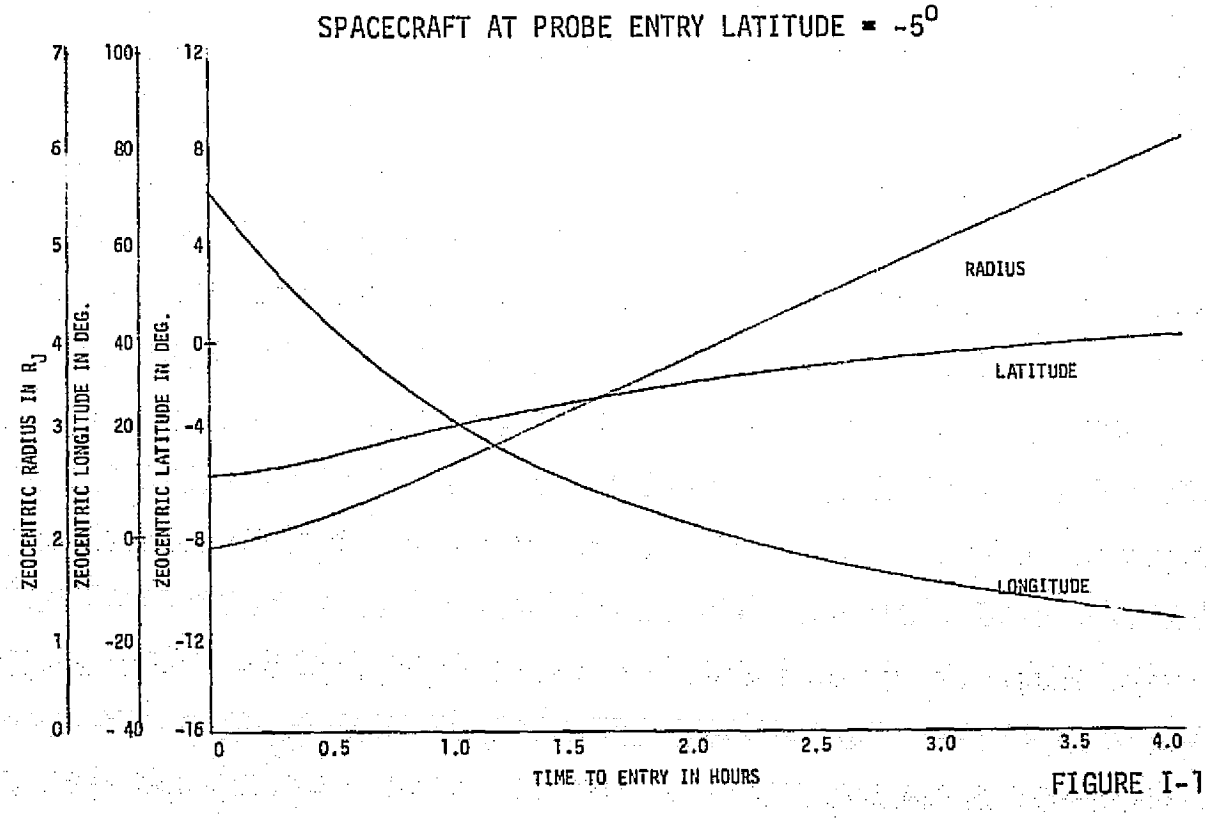

FIGURE I-13

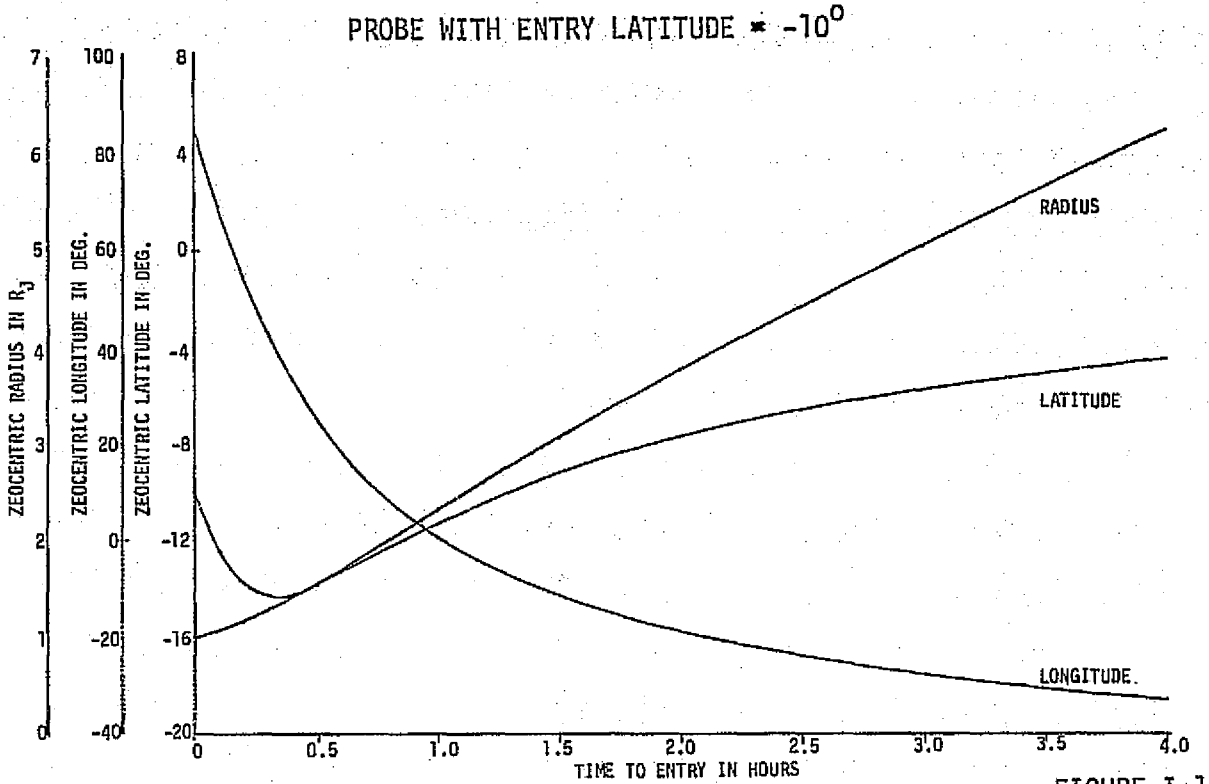

FIGURE I-15

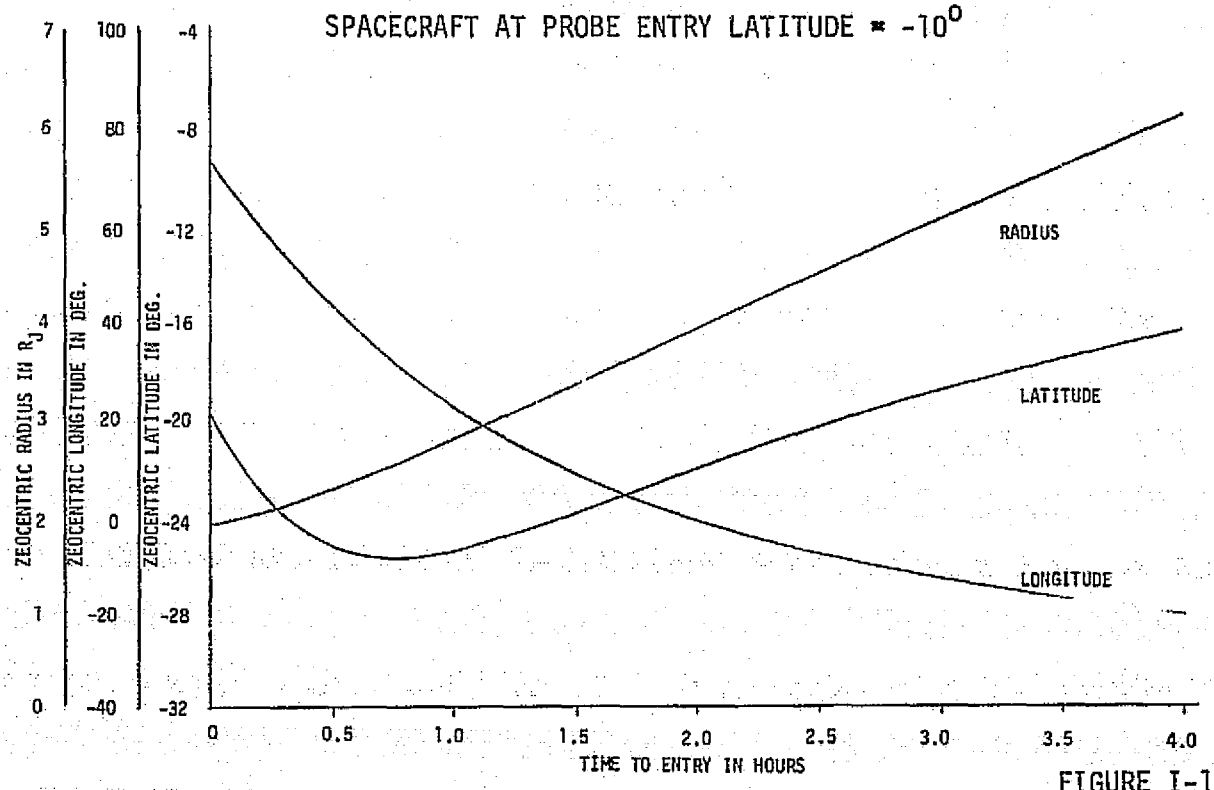

FIGURE I-16

APPENDIX II

REPRESENTATIVE LINK TABLES
PIONEER JUPITER FLYBY-PROBE MISSION
(REFER TO MISSION ANALYSIS)

APPROACH 1

```
 FPO,PRSW,SCBM,SCBC,SCNR  ,TL.
?
    400.0        66.00        50.00        65.00        1.000        2.000
 DATA,RCVL,TH,RM,NPW
?
    44.00        1.500        10.60        290.0        40.00
 EXOATM;10.0R7.5
?7.5
    7.500     NOMINAL ENTRY ANGLE
 LINK TABLE:ENTRY TO JUPITER
 PARAMETER       VALUE       TOLERANCE  COMMENT
 XMTR             46.02       -1.000      40.00     WATTS
 MISC LOSSES     -1.000       -.3000     ASSUMED
 XMT ANT GAIN     5.101        -.8838       66.00     DEG ON
 FREE SPACE     -182.6         -.7347       1.133     RADII
 IONOSPHERE     -.4364E-01     -1.105       .3801E-01 VERTICAL
 ABSORPTION     -.1607E-01     -.2756E-01   .1400E-01 VERTICAL
 RCV ANT GAIN     2.665         -.6195        50.00        65.00     DEG SW&BC
 TOT RCV PWR    -129.9         -4.670      SUBTOTAL
 COSMIC          118.9          568.9      TRW SPACE HB
 THERMAL         414.4          510.6      NASA SP
 SYNCH          3446.          5169.       NASA HB
 RCVR            290.0          360.8      1/2 DB
 SENS           -163.1          1.908      SUBTOTAL
 DATA             10.43         .0000         44.00     BPS
 RCV LOSS         1.500        -.2000      SPEC
 THRESHOLD       10.60          .0000      FSK BT=2
 RCV DATA PWR    28.53         -.2000       SUBTOTAL
 SUM ADVERSE TOLERANCES  -6.779     SUBTOTAL
 MARGIN           4.680
 EXCESS MARGIN   -2.099


 MARGIN HISTORY=1.
?1.
    TIME(HR)                MARGIN HISTORY
                  BEST        NOMINAL       WORST
    .0000         8.827        4.680       -1.916
    .5000E-01     9.271        5.102       -1.859
    .1000         9.460        5.255       -2.055
    .1500         9.444        5.178       -2.065
    .2000         9.264        4.907       -10.33
    .2500         8.955        4.474       -17.82
    .3000         8.546        3.905       -17.44
    .3500         8.060        3.224       -17.19
    .4000         7.570        2.393       -17.04
    .4500         7.006        1.507       -17.01
    .5000         6.339       -14.84       -17.09
    .5500         5.586       -14.99       -17.27
    .6000         4.839       -15.14       -17.56
    .6500         4.019       -15.43       -17.96
    .7000         3.105       -15.80       -18.48
    .7500         2.070       -16.29       -19.12
    .8000        -14.95       -16.89       -19.90
    .8500        -15.29       -17.65       -20.82
    .9000        -16.02       -18.59       -21.90
    .9500        -16.90       -19.75       -23.16
    1.000        -18.08       -21.15       -24.62
    1.050        -19.64       -22.86       -26.31
```


FIGURE II-1

APPROACH 3

```
 FRQ,PPBW,SCBW,SCBC,SCNA,SCPE
?
    400.0        66.00        50.00        65.00        1.000        2.000
 DATA,RCVL,TH,RN,XPW
?21.,,,,,50.
    21.00        1.500        10.60        290.0        50.00
 CMDATM;10.OR7.5
??7.5
    7.500    NOMINAL ENTRY ANGLE
 LINK TABLE;ENTRY TO JUPITER
 PARAMETER      VALUE       TOLERANCE   COMMENT
 XMTR           46.99       -1.000        50.00     WATTS
 MISC LOSSES   -1.000       -.3000     ASSUMED
 XMT ANT GAIN   5.101        -.8838       66.00     DEG 1W
 FREE SPACE    -182.6       -.7347      1.133      RADII
 IONOSPHERE    -.4364E-01   -1.105       .3801E-01 VERTICAL
 ABSORPTION    -.1607E-01   -.2756E-01   .1400E-01 VERTICAL
 RCV ANT GAIN   2.665        -.6195       50.00        65.00     DEG BW&BC
 TOT RCV PWR   -129.0       -4.670     SUBTOTAL
 COSMIC         118.9        568.9     TRW SPACE HB
 THERMAL        414.4        510.6     NASA SP
 SYNCH          3446.        5169.     NASA HB
 RCVR           290.0        360.8     1/2 DB
 SENS          -163.1        1.908     SUBTOTAL
 DATA           13.22        .0000        21.00     BPS
 RCV LOSS       1.500       -.2000     SPEC
 THRESHOLD      10.60        .0000     FSK BT=2
 RCV DATA PWR   25.32        -.2000      SUBTOTAL
 SUM ADVERSE TOLERANCES    -6.779     SUBTOTAL
 MARGIN         8.861
 EXCESS MARGIN  2.083


 MARGIN HISTORY=1.
?
     TIME(HR)                MARGIN HISTORY
                  BEST          NOMINAL        WORST
    .0000         13.01          8.861         2.266
    .5000E-01     13.45          9.284         2.322
    .1000         13.64          9.436         2.126
    .1500         13.63          9.359         1.716
    .2000         13.45          9.089        -14.15
    .2500         13.14          8.655        -13.64
    .3000         12.73          8.087        -13.26
    .3500         12.24          7.405        -13.00
    .4000         11.75          6.575        -12.86
    .4500         11.19          5.688        -12.83
    .5000         10.52         -10.66        -12.91
    .5500         9.768         -10.74        -13.09
    .6000         9.020         -10.96        -13.38
    .6500         8.200         -11.25        -13.78
    .7000         7.286         -11.62        -14.30
    .7500         6.251         -12.10        -14.94
    .8000        -10.77         -12.71        -15.72
    .8500        -11.21         -13.47        -16.64
    .9000        -11.84         -14.41        -17.72
    .9500        -12.72         -15.56        -18.98
    1.000        -13.90         -16.97        -20.44
    1.050        -15.46         -18.68        -22.13
```

FIGURE II-2

APPROACH 5

```
FRQ,PRBW,SCBW,SCBC,SCNA,MODE
?,,,,2.
    400.0        66.00        50.00        65.00        2.000        2.000
DATA,RCVL,TH,PN,XPW
?
    21.00        1.500        10.60        290.0        50.00
EXOATM;10.0R7.5
?
    7.500    NOMINAL ENTRY ANGLE
LINK TABLE;ENTRY TO JUPITER
PARAMETER      VALUE       TOLERANCE   COMMENT
XMTR           46.99       -1.000        50.00     WATTS
MISC LOSSES   -1.000       -.3000      ASSUMED
XMT ANT GAIN   5.101        -.8838        66.00     DEG BW
FREE SPACE    -182.6       -.7347       1.133      RADII
IONOSPHERE    -.4364E-01   -1.105       .3801E-01  VERTICAL
ABSORPTION    -.1607E-01   -.2756E-01   .1400E-01  VERTICAL
RCV ANT GAIN   2.665        -.6195        50.00        65.00     DEG BW@BC
TOT PCV PWR   -129.0       -4.670      SUBTOTAL
COSMIC         118.9        568.9      TRW SPACE HB
THERMAL        414.4        510.6      NASA SP
SYNCH          3446.        5169.      NASA HB
PCVR           290.0        360.8      1/2 DB
SENS          -163.1        1.908      SUBTOTAL
DATA           13.22        .0000        21.00     BPS
PCV LOSS       1.500       -.2000      SPEC
THRESHOLD      10.60        .0000      FSK BT=2
POD DATA PWR   25.32        -.2000       SUBTOTAL
SUM ADVERSE TOLERANCES   -6.779      SUBTOTAL
MARGIN         8.861
EXCESS MARGIN  2.083


MARGIN HISTORY=1.
?
    TIME(HR)              MARGIN HISTORY
                BEST          NOMINAL        WORST
    .0000       13.01         8.861          3.760
    .5000E-01   13.45         9.345          5.586
    .1000       13.64         10.64          5.980
    .1500       13.60         11.62          6.144
    .2000       13.96         11.91          7.127
    .2500       14.05         11.90          8.193
    .3000       14.10         11.74          9.041
    .3500       14.05         12.15          8.983
    .4000       14.00         12.46          8.655
    .4500       13.89         12.66          8.162
    .5000       13.69         12.80          8.235
    .5500       13.59         12.71          8.561
    .6000       13.63         12.36          8.725
    .6500       13.61         11.94          8.723
    .7000       13.52         11.44          8.551
    .7500       13.33         11.04          8.009
    .8000       13.01         10.67          7.144
    .8500       12.53         10.10          6.157
    .9000       11.86         9.268          5.037
    .9500       11.06         8.048          3.767
    1.000       9.902         6.569          2.325
    1.050       8.316         4.789          .6881
```


FIGURE II-3

LINDENBLAD ANTENNA MARGIN ANALYSIS

```
ATMOS CORR=1.
?
 FRQ;PRBW;SCBW;SCBC;SCHA
?
    400.0        66.00        40.00        85.00        1.000
 DATA;RCVL;TH;RN;XPW
?
    44.00        1.500        10.60        290.0        40.00
 EXOATM;RPS=2.0;TT=.4=2040
?2040
   2040
 GAMMA=7.5;RP=2.0;TT=.4
 LINK TABLE;ENTRY TO JUPITER
 PARAMETER       VALUE       TOLERANCE  COMMENT
 XMTR            46.02       -1.000       40.00     WATTS
 XMT LINE       -.3000       -.1000     ASSUMED
 XMT ANT GAIN    5.101        -.7454       66.00     DEG BW 5DTOL
 FREE SPACE    -182.6          .0000       1.133    RADII
 IONOSPHERE     -.1148E-01   -.3816E-01   .9999E-02 VERTICAL MM=E6
 ABSORPTION     -.1607E-01   -.2796E-01   .1400E-01 VERTICAL
 RCV ANT GAIN    4.146        -.5000       40.00        85.00     DEG BW&BC
 RCV LINE       -.5000       -.1000     ASSUMED
 POLARIZ        -.2000       -.1000     ASSUMED
 TOT RCV PWR    -128.4       -2.605     SUBTOTAL
 COSMIC          118.9        568.9     TRW SPACE HB
 THERMAL         414.4        510.6     NASA SP
 SYNCH           3446.        5169.     NASA SP
 RCVR            290.0        360.8     1/2 DB
 SYS TEMP        3543.        5498.     KELVIN
 SENS           -163.1        1.908     SUBTOTAL
 DATA            16.43         .0000       44.00     BPS
 RCV LOSS        1.500        -.2000     SPEC
 THRESHOLD       10.60         .0000     FSK BT=2
 RCD DATA PWR    28.53        -.2000      SUBTOTAL
 SUM ADVERSE TOLERANCES   -4.714      SUBTOTAL
 MARGIN          6.193
 EXCESS MARGIN   1.479


 MARGIN HISTORY=1.
?
     TIME(HR)                MARGIN HISTORY
                  BEST          NOMINAL       WORST
 THRD EXCESS    -.1194E-01
    .0000        6.805          6.193         5.507
    .5000E-01    7.603          7.214         6.771
    .1000        8.221          7.961         7.660
    .1500        8.675          8.451         8.195
    .2000        8.916          8.701         8.458
    .2500        8.965          8.726         8.460
    .3000        8.842          8.542         8.214
    .3500        8.504          8.165         7.797
    .4000        7.987          7.612         7.204
    .4500        7.339          6.896        -14.66
 MAGIC 105 AT     .4624
 THRD EXCESS      .4550
    .5000       -14.62         -14.75        -14.90
 TOTAL RCVD ENERGY METRIC IS     2.067
```

ORIGINAL PAGE IS
OF POOR QUALITY

FIGURE II-4

LOOP VEE ANTENNA MARGIN ANALYSIS

```
ATMOS CORR=1.
?
 FRQ,PRBW,SCBW,SCBC,SCNA
?
    400.0        66.00        50.00        65.00        1.000
 DATA,RCVL,TH,RN,XPW
?
    44.00        1.500        19.60        290.0        40.00
 EXOATM;RPS=2.0;TT=.4=2040
?1740
   1740
 GAMMA=7.5;RP=1.7;TT=.4
 LINK TABLE;ENTRY TO JUPITER
 PARAMETER      VALUE       TOLERANCE  COMMENT
 XMTR           46.02       -1.000       40.00     WATTS
 XMT LINE      -.3000       -.1000     ASSUMED
 XMT ANT GAIN   2.362        -1.123        66.00     DEG BW 5DTOL
 FREE SPACE   -181.0         .0000        .9396     RADII
 IONOSPHERE    -.1369E-01   -.3835E-01    .9999E-02 VERTICAL NX=E6
 ABSORPTION    -.1917E-01   -.3286E-01    .1400E-01 VERTICAL
 RCV ANT GAIN   3.601        -.5000        50.00        65.00     DEG BW@3BC
 RCV LINE      -.5000       -.1000     ASSUMED
 POLARIZ       -.2000       -.1000     ASSUMED
 TOT RCV PWR  -130.1        -2.994     SUBTOTAL
 COSMIC         118.9        568.9     TRW SPACE HB
 THERMAL        414.4        510.6     NASA SP
 SYNCH          3309.        4963.     NASA SP
 RCVR           290.0        360.8     1/2 DB
 SYS TEMP       3429.        5313.     KELVIN
 SENS          -163.3        1.901     SUBTOTAL
 DATA           16.43        .0000        44.00     BPS
 RCV LOSS       1.500       -.2000     SPEC
 THRESHOLD      10.60        .0000     FSK BT=2
 ROD DATA PWR   28.53        -.2000     SUBTOTAL
 SUM ADVERSE TOLERANCES  -5.095     SUBTOTAL
 MARGIN         4.670
 EXCESS MARGIN  -.4257


 MARGIN HISTORY=1.
?
     TIME(HR)              MARGIN HISTORY
                  BEST          NOMINAL       WORST
    .0000         5.521         4.670         3.755
 THRD EXCESS      .1399E-01
    .5000E-01     6.834         6.191         5.506
    .1000         7.740         7.223         6.678
    .1500         8.265         7.805         7.322
    .2000         8.488         7.974         7.435
    .2500         8.395         7.765         7.102
    .3000         7.914         7.210         6.466
    .3500         7.083         6.344         5.555
    .4000         6.028         5.201        -11.48
 MAGIC 105 AT      .4187
 THRD EXCESS       .4003
    .4500        -11.31        -11.52        -11.76
 TOTAL RCVD ENERGY METRIC IS     2.020
```

FIGURE II-5